January 2012

Impact Of Coal Derived Impurities On The Performance Of Hydrogen Separation Membranes

Joshua Stanislowski

IMPACT OF COAL DERIVED IMPURITIES ON THE PERFORMANCE OF HYDROGEN SEPARATION MEMBRANES

by

Joshua Jerry Stanislowski
Bachelor of Science, University of North Dakota, 2000

A Thesis

Submitted to the Graduate Faculty

of the

University of North Dakota

in partial fulfillment of the requirements

for the degree of

Master of Science

Grand Forks, North Dakota
December
2012

This thesis, submitted by Joshua Jerry Stanislowski in partial fulfillment of the requirements for the Degree of Master of Science from the University of North Dakota, has been read by the Faculty Advisory Committee under whom the work has been done, and is hereby approved.

_____
Dr. Steven A. Benson

_____
Dr. Michael D. Mann

_____
Dr. Brian M. Tande

This thesis is being submitted by the appointed advisory committee as having met all of the requirements of the Graduate School at the University of North Dakota and is hereby approved.

_____
Wayne Swisher
Dean of the Graduate School

_____
Date

Title Impact of Coal Derived Impurities on the Performance of Hydrogen Separation Membranes

Department Chemical Engineering

Degree Master of Science

In presenting this thesis in partial fulfillment of the requirements for a graduate degree from the University of North Dakota, I agree that the library of this University shall make it freely available for inspection. I further agree that permission for extensive copying for scholarly purposes may be granted by the professor who supervised my thesis work or, in his absence, by the Chairperson of the department or the dean of the Graduate School. It is understood that any copying or publication or other use of this thesis or part thereof for financial gain shall not be allowed without my written permission. It is also understood that due recognition shall be given to me and to the University of North Dakota in any scholarly use which may be made of any material in my thesis.

Name: Josh Stanislowski

Date: November 27, 2012

TABLE OF CONTENTS

LIST OF FIGURES

LIST OF TABLES

ACKNOWLEDGMENTS

I wish to express my sincere appreciation to Dr. Steven Benson, Dr. Michael Mann, Dr. Brian Tande, and other faculty members of the University of North Dakota for their guidance and support during my time in the master's program.

Special thanks goes to my friends and family that supported this endeavor.

I would like to thank the US Department of Energy and the State of Wyoming through the Clean Coal Technologies Research Program for providing the funding for completing the experimental and modeling portion of this work.

My deepest thanks go out to Dr. Bret Howard and Dr. Bryan Morreale of the National Energy Technology Laboratory and Dr. Sean Emerson of United Technologies Research Center for providing analytical results.

The support of the staff at the Energy & Environmental Research Center was key to completing this work. I would like to thank Angie Morgan, Scott Tolbert, Tyler Curran, Mike Swanson, Jason Laumb and Nick Lentz and for all of their help, guidance, and support through the course of this project.

ABSTRACT

In order to facilitate the use of hydrogen in integrated gasification combined-cycle (IGCC) applications or as a transportation fuel, hydrogen-from-coal technologies that are capable of managing carbon will be needed. Many technologies are under development for the separation of hydrogen from coal-derived syngas, and among the most promising are hydrogen separation membranes. Studies indicate a significant IGCC plant efficiency increase can be realized if warm-gas cleanup and hydrogen separation membranes are used in place of conventional technologies. These membranes provide the potential to produce hydrogen while simultaneously separating CO_2 at system pressure. Membrane development to date has primarily occurred on bottle-derived syngas, and the impact of coal-derived impurities is largely unknown. Gasification syngas typically has many impurities that, if not removed, will poison most hydrogen separation materials. In order to commercialize this promising technology, scale-up to bench- and pilot-scale gasifiers is required so that the impact of impurities can be evaluated.

Sulfur and other coal derived impurities such as chlorine, sodium, mercury, and arsenic have the potential to deteriorate the performance of hydrogen separation membranes. It is unknown if species such as mercury will have an impact on the membrane performance, but mercury does remain in the gas phase and can cause environmental concerns. Commercially available technologies exist today to remove the contaminants from the syngas prior to exposure to the membranes. The goal of this work was to determine if the warm gas clean up techniques available today are adequate to

protect hydrogen separation membranes from performance degradations caused by the impurities found in coal. To test this hypothesis, pilot-scale gasifiers at the Energy & Environmental Research Center (EERC) were used to produce coal-derived syngas, and solid sorbents were used for warm-gas cleanup and water–gas shift. Three hydrogen separation membranes were exposed to coal-derived syngas for several hundred hours. Membrane materials that were exposed to coal derived syngas during the testing were acquired and analyzed for contaminants. This work explores whether the warm gas cleanup techniques employed were adequate to prevent performance degradation of hydrogen separation membranes. The U.S. Department of Energy's National Energy Technology Laboratory and the State of Wyoming funded the experimental effort.

CHAPTER 1

INTRODUCTION

Hydrogen provides a unique opportunity for the future energy portfolio of the United States, because hydrogen can be produced in large scale facilities domestically, and because only water is emitted when the energy is utilized. Hydrogen has the potential to play an important role in both zero emissions electrical generation and transportation. Carbon capture and storage technologies will enable hydrogen to be produced from coal without carbon emissions. Coal gasification combined with advanced gas cleanup technologies and carbon capture will enable the production of hydrogen from coal with near zero emissions. Hydrogen separation membranes have the potential to play an important role in these near zero emission plants because membranes can produce hydrogen economically and at large scale. Therefore, development and deployment of hydrogen separation membrane technologies is a critical path forward toward energy sustainability in a carbon constrained world.

Hydrogen separation membranes are commercially available today, but most developments have spurred from advancements in hydrogen separation from steam-methane reforming plants or refineries. Most membranes used today are highly susceptible to poisons commonly found in coal derived syngas such as sulfur, ammonia, mercury, and trace metals. Gas cleanup technologies will eliminate many of these contaminants, but trace amounts of poisons will breakthrough and system upsets will

inevitably occur. Considering that most membrane materials are very expensive, new separation materials are needed that will have some resistance to common poisons.

Several promising advanced membrane technologies for hydrogen separation are currently under development that have the potential to efficiently separate hydrogen while having an inherent resistance to poisons found in syngas. Unfortunately, most of the development performed to date has occurred on the laboratory scale using bottle-derived syngas. Demonstration of the performance of these advanced membranes must occur on coal derived syngas in order to move the technologies into the commercial market place. Impurities from coal-derived syngas that could poison a hydrogen separation membrane include H_2S, COS, NH_3, CO, and HCl. Long-term success of membrane technology will require long-term exposure to coal-derived syngas to understand the impact of the impurities. While the majority of the impurities will be removed in a gas cleanup process, concentrations to less than 1 ppm may be required for long-term viability.

Five main types of membranes are currently under development: dense polymer, microporous ceramic, porous carbon, dense metallic, and dense ceramic (1). Of these types, dense metallic and dense ceramic have the highest hydrogen selectivity. Dense metallic membranes also have very high hydrogen flux rates, making them potential candidates for large-scale commercial application if poisoning issues can be overcome. Palladium is the typical base metal for metallic membranes, and alloy combinations such as Pd–Cu, Pd–Au, and Pd–Ag have been tested. Many other formulations exist, but most are closely guarded trade secrets.

The development of warm-gas cleanup techniques is essential to the successful deployment of hydrogen separation membranes. Metallic membranes operate optimally between 300° and 600°C. Cold-gas-cleaning techniques that cool the syngas to ambient temperature or less will result in a substantial energy penalty from having to reheat the syngas before hydrogen separation. Additionally, water–gas shift (WGS) catalysts require higher temperatures to run efficiently, and some level of heating is achieved in the shift catalyst bed. Most membranes are not sulfur tolerant and require syngas with very low sulfur content to operate optimally.

Sulfur and other coal derived impurities such as chlorine, sodium, mercury, and arsenic have the potential to deteriorate the performance of hydrogen separation membranes. It is unknown if species such as mercury will have an impact on the membrane performance, but mercury does remain in the gas phase and can cause environmental concerns. Commercially available technologies exist today to remove the contaminants from the syngas prior to exposure to the membranes. The goal of this work was to determine if the warm gas clean up techniques available today are adequate to protect hydrogen separation membranes from performance degradations caused by the impurities found in coal. To test this hypothesis, pilot-scale gasifiers at the Energy & Environmental Research Center (EERC) were used to produce coal-derived syngas, and solid sorbents were used for warm-gas cleanup and water–gas shift. Three hydrogen separation membranes were exposed to coal-derived syngas for several hundred hours. Membrane materials that were exposed to coal derived syngas during the testing were acquired and analyzed for contaminants. This work explores whether the warm gas cleanup techniques employed were adequate to prevent performance degradation of

hydrogen separation membranes. The U.S. Department of Energy's National Energy Technology Laboratory and the State of Wyoming funded the experimental effort.

Hydrogen separation membranes were acquired for this testing from organizations currently developing the technology. A fluid bed gasifier and an entrained flow gasifier at the EERC produced a syngas stream derived from Powder River Basin coal. The gas was cleaned using warm gas cleaning techniques; removing particulate, sulfur, chlorine, and possibly trace metals. The gas was cleaned above a temperature of 400°F, and then the membranes were exposed to coal derived syngas. Because the gas temperature remains warm through the cleaning process, the membranes had the potential to see contaminants such as ammonia, chlorine, and trace metals. Performance of the hydrogen separation membranes was monitored on a continuous basis. Syngas composition, hydrogen purity, hydrogen flux, and hydrogen recovery are all key metrics that provide clues to possible performance deterioration.

CHAPTER 2

BACKGROUND

Two main applications for hydrogen separation membranes employed a large scale are envisioned. Large scale hydrogen production facilities could provide fuel for fuel cell vehicles. Power generation facilities with CO_2 capture could employ hydrogen separation membranes to reduce the cost of separation. Both scenarios are likely to employ coal gasification to produce the hydrogen.

2.1 Membranes for Hydrogen Production for Transportation Applications

The US Department of Energy (DOE) views hydrogen as an energy carrier of the future because it can be derived from domestic resources that are clean and abundant; and because hydrogen is an inherently clean fuel. According to DOE, the deployment of hydrogen technologies could lead to the creation of 675,000 green jobs in the United States (2). Coal gasification plants can separate hydrogen from the synthesis gas, purify the carbon for storage, and burn the hydrogen to produce power in an integrated gasification combined cycle (IGCC) configuration. In this type of configuration, the only major emission from the plant is water. Hydrogen can also play a key role as a transportation fuel. If all vehicles in Los Angeles were converted to hydrogen, the urban smog problems would be virtually eliminated. Hydrogen fuel cell technologies have undergone rapid development over the past decade, and the technology exists today to produce commercial hydrogen fuel cell vehicles that have a transportation range of up to 280 miles (3). The main challenges that remain today are the economical production of

hydrogen, economical production of fuel cell vehicles, and the development of hydrogen transportation, storage, and dispensing infrastructure.

The National hydrogen Association views hydrogen as the best pathway to both reduce the oil consumption in the US and reduce transportation based CO_2 emissions. Figure 2.1 compares three different vehicle market penetration scenarios for light duty vehicles (4). The bar on the left represents 100% gasoline internal combustion engines, the middle bar represents market penetration for plug-in hybrid electric vehicles, and the bar on the right represents hydrogen fuel cell vehicles. Each scenario is compared to the annual oil consumption for that time period. It can be seen that if nothing changes and the US continues to rely solely on gasoline powered vehicles, the annual oil consumption is predicted to increase from 4 billion barrels per year (bby) to over 7 bby by the year 2100. With a significant market penetration of plug in hybrid vehicles, oil consumption can be reduced to about 2.5 BBY by 2100. However, with 98% market penetration of fuel cell vehicles, dependence on oil is virtually eliminated. While the future of transportation will certainly be a mix of several technologies, this graph illustrates that hydrogen is one of the only pathways toward eliminating the use of oil.

Figure 2.2 shows a similar set of scenarios, but compares the market penetration with annual CO_2 emissions from vehicles (4). It should be noted that the study assumes hydrogen production is occurring with carbon capture and storage or hydrogen is supplied from a renewable source. The graph shows that carbon dioxide emissions from vehicles will almost double by the year 2100 if gasoline vehicles are continued to be used exclusively. A reduction in CO_2 emissions is achieved if the course of plug in hybrid vehicles is followed. However with the fuel cell vehicle scenario, CO_2 emissions are

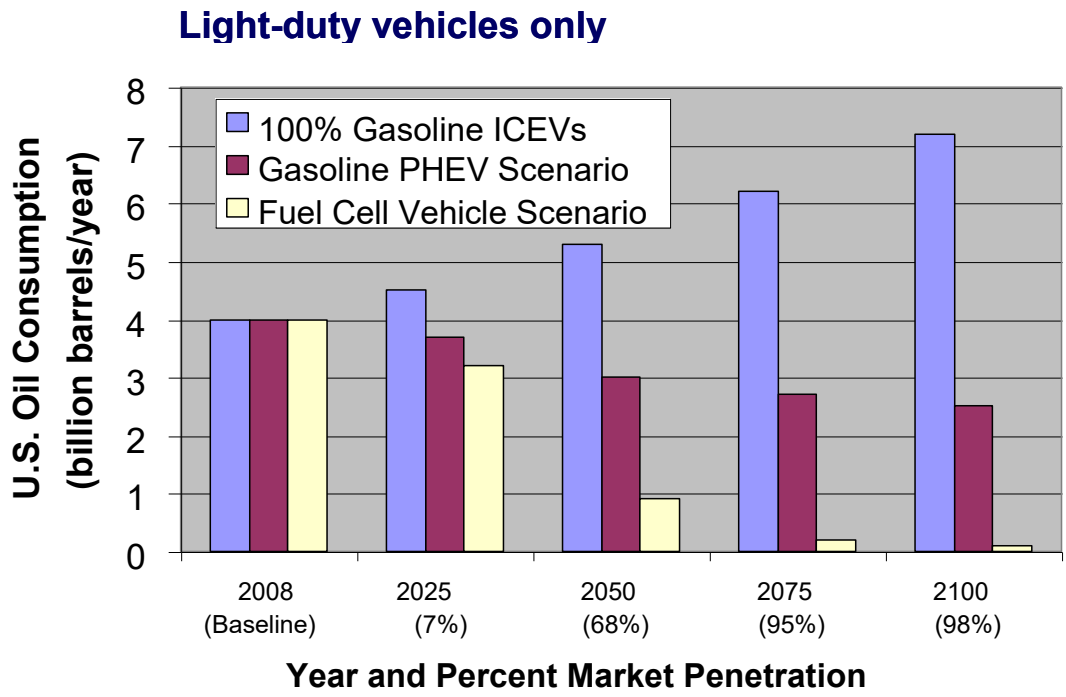

Figure 2.1. US Oil Consumption for Various Vehicle Scenarios (4).

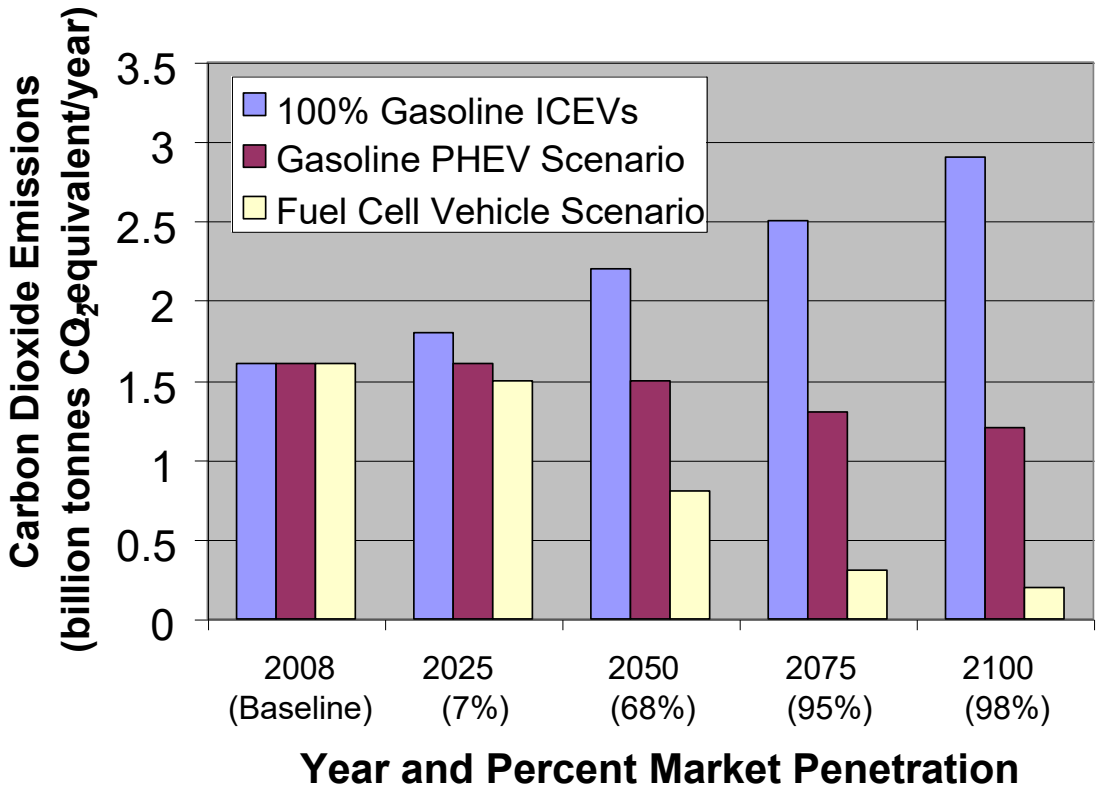

Figure 2.2. Carbon Dioxide Emissions for Various Vehicle Scenarios (4).

reduced by over 80% in the year 2100. This illustrates that hydrogen is a potential fuel pathway in a carbon constrained world. Increased production of natural gas and coal will be needed to meet these targets, and the data assume that the hydrogen production facility is equipped with carbon capture technology.

2.2 Membranes Integrated with Power Systems

Coal gasification is of significant interest to the future of power generation in the United States because it can be performed more efficiently and with less emission than conventional combustion. Integrated gasification combined cycle (IGCC) systems fire the syngas produced directly in a gas turbine, and recover the heat produced, resulting in more efficient conversion of energy to electricity than a conventional steam cycle. Currently the costs of gasification systems produce electricity at a higher cost than conventional combustion systems. One significant advantage of gasification over combustion is the ability to capture CO_2 at a much lower cost and energy penalty. The CO_2 in gasifier syngas streams is at much higher concentration and typically at elevated pressure, therefore less energy is required to perform the separation. When the cost of CO_2 capture is considered in the overall capital and operating cost of a power system, gasification units can have advantages in the cost of electricity over conventional combustion. Figure 2.3 compares the cost of electricity for gasification versus conventional power systems with and without CO_2 capture (5). The Figure shows that for conventional power systems, the cost of electricity is significantly less if CO_2 capture is not required. In the cases where CO_2 capture is needed, the IGCC plant produces electricity at a lower cost than the pulverized coal (PC) systems. The cost of natural gas combined cycle (NGCC) is heavily dependent on the price of natural gas. With recent

natural gas prices as low as $2/MMBtu, the current cost of NGCC is significantly lower than the competing technologies.

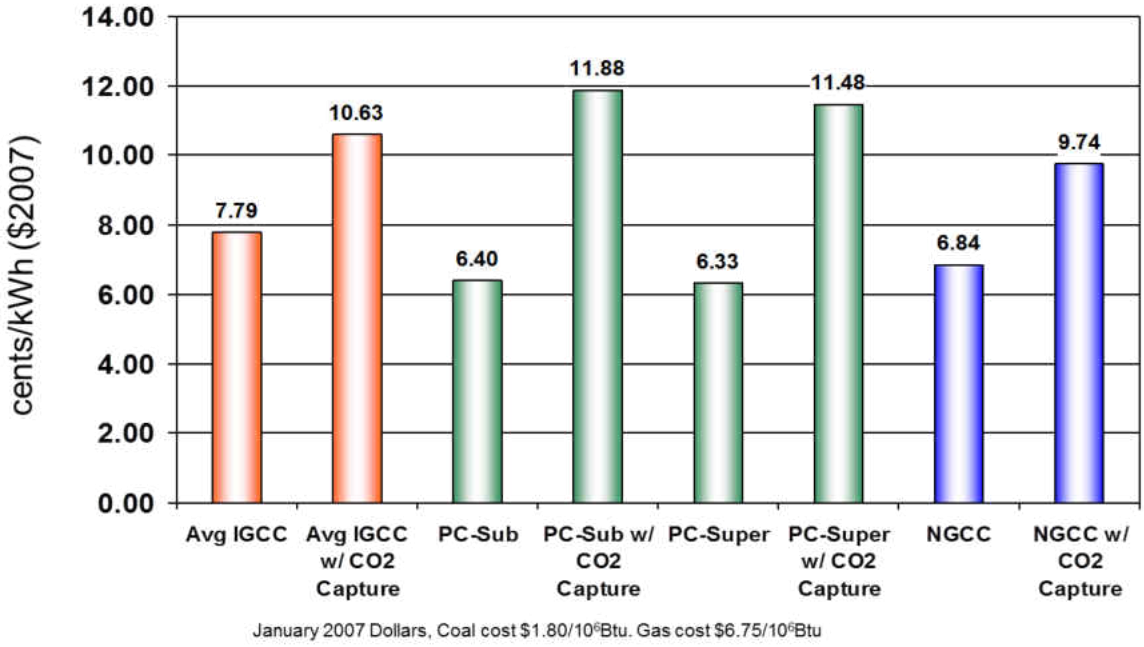

Figure 2.3. Comparison of the Cost of Electricity for Gasification vs. Conventional Systems with and without CO_2 Capture (5).

The cost of gasification with CO_2 capture utilizing technologies that are commercially available today is still relatively high compared to the cost of electricity production with no capture. Advanced technologies are needed to further reduce the costs of capture and improve the overall efficiency of the plants. Several critical research pathways and technologies have been identified by the National Energy Technology Laboratory (NETL) that will greatly improve the efficiency of gasification based power systems. Figure 2.4 depicts the technology advancements and the incremental increase in net plant efficiency if each technology is implemented (6). The figure indicates that the technology with the highest potential for reducing the cost of gasification systems is hydrogen and CO_2 separation using hydrogen selective membranes. According to NETL

the implementation of membrane technology can result in a nearly 3% efficiency point increase for a gasification system over using a conventional Selexol process. If all of the advanced pathway technologies are realized, the efficiency of an IGCC system with hydrogen separation membrane technology and CO_2 capture and compression could reach 40%. Advanced gasification fuel cell (IGFC) technologies could push the efficiency over 50%.

Case Title	Efficiency (% HHV)	Delta* Efficiency (% points)	TPC** ($/kW)	Delta* TPC** ($/kW)	20-yr Levelized COE (¢/kW-hr)	Delta* COE (¢/kW-hr)
Reference IGCC	30.4	0	2,718	0	11.48	0
Adv "F" Turbine	31.7	1.3	2,472	-246	10.64	-0.84
Coal Feed Pump	32.5	0.8	2,465	-7	10.54	-0.10
85% CF	32.5	0.0	2,465	0	10.14	-0.40
WGCU/Selexol	33.3	0.8	2,425	-40	10.00	-0.14
WGCU/H_2Membrane	36.2	2.9	2,047	-378	8.80	-1.20
AHT-1 Turbine	38.0	1.8	1,855	-192	8.14	-0.66
ITM	38.3	0.3	1,724	-131	7.74	-0.40
AHT-2 Turbine	40.0	1.7	1,683	-41	7.61	-0.13
90% CF	40.0	0.0	1,683	0	7.36	-0.25
IGCC Pathway		+9.6%pts (+32%)		-1,035 (-38%)		-4.12 (-36%)
Advanced IGFC	56.3	+26%pts +85%	1,759	-959 (-35%)	7.45	-4.03 (-35%)

* Delta shown is the incremental change as each new technology is added to previous case configuration
** TPC is reported in January 2007 dollars and excludes owner's costs

Figure 2.4. Advanced Gasification Pathways Toward Improving Efficiency and Reducing the Cost of Electricity for IGCC Systems (6).

2.3 Coal Gasification Fundamentals

Coal gasification is a process in which coal is reacted with steam and oxygen at temperature and pressure to form H_2 and CO. Pressures can range from atmospheric pressure to 1200 psi, and temperatures range from about 1200°F to over 2900°F. Besides the typically desired products, H_2 and CO, many other byproducts are formed during

gasification such as CO_2,CH_4, H_2S, COS, HCl, NH_3 , higher hydrocarbons, tars and oils, and particulate matter. The biggest challenge with any gasification system is dealing with the inorganic components in the coal and matching gasifier design to fuel specific properties and desired end products. Gasifiers are typically configured as fixed beds, fluidized beds, moving beds, or entrained flow. Each gasifier type has strengths and weaknesses depending on the fuel used and the desired end products.

Entrained flow gasifiers operate at very high temperatures and pressures, usually exceeding 2700°F and 600 psig. Systems are either up-fired or down-fired, and the gasifier operates like a plug flow reactor with the pulverized solids entrained in the gas stream. Residence times are on the order of seconds. The main advantage of entrained flow gasifiers is that the high temperature results in the destruction of heavy organic materials, light aromatics, and hydrocarbons including methane. Carbon conversions of low-reactivity high-rank coals and petroleum coke can exceed 99%, and most entrained flow gasifiers are designed for high rank fuels. The inorganic components are melted in the high temperature environment and flow out of the gasifier as liquid slag. The elevated temperature results in lower cold gas efficiencies (CGE) with entrained flow gasifiers, and most gasifiers average near 80% CGE. Entrained flow gasifiers are commercially available today and are backed by large companies such as Shell, GE, Siemens, and Phillips 66.

Fluid bed gasifiers operate with a fluidized bed of unconverted carbon and inorganic particles, typically sized to approximately 0.075 in. Solids residence times are typically 0.5 to 2 minutes. The temperature of the system is kept below the ash melting point, usually below 1600°F, and the systems typically operate at elevated pressure.

These systems are well suited for high reactivity, low rank fuels. Fluid beds can produce high levels of tars and organic materials, can achieve cold gas efficiencies of 90%, and carbon conversions over 95%. Commercial systems include the High Temperature Winkler offered by ThyssenKrupp and the U-Gas technology developed by the Gas Technology Institute and licensed to Synthesis Energy Systems.

Fixed bed gasifiers operate with a bed of larger coal particles, ranging from 0.5 to 2 inches in size. Both slagging and non-slagging fixed beds have been develped. Depending of the operating condition, fixed beds can produce high levels of tars, organics, and methane. The low temperature and relatively simple operation of non-slagging systems can leads to high cold gas efficiencies and low cost operation. The Lurgi gasifier offered by Air Liquid is currently deployed commercially at Sasol in South Africa and the Great Plains Synfuels Plant in North Dakota.

For the purposes of this test program, syngas was produced from a small pilot scale entrained flow gasifier and fluid bed gasifier. These systems were chosen because they are commercially available and tend to produce less methane than fixed bed gasifiers. While methane is not expected to harm membrane materials, elevated levels in syngas reduces the overall capture efficiency of an IGCC facility.

Coal gasification has taken on a renewed interest in the last five years because of the rising price of oil and pending carbon legislation. Falling natural gas prices over the last two years has made recent deployment and financing of gasification technologies more difficult. Historically, studies have shown that if carbon capture and storage is required, IGCC plants will have a significant cost advantage over conventional pulverized coal boilers with retrofit carbon capture (7.8). However, the most recent

studies to come out have stated that the costs may be similar between the two technologies, especially when considering ultrasupercritical boilers (9,10,11). At this point it is difficult to accurately estimate the cost of carbon capture from a pulverized coal power plant because no commercially available technology exists. Therefore, these studies must be re-evaluated once technologies are commercially available.

2.4 Gas Cleanup Fundamentals

Conventionally, cold gas cleanup methods have been employed to remove contaminants from coal gasification syngas streams. Methods such as Rectisol or Selexol are commercially available and do a very good job removing contaminants, but are also very costly from a capital and operational perspective. Significant economic benefits can be realized by utilizing warm or hot gas cleaning techniques. The DOE has stated thermal efficiency increases of 8% over conventional techniques can be realized by integrating warm gas cleanup technologies (7) into IGCC plants. Hydrogen separation membranes typically operate at warm gas cleanup temperatures, so they are a good match for IGCC projects looking to employ warm gas cleanup and carbon capture.

Work has been performed at the Energy & Environmental Research Center (EERC) in conjunction with the DOE to develop methods to remove contaminants from syngas to levels suitable for a hydrogen separation membrane. The warm gas cleanup train is capable of removing sulfur, particulate, chlorine, and trace metals including mercury at temperatures above 400°F. All of the technologies utilized are considered either commercial or near commercial in development. One such test involved gasification of Texas lignite in the EERC's Transport Reactor Demonstration Unit

(TRDU), with a slipstream of gas being sent to the warm gas cleanup train (12). Figure 2.5 shows the test setup and a sampling of the results from the test.

Sulfur in the form of hydrogen sulfide and carbonyl sulfide was removed in a transport-style gas solid contactor at temperatures between 600 and 1000°F. The system was capable of reducing sulfur to single-digit ppm levels in the syngas. Particulate was removed in a hot gas filter vessel that provided near absolute filtration using candle filters. Mercury and trace elements were removed with a proprietary sorbent. A high temperature water gas shift catalyst significantly increased the hydrogen concentration in the gas stream while reducing CO. A sulfur polishing bed removed hydrogen sulfide to concentrations below 0.2 ppm. A chlorine guard bed was used in front of the low temperature water gas shift catalyst to prevent poisoning. Carbon monoxide was reduced to 0.1% in a low temperature shift bed, and hydrogen was maximized. If the system were run under oxygen-fired conditions, the resulting syngas would have had combined H_2 and CO_2 levels greater than 90%. After passing through the cleanup train, the syngas was ready for hydrogen and CO_2 separation in a hydrogen separation membrane.

2.5 Conventional Hydrogen Separation Processes

The most commonly employed method used today for hydrogen separation is a process called pressure swing adsorption (PSA). PSA technology is based on an adsorbent bed that captures the impurities in the syngas stream at higher pressure and then releases the impurities at low pressure. Multiple beds are utilized simultaneously so that a continuous stream of hydrogen may be produced. This technology can produce hydrogen with purity greater than 99.9% (13). Temperature swing adsorption is a variation on PSA, but is not widely used due to the relatively long time it takes to heat

and cool sorbents. Electrical swing adsorption has been proposed as well, but is currently in the development stage. Cryogenic processes also exist to purify hydrogen, but require extremely low temperatures and are therefore very expensive (14).

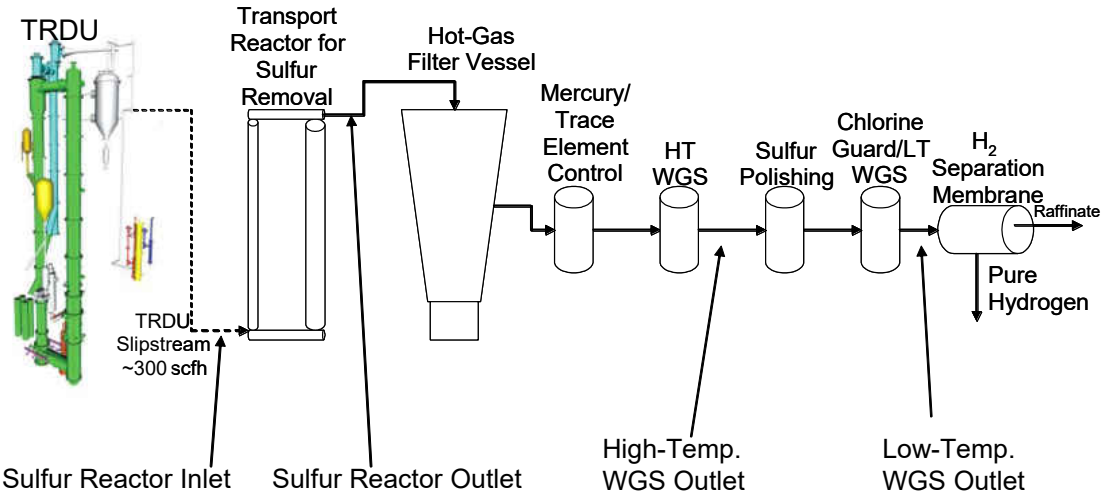

Component	Concentration	Unit
H_2	8.3	%
CO	4.8	%
CO_2	15.0	%
N_2	69.1	%
CH_4	1.7	%
H_2S	3455	ppm
H_2/CO	1.7	ratio

Component	Concentration	Unit
H_2	7.7	%
CO	4.4	%
CO_2	13.8	%
N_2	72.3	%
CH_4	1.5	%
H_2S	4.4	ppm
H_2/CO	1.8	ratio

Component	Concentration	Unit
H_2	10.9	%
CO	1.0	%
CO_2	16.7	%
N_2	68.6	%
CH_4	1.5	%
H_2S	3.0	ppm
H_2/CO	11.0	ratio

Component	Concentration	Unit
H_2	13.3	%
CO	0.1	%
CO_2	18.4	%
N_2	65.5	%
CH_4	1.6	%
H_2S	0	ppm
H_2/CO	98.3	ratio

Figure 2.5. Gasification and Gas Cleanup Process Diagram with Test Results (12).

2.6 Principles of Hydrogen Separation Membranes

Most hydrogen separation membranes operate on the principle that hydrogen selectively penetrates through the membrane due to the inherent properties of the material. The mechanism for hydrogen penetration through the membrane depends on the type of membrane in question. Most membranes rely on the partial pressure of hydrogen in the feed stream as the driving force for permeation, which is balanced with the partial pressure of hydrogen in the permeate stream. Kluiters has categorized membranes into five main types that are commercial or appear to have commercial promise: dense polymer, microporous ceramic, porous carbon, dense metallic, and dense

ceramic (1). Each membrane type has advantages and disadvantages, and research organizations and companies continue to work to develop better versions of each (15). Figure 2.6 illustrates the basic operating principles of hydrogen separation membranes for use in coal derived syngas (12). This figure shows a dense metallic tubular membrane, but plate and frame style membranes have also been developed. The "syngas in" stream refers to the feed gas into the membrane module. The permeate stream has permeated through the membrane wall, and in this case is made up of mostly hydrogen. The raffinate stream is what is left of the feed stream once the permeate is separated. A sweep gas such as nitrogen may be used on the permeate side to lower the partial pressure of hydrogen and enable more hydrogen to permeate the membrane.

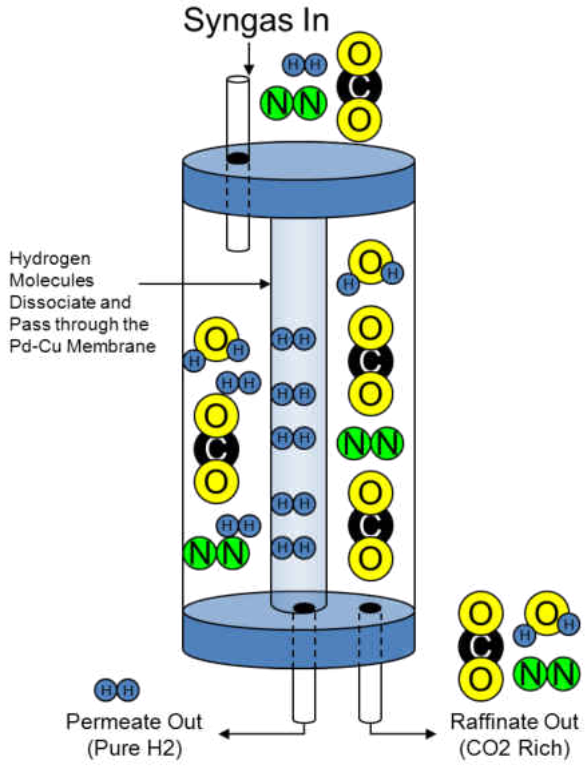

Figure 2.6. Illustration of the Operating Principle of Hydrogen Separation Membranes (12).

The mechanisms for hydrogen transport through each membrane type are different. However, the performance of each membrane is gauged by two main principles: hydrogen selectivity and hydrogen flux. Hydrogen selectivity is defined by Equation 2.1 (1):

$$\alpha_{A/B} = \frac{y_A / y_B}{x_A / x_B} \qquad [2.1]$$

where α is the selectivity factor of component A over component B in the mixture, y_A and y_B are the fractions of those components in the permeate, and x_A and x_B are the fractions of those components in the feed. Components A and B are usually defined so that a higher the selectivity factor refers to better membrane performance. A selectivity factor of 1 means there is no component separation.

Hydrogen flux is a measure of the rate of permeation of hydrogen through a membrane wall. The general equation for flux is shown by Equation 2.2 (1, 14):

$$J_x = \frac{P(p_{x,feed}^n - p_{x,permeate}^n)}{t} \qquad [2.2]$$

where J_x represents the flux of species x, P_x represents the permeability of species x, $p_{x,feed}$ and $p_{x,permeate}$ are the partial pressures of species x in the feed and permeate streams, t is the membrane thickness, and n is the partial pressure exponent. The value of n is usually between 0.5 and 2, and like the value of P, depends on the transport mechanism assumed. When n = 1, the equation is called Fick's law. For hydrogen transport through a metal membrane, the value of n is usually 0.5, and the equation reduces to what is referred to as Sievert's law. Sieverts law is a useful way of measuring membrane performance because it takes into account the membrane thickness and the partial pressure of hydrogen on each side of the membrane.

Since most membranes operate on a partial pressure differential, there will always be some hydrogen left behind in the raffinate stream. Therefore, an additional measurement of performance is the recovery or yield as shown by Equation 2.3 (1):

$$S = \frac{q_p}{q_f} \qquad [2.3]$$

where S is the yield, qp is the permeate flow, and qf is the feed flow. There are numerous other ways to quantify the yield, including calculating the volume reduction in the raffinate or the percentage hydrogen recovery from the feed.

The five basic types of membranes mentioned earlier each have inherent advantages and disadvantages, depending on the desired operating conditions and necessary product specifications. With data presented by Kluiters (1) and modified with Adhikari (14) and Ockwig (16), Table 2.1 compares in general the relative operational performance of these five membrane types. Typical operational temperature will vary by specific membrane type, but it can be seen that the dense polymer membranes are only applicable at low temperature. Dense ceramic and dense metallic membranes have the highest hydrogen selectivity and hydrogen flux is highest with dense metallic or micro-porous ceramic membranes. While dense metallic membranes seem to have the best performance relative to hydrogen, they are also very susceptible to poisoning from many compounds found in syngas, and metal alloys can be very expensive. Dense ceramic membranes also have high potential for commercial applications. They are less susceptible to poisoning than metallic membranes, and depending on the material can be significantly less inexpensive. Development work is underway with each of these membrane types to increase the resistance to poisoning and reduce cost.

Table 2.1. Properties of Five Hydrogen Selective Membranes (1,14,16)

	Dense Polymer	Micro porous ceramic	Dense ceramic	Porous carbon	Dense Metallic
Temperature Range	<100 °C	200-600°C	600-900°C	500-900°C	300-600°C
H_2 Selectivity	low	moderate	very high	Low	very high
H_2 Flux	low	high	moderate	moderate	High
Known Poisoning Issues	HCl, SOx, CO_2		H_2S	Organics	H_2S, HCl, CO
Example Materials	Polymers	Silica, alumina, zirconia, titania, zeolites	$SrCeO_{3-\delta}$, $BaCeO_{3-\delta}$	Carbon	Palladium Alloys, Pd-Cu, Pd-Au
Transport Mechanism	Solution/ diffusion	Molecular sieving	Solution/ diffusion	Surface diffusion, molecular sieving	Solution/ diffusion

2.6.1 Hydrogen Transport Mechanisms

For porous membranes, there are four types of diffusion mechanisms that can effect hydrogen separation. They are Knudsen diffusion, surface diffusion, capillary condensation, and molecular sieving. Knudsen diffusion occurs when the Knudsen number, Kn defined by Equation 2.4, is large (16).

$$Kn = \frac{\lambda}{L} \qquad [2.4]$$

The variable λ in equation D represents the mean free path of the gas molecules, and L is the pore radius. At Knudsen numbers larger than 10, Knudsen diffusion becomes significant. Surface diffusion refers to gas molecules that are absorbed on the pore wall and migrate along the surface to the other side. Surface and Knudsen diffusion can occur simultaneously. Capillary condensation occurs if a partially condensed phase fills the pores and does not let other molecules penetrate. Molecular sieving occurs when the pores are so small that only the smaller molecules can fit through. Selectivity toward

hydrogen is greatest with molecular sieving and is least with the Knudsen diffusion mechanism (1, 16).

This work focuses on palladium-based dense metallic membranes, which rely on a solution/diffusion mechanism to transport hydrogen. The solution/diffusion mechanism is somewhat more complex than the porous diffusion mechanisms, although relatively straightforward in nature. Ockwig (16) has presented a seven step mechanism in which 1) the hydrogen mixture moves to the surface of the membrane; 2) dissociation of the H_2 molecules into H+ ions and electrons; 3) adsorption of the ions into the membrane bulk; 4) diffusion of the H+ ions through the membrane 5) desorption of the H+ ions from the membrane; 6) recombination of the H+ ions and electrons back to H_2 molecules and 7) diffusion of the H_2 from the surface of the membrane. In the case of metal membranes, only hydrogen undergoes the solution/diffusion mechanism, and therefore the membranes are considered 100% selective to hydrogen.

Figure 2.7 illustrates the mechanism of separation in a 7 step process that depicts hydrogen transport through dense metallic membranes as atoms. The mechanism is very similar to that proposed by Ockwig in the case of ion transport membranes. Key points for the mechanism of separation are the catalytic dissociation of hydrogen on the membrane surface and absorbtion of H atoms into the alloy structure. Both of these key steps can be hindered by the presence of sulfur on the surface of the membrane, reducing the overall flux rate. Sulfur could also be present on the reassociation side of the membrane if a significant leak in the material were ever present during operations. Diffusion of the hydrogen away from the surface is also an important point because under normal operating conditions, the gas is pure hydrogen and therefore the partial pressure

of hydrogen can be high. In IGCC cases, a sweep gas of nitrogen would be employed to improve the overall efficiency of the separation, temper the combustion flame in the gas turbine, and provide additional mass to drive the turbine.

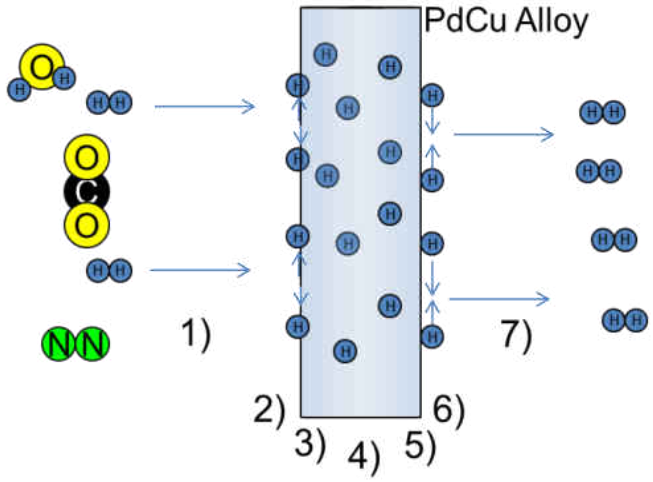

1. Diffusion of H2 to membrane surface
2. Adsorption and catalytic dissociation of H2 into H atoms
3. Absorption of H atoms into the alloy structure
4. "Hopping" or "Jumping" of H atoms through interstitial sites of FCC or B2 PdCu lattice
5. Reassociation of the atoms to molecules
6. Desorption of H2 from the membrane surface.
7. Diffusion of hydrogen away from the membrane surface

Figure 2.7. Seven Step Mechanism of Hydrogen Separation through Dense Metallic Membranes.

2.6.2 Impact of Pd-Cu Crystalline Structure and Sulfur on Membrane Performance

Dense metallic Pd-Cu based membranes are of great interest to researchers because they hold properties of high selectivity, high flux rates, and have shown the potential to have resistance to sulfur poisoning (17,18). The nature of the Pd-Cu structure is of great importance when it comes to the permeation of hydrogen through the membrane. Pd-Cu either forms a body centered cubic (bcc or b2) structure, or a face

centered cubic (fcc) structure. Figure 2.8 depicts the crystalline structure of each. The bcc structure contains copper atoms at each of the eight corners of the cubic matrix, with a palladium atom at the center of the cube. The fcc structure also contains eight copper atoms at the corners, but also a palladium atom at the center of each face of the cube.

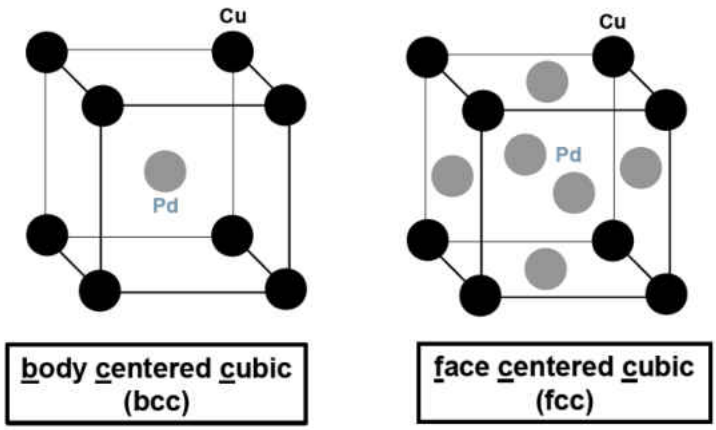

Figure 2.8. Palladium-Copper Crystalline Structure in bcc and fcc Orientations (17).

As shown in Figure 2.9, the type of crystalline structure formed depends on both the composition and temperature of the material (17,19,20). The bcc cubic structure is encountered in the widest temperature range at a concentration of 53wt% Pd and 47wt% Cu. It is for this reason that many studies have evaluated this particular composition. Studies also indicate that the bcc structure has higher hydrogen permeability, but lower resistance to sulfur than the fcc structure. Rothenberger et. al. reported that performance degradations of an order of magnitude were observed when exposing bcc cubic structures to 1000 ppm H2S, but performance degradations of less than 20% were observed when exposing fcc-crystaline phase materials to the same conditions (17).

The diffusion of hydrogen through a palladium membrane or a palladium copper alloy has been described in detail by a number of authors (21, 22, 23). Work by Sholl et.

al. has attempted to understand and predict the energies required to for hydrogen atoms to diffuse through Pd-Cu lattices. Figure 2.10 depicts possible positions for H atoms to exist in bcc Pd-Cu. Sholl described the movements to and from tetrahedral sites and determined the activation energy required for each of these movements. Understanding of the first principles of hydrogen diffusion through metal materials can lead to breakthroughs in development of new materials and crystal arrangements. Sholl has also studied the impact of ternary alloys on hydrogen diffusion (24) and has undertaken a number of studies involving novel metals and amorphous materials for hydrogen separation (25, 26, 27).

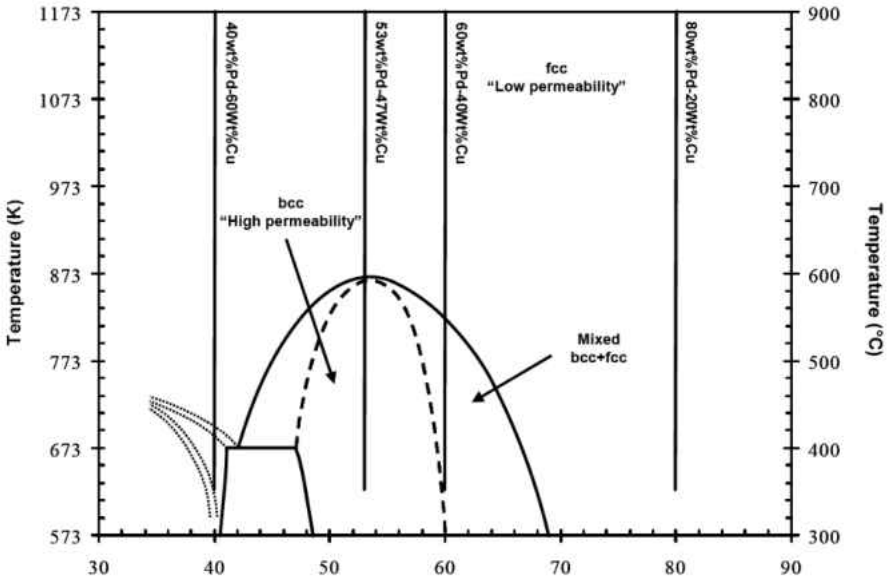

Figure 2.9. Palladium-Copper Phase Diagram (17,19,20).

Sulfur poisoning is known to impact the flux rate of hydrogen through Pd and Pd-Cu alloys. Obrien (28) theorized that hydrogen transport across a membrane is impacted by sulfur poisoning in two manners: 1) by producing a thin sulfide film on the surface of the membrane with low hydrogen permeability and 2) by blocking Pd from catalyzing the hydrogen dissociation reaction and therefore slowing the rate of dissociation. Obrien's

permeation experiments and H_2-D_2 experiments showed that both mechanisms indeed impact hydrogen flux rates through Pd-Cu membranes. The study also showed that at elevated temperature (900 K), H_2S has no impact on hydrogen permeation through $Pd_{47}Cu_{53}$ alloys.

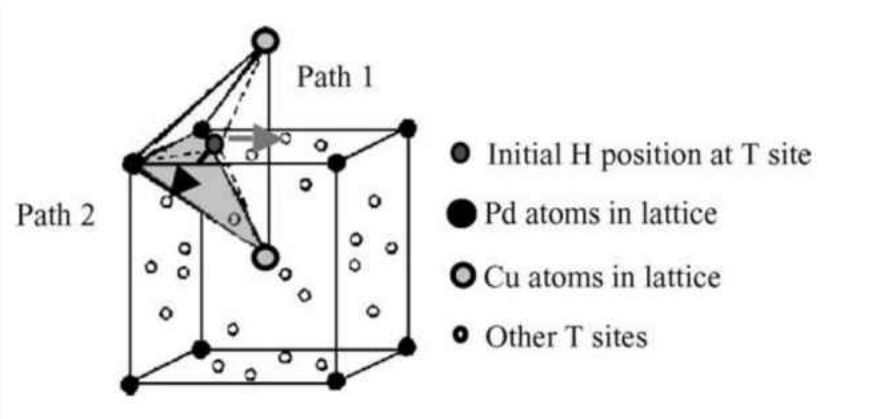

Figure 2.10. Possible Pathways for H Motion in bcc Pd-Cu (23).

Studies by Gabitto and Tsouris (29) concluded that $Pd_{60}Cu_{40}$ alloys represent the best combination of high hydrogen flux and sulfur resistance. Studies by Ma et al have showed that sulfur poisoning of a thin membrane of fcc $Pd_{81}Cu_{19}$ was completely reversible if the sulfur was exposed to the membrane above 450°C (30). If the sulfur was exposed at 400°C, the original membrane performance could not be reestablished. Yang et. al. evaluated the performance of a $Pd_{60}Cu_{40}$ membrane covered with a thin coating of nickel to promote resistance to H_2S (31). The results of this study indicated that the H_2S poisoning was reversible, and that the membrane shows little performance degradation when operated above 573 K.

2.7 Membrane Development Activities

The US Department of Energy has developed a set of performance goals based on the primary metrics of hydrogen separation membranes. These goals are listed in Table

2.2 (32). In order to meet these goals, membranes will have to be developed that have high hydrogen flux and selectivity, and are durable to the contaminants found in coal derived syngas.

Table 2.2. DOE Technical Targets for Hydrogen Separation Membranes (32)

Performance Criteria	Units	2010 Target	2015 Target
Flux (100 psi dp basis)	ft3/hour/ft2	200	300
Temperature	ºC	300–600	250–500
S tolerance	ppmv	20	>100
Cost	$/ft2	100	<100
WGS activity	-	Yes	Yes
ΔP Operating capability	psi	Up to 400	Up to 800 to 1,000
Carbon monoxide tolerance	-	Yes	Yes
Hydrogen purity	%	99.5%	99.99%
Stability/durability	Years	3	5

Many companies and organizations are actively researching new hydrogen separation materials that have the potential to meet the performance goals as laid out by the US Department of Energy. This section describes several membranes currently under development and discusses the challenges and opportunities of each. Comparisons are also made to the current DOE targets.

2.7.1 U.S. Department of Energy National Energy Technology Laboratory (NETL)

The U.S. DOE through the NETL has developed a comprehensive program on hydrogen membrane research. NETL is performing in-house laboratory scale research on hydrogen separation materials and is mainly focused on metallic membranes. NETL is also co-funding basic membrane research activities with numerous other companies and organizations including (but not limited to) Argonne National Laboratory, REB Research and Consulting, Eltron Research, Southwest Research Institute, University of North Dakota Energy & Environmental Research Center, Ohio State University, Media and Process Technology, Inc; Praxair, Inc.; United Technologies Research Center; Western

Research Institute; Worcester Polytechnic Institute; Lehigh University; and Carnegie Mellon University. Most of the companies listed above are performing basic research on material types and testing these materials in the laboratory under simulated syngas conditions. Of the membrane developers listed above, the membranes with the most potential were shown to be provided by Eltron Research, Praxair, United Technologies Research Center (33).

In-house research at NETL is focused on membrane screening test units that can quickly establish capacity for hydrogen separation expose the material to simulated syngas. One of the reactor systems is focused on sulfur laden gas streams, and can evaluate the membrane's performance with exposure to sulfur-laden gasses. Testing at NETL has shown that a Pd foil can withstand some exposure to H_2S, but flux is reduced quickly and a slow deactivation is noted during the test period. By contrast, exposure of a Pd-Cu alloy to the same syngas shows almost immediate, irreversible deactivation (34). A wide variety of additional alloys continues to be evaluated at NETL to determine which perform the best in the presence of sulfur. Some alloys have been identified through these studies that show almost no performance loss in the presence of sulfur (35).

2.7.2 Eltron Research

Eltron Research has developed a non-palladium based metallic membrane that is comprised of three layers: 1) a hydrogen dissociation catalyst 2) metal transport membrane 3) hydrogen desorption catalyst (36). This membrane may be more resistant to common poisons found in coal derived syngas than a single layer palladium based membrane because the transport membrane itself is not exposed to the syngas. Eltron has not disclosed the metal used in the membrane, but has stated that it is not palladium.

With reported flux measurements of >400scfh/ft^2 and ultra-pure hydrogen product, Eltron's membrane performs as good as any other currently under commercial development.

Eltron has very recently tested its membrane on coal-derived syngas, but the results are not yet available. Eltron's development activities appear to be focused on a FutureGen type facility, where the membrane is utilized in conjunction with a coal gasification plant and a reasonable level of gas cleanup is achieved. Eltron has stated that a thermal efficiency of 33.6% can be achieved using the membrane technology with RTI's warm gas cleaning technique, compared to 27.4% efficiency with a standard Selexol unit equipped with CO_2 capture (37).

According to Eltron, the current cost of the membrane is less than $200/ft^2, which may be slightly behind current DOE performance goals (37). The membrane is expected to be resistant to sulfur up to 20 ppm. Eltron is looking to perform scale-up activities to coal derived syngas in the near future.

2.7.3 Praxair

Praxair has worked with DOE and RTI to develop an integrated ceramic and metal membrane, where the metal portion is made up of Pd-Au. These types of membranes are often referred to as "cermet" membranes, and tend to offer the high flux benefits of metallic membranes, and additional corrosion resistance is provided by the ceramic component. Flux measurements are based on the rate of transport through the metal substrate. Praxair has achieved flux measurements >200scfh/ft^2 with this membrane technology (38). Membrane cost as of 2007 is very significant at $1500/ft^2. In an effort to reduce the overall cost of system implementation, Praxair is working

toward integrating this system with a water gas shift catalyst. Initial cost estimates with the integrated system show that the DOE cost targets can be met.

2.7.4 United Technologies Research Center (UTRC)

UTRC is developing a tri-metallic palladium-copper membrane that has high stability and resistance to syngas contaminants. The third metal has not been disclosed. This membrane has achieved a hydrogen flux of 256 scfh/ft^2 and has shown some tolerance to sulfur. Cost evaluations were not readily available. SEM evaluations of the membrane surface showed that approximately 5% of the membrane surface was made of up the desired ternary alloy, and most of the surface contained a binary alloy that essentially acted as a H_2 diffusion barrier. Work is underway to improve the surface area of the trimetallic alloy through some annealing and etching processes; as well as re-evaluating the production process for the alloy. With these improvements, the hydrogen flux is expected to improve significantly (39). To date, testing of the membrane has been limited to bottle-derived syngas.

2.7.5 Argonne National Laboratory

Argonne National Laboratory is working to develop a cermet membrane capable of separating hydrogen from a coal gasification stream. The membrane consists of 40-50% by volume of a metal or alloy, which is dispersed in a ceramic matrix. The metal increases the permeability of the ceramic by increasing the electron conductivity. Early results showed relatively low H_2 fluxes (40), but with the development of thinner materials, Argonne has achieved a hydrogen flux of greater than 100 scfh/ft^2 at 900° C (41). Work is currently underway to understand and quantify the impact of H_2S on cermet membranes and on the development of tubular membranes as opposed to flat

plates. Preliminary studies suggest that 400 ppm H_2S can be fed to the membrane with no performance degradation. Testing of the membrane to date has been limited to laboratory derived syngas from gas bottles.

2.7.6 Colorado School of Mines (CSM)

Development work at the Colorado School of Mines has focused on deposition of very thin (some less than 1micron thick) Pd alloys onto Pall AccuSep filters that are coated with a ZrO2 diffusion barrier. This combination gives the overall membrane the mechanical strength as provided by the filter and the potential for very high hydrogen flux rates. Also, the thinner materials are by nature cheaper because less precious metal is used in the construction. Alloy combinations tested to date include Pd-Cu, Pd-Ag, and Pd-Au. H_2 fluxes of over 337 scfh/ft^2 have been achieved at a differential pressure of 20 psi with a 0.93 micron thick membrane of pure Pd(42). The reported tests occurred on mixtures of H_2 and N2 gases. No testing was noted to have occurred on simulated syngas mixtures that may include CO, CO_2, or CH_4 or H_2S. Some literature exists stating the membrane has tolerance to CO and H_2S, but no specific testing examples were listed (43).

2.7.7 Worcester Polytechnic Institute (WPI)

WPI has produced a thin Pd Inconel membrane that has achieved a flux of 359 scfh/ft^2 with a differential pressure of 100 psi at 442°C (44). The flux test was demonstrated using mixed gases of H_2, CO, CO_2 and H_2O. The goal of the activity is to develop sulfur-tolerant Pd-Cu alloy membranes and to work on process intensification that will incorporate the water-gas shift reaction with the membrane technology. WPI continues to be very active in developing synthesis methods for the membrane (45, 46).

Recent developments have included the testing of Pd-Au membranes on coal derived syngas at the National Center for Carbon Capture in Wilsonville, AL. Three hydrogen separation membranes were exposed to coal derived syngas for several hundred hours (47). Contaminants including sulfur, arsenic, and sodium were found on the surface of membrane materials. Most of the analytical work reported focused on deposition found on some coupons placed ahead of the sulfur control beds. Some reduction in hydrogen permeance was noted through the testing, and the deactivation was only partially reversible.

2.7.8 Western Research Institute (WRI)

WRI is working on developing an integrated water gas shift catalyst and metallic membrane. The three module membrane situates a ceramic water gas shift catalyst and a vanadium hydrogen separation membrane into the same system (48). Testing to date has occurred on the back end of a pilot scale fluid bed gasifier with Wyoming coal. A gas cleanup train on the back end of the fluid bed system is capable of removing particulates, condensate, sulfur and mercury. Flux measurements with a driving force of 250 psi at 400°C were 52 scfh/ft^2. Additional testing is currently underway to understand the longevity of the material as it is exposed to trace levels of coal derived contaminants including sulfur.

2.7.9 Energy & Environmental Research Center (EERC)

The EERC is not actively involved in developing hydrogen separation membrane materials. The focus of the EERC has been on the demonstration of hydrogen separation membranes on coal derived syngas. Testing performed demonstrated that a pure stream of hydrogen could be produced from a Texas lignite derived syngas (12). Syngas was

produced in an EERC pilot scale gasifier, and a slipstream was purified through a warm gas cleanup train. The clean syngas was shifted to maximize hydrogen, and the hydrogen and CO_2 were then separated in a Pd-Cu membrane. The membrane was shown to operate for over 50 hours on coal derived syngas with no loss in activity. Neglecting leaks in the sample system, hydrogen with a purity of greater than 99.9% was produced. Future testing is planned at the EERC with this and other membranes over a duration of several hundred hours.

2.7.10 University of Southern California, Los Angeles

Studies by Liu et. al at the University of Southern California, Los Angeles, have focused on development of hydrogen separation membranes at scales that might be encountered in a commercial application. Tubes that are considered to be one bundle or section of a commercial scale system have been tested on simulated syngas. Long duration testing of over 10,000 hours in N_2/H_2 atmospheres with thermal cycling has occurred with Pd based membranes, and no performance degradation has been noted (49). Development of both carbon molecular sieve and Pd based membranes is on-going (50, 51).

2.7.11 Energy research Center of the Netherlands (ECN)

Li and others at the Energy research Center of the Netherlands (ECN) have built a Process Development Unit (PDU) to test the performance of hydrogen separation membranes at rates greater than the typical laboratory scale (52). Testing has focused in the inhibition of water gas shift components water and CO on the performance of palladium based membranes. A 20% drop in hydrogen permeation was observed when the membrane had been exposed to steam and CO at 673K over short duration testing, as

compared to the permeation rates in mixtures of H_2 and N_2 (53). This finding further emphasizes the need to test membranes on coal derived syngas.

2.7.12 Additional Research Activities

Many other research institutes and companies are developing hydrogen separation membranes that have achieved high flux rates. A patent search for "hydrogen membrane" in the title yielded 97 patents filed since 1976. The majority of the research to date is focused on materials development and testing of the membranes in laboratory conditions with bottle-derived syngas. More development work needs to be performed on promising membrane technologies with coal derived syngas in order to move the technology from the laboratory to the commercial market place.

2.8 Commercially Available Membranes

Most of the hydrogen separation membranes that are commercially available today are based on use in a refinery or steam-methane reforming plants. Air Liquide has a hydrogen separation membrane technology called MEDAL^{TM} that is commercially available and typically used in refinery applications for hydrotreating. The membrane is selective to other components than hydrogen, including H_2O, NH_3, and CO_2, and therefore would probably not be a good fit in a coal gasification (54).

Air Products offers a line of hydrogen recovery membranes referred to as PRISM® membrane systems (55). The PRISM membrane is intended for separations in hydrocracker and hydrotreater systems, or for CO purification in reformer gasses. The systems are low temperature and not intended for processing on coal derived syngas.

Wah-Chang offers small scale Pd-Cu membranes for commercial sale that are capable of producing an ultra-pure stream of hydrogen from syngas. The one drawback

of the membrane (like many Pd based membranes) is that is has a very low tolerance to H_2S and HCl, both of which are commonly found poisons in coal derived syngas.

2.9 Future Research Needs

Many good membrane candidates have been found through the DOE program. Additional laboratory-scale testing needs to occur to establish baseline durability and improvements in hydrogen flux. If operation with a coal gasification system is desired, long-term testing on coal-derived syngas must occur to understand the impacts of trace impurities over the life of the membranes. Additional materials development will also occur to find even better candidates for hydrogen separation, but some of today's materials are promising enough to move to pilot-scale testing.

The next step for several of these membranes is testing on a bench- or pilot-scale coal gasification unit, where the syngas is cleaned to levels that would mimic a typical commercial-scale gasification operation. Successful demonstration at the pilot scale would include demonstrating that high hydrogen flux can be maintained over long durations, little or no performance degradation due to impurities, high hydrogen recovery rates, and low operating cost. Membranes that successfully meet these criteria and the 2015 criteria listed by DOE may be candidates for scale-up to a demonstration-scale facility, followed by potential inclusion as a slipstream in an advanced gasification or IGCC-style facility.

CHAPTER 3

EQUIPMENT AND METHODOLOGY

To test the central hypothesis, a test system was built to enable the evaluation of three hydrogen separation membranes simultaneously on coal derived syngas that has passed through a warm-gas cleanup train. Two gasifiers at the EERC were used to produce the syngas for testing, and an existing warm gas cleanup train was used to remove contaminants from the syngas. Both the entrained flow gasifier (EFG) and high pressure fluid bed gasifier (HPFBG) were chosen for testing. Both types of systems are available commercially, and therefore each system warranted test time with hydrogen separation membranes. Commercially, the entrained flow gasifier is probably the best choice for inclusion in a test program because of the lower methane production, but the more efficient conversion of low rank fuels in a fluid bed warrants investigation. Additionally, the pressure rating of the EERC's HPFBG enables testing at higher pressure, enabling the membranes to achieve higher flux rates.

The overall process flow diagram for integrating the membranes with the gasification system is shown in Figure 3.1. This figure depicts the system with the HPFBG on-line with the warm gas cleanup train and hydrogen separation membranes. A hot-gas filter vessel was used for particulate control, and six fixed-bed reactors were used to remove syngas contaminants and maximize the hydrogen content of the syngas. The raffinate stream from the full-stream membrane was recycled back to the gasifiers to increase velocity and replace nitrogen purges. This section describes the construction of

the membrane test skid and the integration of the hydrogen separation membranes with the gasifiers and warm gas cleanup train in detail.

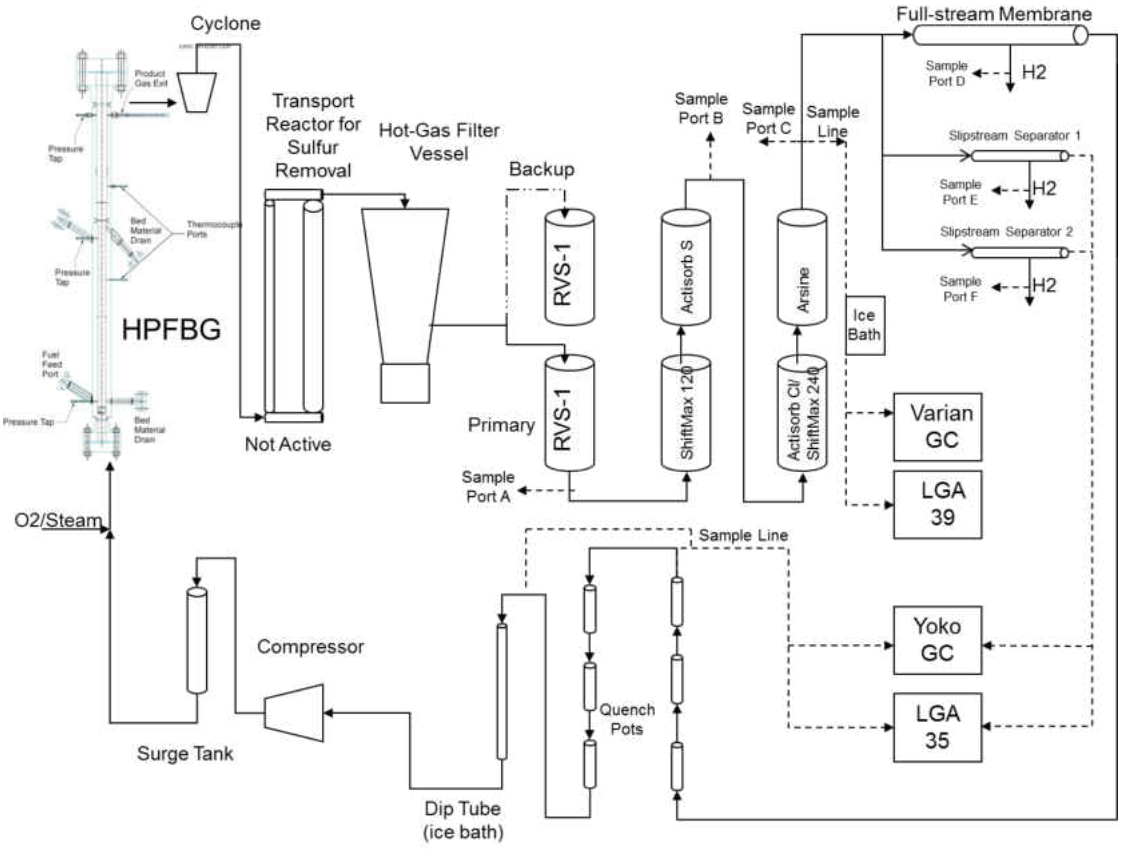

Figure 3.1. Process Flow Diagram.

3.1 Description of Hydrogen Separation Membranes

Three membranes were acquired for testing of the central thesis. One membrane was larger and was capable of handling all of the syngas from the gasifier. The other two were smaller and took a slipstream from the gasifier. The FS membrane is a palladium–copper membrane. High hydrogen flux rates and high hydrogen purities are anticipated with this membrane, but it is also expected to have a low tolerance for impurities. The full-stream (FS) membrane is capable of operation up to 600 psi. Slipstream separator 1 (SS1) membrane is a palladium–gold-based material that is also expected to produce

good flux rates and high purities. This membrane may have more resistance to impurities than a copper-based membrane. It is capable of operation up to 300 psi. Slipstream separator 2 (SS2) membrane is a palladium-copper membrane that is expected to have high flux and purity rates and has shown some resistance to sulfur. Sulfur has been shown to reduce performance during exposure, but performance returns to baseline when the sulfur is removed. This membrane is capable of operation up to 200 psi. Table 3.1 describes the membranes used in this program.

Table 3.1. Description of Membranes to be Tested

Membrane Designation	FS	SS1	SS2	DOE 2015 Goal
Materials of Construction	Pd–Cu	Pd–Au	Pd-Cu	N/A
Flow Range, scfh	200–400	<20	<20	N/A
Operating Temp, °C	200–300	350–600	350–600	250–500
ΔP Operating Capability, psi	600	300	200	800
CO Tolerance	Yes	Yes	Yes	Yes
S Tolerance, ppm	None	Not specified	78 ppm	>100
Hydrogen Purity, %	99.9+	99.9+	99.9+	99.99

3.2 Membrane Test Skid Design, Procurement, and Construction Activities

The objective was to build a system capable of testing three hydrogen separation membranes at the back end of the gasification system. Running three membranes simultaneously was deemed essential to maintain the cost-effectiveness of the project and stay within time constraints. To this end, a modular membrane test skid was designed to run the three membranes in a parallel flow fashion. An advanced data acquisition and control system was designed to facilitate the independent control of various operational parameters for each membrane and log data. Post-processing of data was conducted to elicit the detailed performance characteristics of each membrane.

Initial performance data for each of the membranes were furnished by their providers. Anticipated maximum ratings for the membranes can be seen in Table 3.2.

These ratings were used as a basis for the system design and component selection. The FS membrane was capable of taking the full gas stream from the gasifiers. SS1 and SS2 only required a small syngas slipstream for operation.

A detailed piping and instrumentation diagram (P&ID) was developed for simultaneous control of 3 membranes. Details of the P&ID can be seen in Figure 3.2. Each of the membranes' parallel pathways was designed to be double-valved to facilitate safe isolation, if needed, while other membranes were operating under pressure. Low cracking pressure check valves were used to prevent backflow of process gases and cross-contamination of samples. The system was designed such that the entire unit be transportable and subsystems must be modular. Redundancy of components was also promoted. Gases discharged from the membrane test system, identified as "To Vent" in Figure 3.2, are recombined prior going to the thermal oxidizer. The thermal oxidizer is a down-fired natural gas-fired combustor specifically designed to run with a high level of excess oxygen to promote complete syngas oxidation.

The membrane test skid is located in Room 120 of the EERC's National Center for Hydrogen Technology® (NCHT®) building. The area where the system is operated is rated as a Class I, Division 2, Group B hazardous area. Equipment for use in Class I hazardous locations, as defined in the NEC (National Electrical Code), is tested with respect to acceptability of operation in the presence of flammable and explosive mixtures of specific vapors and gases with air. Division 2 specifies that ignitable concentrations of flammable gases, vapors, or liquids are not likely to exist under normal operating conditions. Group B specifies atmospheres containing acrolein, butadiene, ethylene oxide, propylene oxide, hydrogen, or fuel and combustible process gases containing more

than 30% hydrogen by volume. Room 120 has a combustible and carbon monoxide gas detection system. A hydrogen flame detection system is also integrated into the gas detection system. In the event of a combustible or carbon monoxide gas alarm condition, the overhead 16’ x 16’ door is programmed to open, and the emergency exhaust system starts. The rooms air exchange rate is 17 air changes an hour under this alarm condition. In the event of the aforementioned alarm condition or a hydrogen flame detection alarm condition, procedures are enacted for a response by the fire department. The gasifier control program is also connected to the gas and flame detection system for monitoring of the room’s environmental conditions.

Table 3.2. Membrane Anticipated Maximum Ratings

Membrane	H_2 Flow, scfh	Syngas Flow, scfh	Temperature, °F	Pressure, psi
Full Stream (FS),	600	1200	650	600
Slipstream Separator 1 (SS1)	21	42	750	300
Slipstream Separator 2 (SS2)	10.5	21	900	200

3.3 Membrane Test System Description

The membrane test skid was designed to test three membranes in parallel using syngas generated by either the entrained flow gasifier (EFG) or the high-pressure FBG (HPFBG) at the EERC. Of critical importance to design of the test system is the ability to control the permeate (hydrogen that diffused through the membrane) and raffinate (remaining syngas after hydrogen separation) streams. Referring to the P&ID shown in Figure 3.2, each membrane subsystem has the following individual components:

- Syngas preheat temperature control
- Membrane temperature control
- Raffinate cooling
- Permeate cooling

- Raffinate flow control
- Raffinate flow measurement
- Permeate flow measurement
- Sweep and purge gas flow control
- Permeate and raffinate gas sample ports downstream of dry gas meters
- Data logging of flows, temperatures, pressures, and gas composition

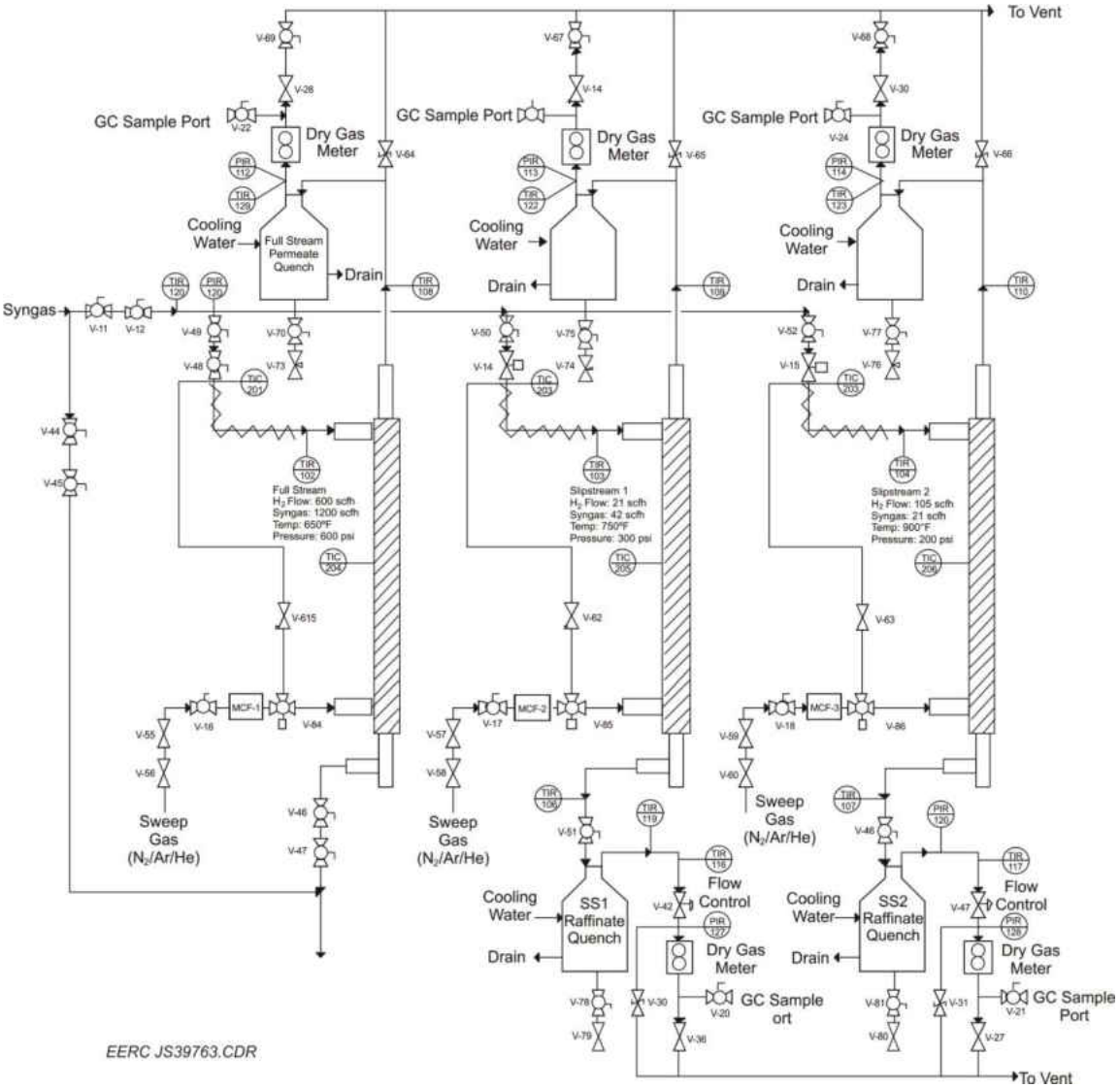

Figure 3.2. Membrane Test Skid P&ID.

The FS membrane has a maximum inlet flow capacity of 1200 scfh, which is approximately twice the capacity of the gasifiers used for these tests. The other two membranes are able to run as slipstreams off the main flow. In all cases, any of the three membrane subsystems can be isolated for maintenance or troubleshooting without disrupting ongoing tests with the other membranes.

The membrane test skid was fabricated and constructed entirely within the EERC, including welded pressurized quench vessels and the electrical and controls systems. All fittings, valves, and quench pots that are in contact with process gases are stainless steel. Swagelok tube fittings, instrumentation valves, and stainless steel tubing were used throughout. Tubing is of moderately heavy wall designation for the sizes used, for example, 0.500-in. diameter tubing has a wall thickness of 0.065- and 0.250-in. diameter tubing has a wall thickness of 0.049-in. All tubing is of fully annealed, drawn, 316/316L grade with a hardness of 80 HRB or less. All connections were inspected for scratches and other imperfections prior to final assembly. Assembly of the tubing and fittings followed procedures outlined in Swagelok's Tube Fitter's Manual. All fittings were leak-checked under pressure with a soap and water solution.

Each membrane has purge gas capability for flushing either side of the membrane during heat up and cool down. Purging residual hydrogen during the cool down period is critically important since hydrogen in contact with membrane media degrades the membrane's performance. Purge flow rates are controlled by mass flow controllers (MFC). Pressure is controlled by a pressure regulator upstream of the MFC. The purge system may also be used for permeate-side sweep gas control. Although various purge gases may be used, this testing was limited to nitrogen. SS1 and SS2 membranes are

small enough to be mounted on the skid. Figure 3.3 shows the 12 inch long SS1 membrane and heat trace. The FS membrane is mounted on a small cart near the test skid. A heater cable is spiral wound around each of the small membranes, SS1 and SS2.

Figure 3.3. SS1 Membrane Mounts and Heat Trace.

Quench pots, Figure 3.4, were of sufficient size to cool permeates and raffinates to approximately 12°C (54°F). Municipal water is used to externally cool quench pots that the gases pass through. The temperature of the cooling water was approximately 3°C (38°F) during the testing period. Cooling water flow is controlled by needle valve and monitored by a rotameter. Since water is present in the raffinate streams, double-valved drains are used on the bottom of each quench pot to facilitate removal of condensates. Although water should not be present in the permeate, permeate quench pots may be periodically checked for condensate, which would be an indicator that syngas is flowing through the membrane into the permeate stream. Because of tubing runs being

sufficiently long and of large enough diameter, the gases were rewarmed to room temperature prior to flow measurement at the dry gas meters.

Flow control valves are used on the raffinate streams to regulate the syngas flow rate past the membrane. In this way, the percent capture of hydrogen may be measured as a function of the flow across the membrane. The flow control valves (shown in Figure 3.5) are of a pneumatic fail-open design. The supply valves at the syngas inlet to the system are a pneumatic fail-closed type. If the operator initiates an emergency stop, power is lost, or compressed air pressure is lost, the pneumatically actuated supply valves close and the back-end flow control valves open, allowing the system to depressurize. The valve flow coefficient of the flow control valves is sufficient to provide a gradual depressurization, thereby eliminating the possibility of flooding the thermal oxidizer with raffinate gas. The valves employ a position encoder giving resulting closed-loop operation and accurate position data being fed back to the control computer.

Figure 3.4. Quench Pots.

Instrumentation consists of Type K thermocouples, pressure transmitters, dry gas meters, gas chromatographs, and laser gas analyzers. Yokogawa EJA series pressure transmitters use a silicon resonant sensor formed from monocrystal silicon, which has no hysteresis in pressure or temperature changes. The sensor minimizes overpressure, temperature change, and static pressure effects, thus offering long-term stability. Output signals are of the 4–20-mA analog type. A 24 bit analog-to-digital converter is employed in the data acquisition and control system employs, thereby yielding high resolution to the measurements.

Figure 3.5. Raffinate Flow Control.

DTM-200A diaphragm type, dry test meters were acquired from Elster American Meter. The DTM-200A meters were used to measure permeate and raffinate flows from SS1 and SS2 membranes. The dial face is calibrated for 1/10 cubic foot/revolution. Resolution is 1/100 cubic foot. A high-resolution optical encoder has been added to the meter's main shaft for real-time data acquisition. Capacity of the gas meter is 200 scfh,

and the maximum allowable operating pressure is 5 psig. A 1/3 psi check valve is employed downstream of the meter to prevent backfeeding of gas into the meter and contamination at the sample port. The check valves were checked for correct operation if gas meter readings were suspect. A thermocouple is used to measure internal gas temperature, and pressure is sensed by a Yokogawa pressure transmitter. The control program calculates pressure and temperature compensation of the flow. During testing, SS2 permeate was sufficiently low to produce no perceptible flow through the meter. As a result, a Gilibrator-2 was used to log flows on an hourly basis. Ten values were averaged for each of these readings. The low-flow Gilibrator-2 test cell, with a range of 1–250 cm^3/minute, was used.

An Elster American Meter AL-1000 diaphragm meter was used to measure FS raffinate flow. The capacity of the meter is 1000 scfh. This meter has a 100 psi maximum allowable operating pressure. An Elster American Meter AL-800 diaphragm meter was used to measure FS permeate flow. The capacity of the meter is 800 scfh. The meter has a maximum allowable operating pressure of 25 psi. Dial resolution of both meters is 5 cubic feet per revolution. The encoding resolution is one pulse per revolution or 5 cubic feet per pulse. Both meters are temperature-compensated; however, thermocouples and pressure transmitters are used to provide real-time standard flow rate calculations.

Control is done with National Instruments LabVIEW software, National Instruments Compact RIO hardware, and a personal computer. All control components, with the exception of the personal computer, are located in a purged cabinet that is mounted on the skid. The computer is located in the control room. Communication between the computer and the skid uses a conventional Ethernet protocol. The physical

network communications media is dedicated to the systems used for testing. Thermocouple and analog input modules have 24-bit resolution. The time span between saved data is a user-selectable parameter. For these tests, 30 seconds was used. Many of the saved data values were a time-weighted average to reduce the effects of spurious signals or non-uniform pulse train signals. The control cabinet, seen in Figure 3.6, is mounted to the skid and houses the Compact RIO controller, 24-volt power supply, pneumatic solenoid valves, mass flow controllers, fuse block, heater relays, main power switch, and an uninterruptable power supply. Watlow temperature controllers are panel-mounted to the front of the control cabinet. The temperature controllers are networked with the main control system to provide integrated temperature control and temperature ramping features. Gradual temperature ramping of the membrane assemblies is required to maintain uniform linear thermal expansion between the internal and external components of the membrane.

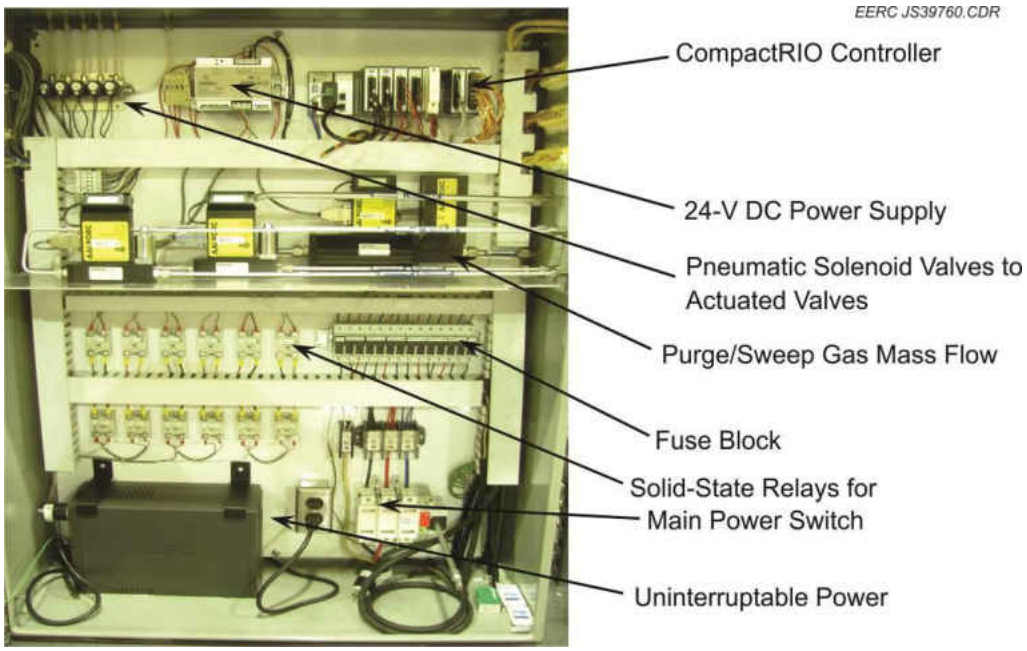

Figure 3.6. Control Cabinet.

The membrane test system uses a control system that was developed in-house using National Instruments LabVIEW software. The main control page can be seen in Figure 3.7. The layout is similar to the P&ID. All control and sensor data are accessible on the main page. The flow rate of purge gases is controlled by mass flow controllers. Three-way valves are used to direct the flow across the outface membrane face media or through the inner permeate portion of the membrane. The latter also enables a membrane to be tested using a sweep gas. Gas meter values shown on the main page are based on a time-weighted average.

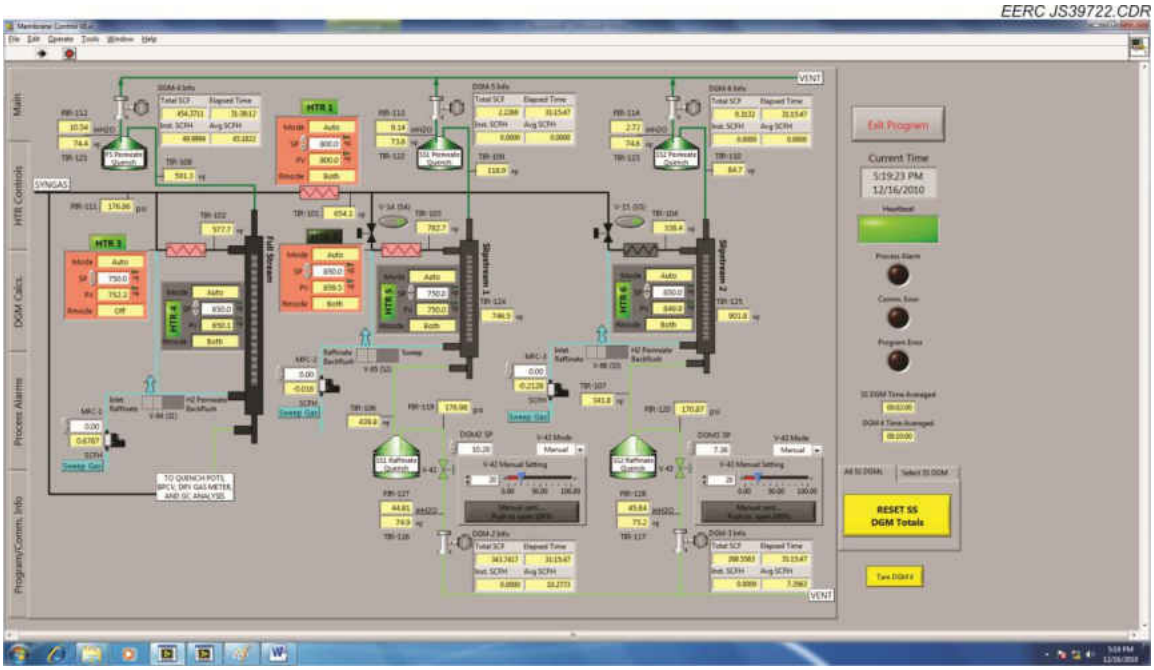

Figure 3.7. Control Program – Main Page.

Numerous acquisition points are set up with alarm conditions if their value lies outside a set range. The alarm condition is signaled by a flashing red background color for the displayed value. The low and high alarm limits are operator-defined values in the left columns. The current status is also displayed in the right columns. The LO or HI red

light indicator will enunciate an alarm condition, thereby giving the operator a quick indication why an alarm condition may exist.

Power to the heaters is controlled by Watlow EZ-Zone PM temperature controllers. The heater controllers use low-voltage signals to control solid-state power relays. Generally, the operator inputs temperature set points (SP) in a heater controller's block on the main page. The Watlow temperature controllers have built-in ramp functions. The control program utilizes the ramp function to allow the operator to specify the ramp rate. The operator may specify ramp up, ramp down, or both. By specifying a gas preheat temperature SP to be the same as the membrane temperature SP and using the same ramp rate, thermal stress in the membrane can be minimized. During heat up, the low flow rate of heated purge gas helps to heat up the internal portion of the membrane at the same rate as the external portion.

Syngas, permeates, SS1 raffinate, and SS2 raffinate gas compositions are monitored with two gas analyzers. Sample ports are located downstream of gas meters. Sample gas streams are manually switched via valves at the sample ports. Sample gas tubing from sample ports to the analyzers is polyethylene with no line longer than 50 feet. Sample gas transit times to the analyzers are estimated to be less than 1 minute, depending on the individual sample gas flow rate. The first analyzer is a laser gas analyzer (LGA) that is capable of detecting and measuring the concentration of eight gases at once: H_2, CO, CO_2, N_2, O_2, H_2S, CH_4, and total hydrocarbons. The LGA provides real-time feedback of the gas composition and is typically used to aid in the control of the system. The second analyzer used is a gas chromatograph (GC) equipped with two thermal conductivity (TC) detectors and a pulsed flame photometric detector for

ultralow sulfur detection. The first TC detector is dedicated solely to analyzing hydrogen and provides three hydrogen measurements for each 15-minute analysis cycle. The second detector analyzes the gas stream for CO, CO_2, N_2, O_2, H_2S, COS, CH_4, ethane, ethene, propane, and propene. One measurement is provided every 15 minutes for each of those gases. The third detector is capable of ultralow sulfur detection, down to 50 ppb. It provides three H_2S and COS measurements per 15-minute cycle. In a similar, but continuous and dedicated manner, the FS raffinate is analyzed by a separate set of paired analyzers, LGA and GC. Dräger tube and gas bag samples may be drawn from each of the sample ports on the membrane skid, as well as from several other ports on the gasifier system. Gas bag samples were analyzed by a GC as an additional check of gas compositions.

3.4 Entrained-flow Gasifier Description

Figure 3.8 shows a cross-sectional view of the EFG. The EFG is dry feed, down-fired system. The reactor tube is vertically housed in a pressure vessel approximately 24 in. in diameter and 7 ft in length. The EFG fires nominally 8 lb/hr of coal and produces up to 20 scfm of fuel gas. The maximum allowable working pressure is 300 psig. The reactor has the capability to run in oxygen- or air-blown mode. The supplemental electrical heating system is capable of reaching a nominal temperature of 1500°C (2732°F) and is separated into four independent zones so that a consistent temperature can be maintained throughout the length of the furnace. The radially spaced heating elements provide the initial heat for the centrally located alumina reactor tube, and refractory walls outside the heating elements provide insulation. Type S thermocouples are used to monitor and control the temperatures of the heating zones and reactor tube.

All of the gasification reactions occur inside the reactor tube, and slag is able to flow on the tube walls. Pressure inside the alumina reactor tube is balanced with a slight positive nitrogen pressure outside of the alumina reactor tube.

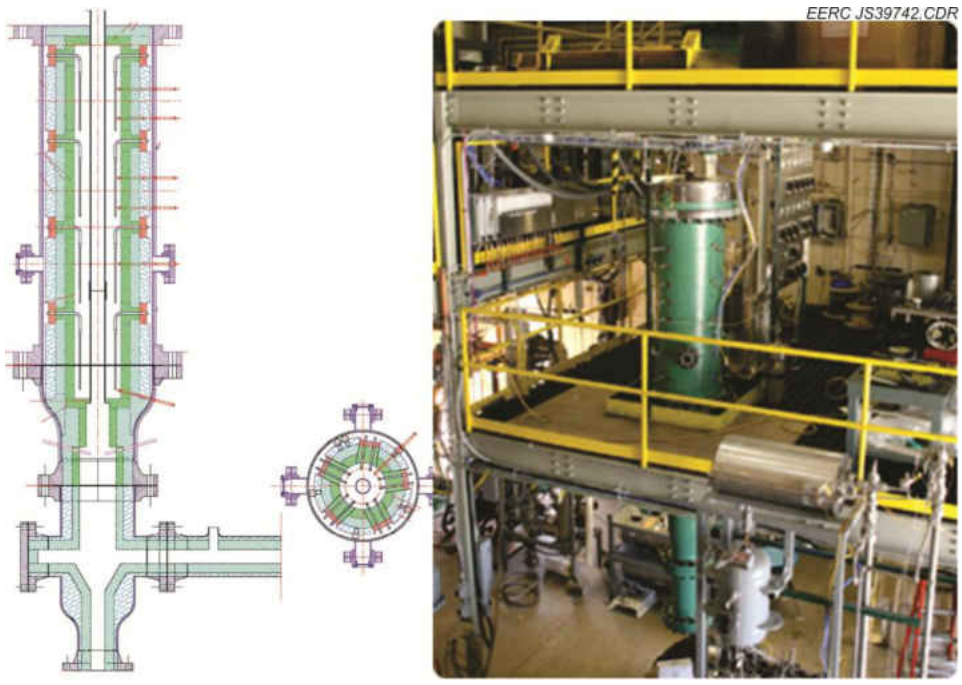

Figure 3.8. Entrained-flow Gasifier.

Pulverized coal is fed into the top of the furnace via a twin screw feeder and scale contained in a pressurized vessel. A lock hopper is in place that allows the system to be refilled while running, thereby facilitating continuous mode operation. Feed rates are calculated in real time. The feed system can be run in either volumetric mode or gravimetric mode. Nitrogen or syngas is used to convey the solid pulverized coal into the combustion zone.

Product gas exits the bottom of the furnace tube and enters a reducing section that houses a quench system capable of injecting water, syngas, or nitrogen as the quench fluid. The product gas then enters a cross, making a 90° turn, and exits the main unit on its way to the back end control devices. The main components in the syngas leaving the

reactor are typically equal parts of H_2, CO, CO_2, and N_2. Methane concentration is typically near zero during steady state operation. Slag, ash, and char drop through the cross and are collected in a refractory-lined slag trap. Fine particulate is able to flow with the gas through the 90° turn and is collected in a downstream filter.

3.5 High Pressure Fluid-bed Gasifier Description

The pilot-scale HPFBG (Figure 3.9) has been used to gasify a range of fuels, including lignite, subbituminous coal, petroleum coke, both untreated and treated biomass, and various mixes thereof. Syngas has been generated for use in Fischer–Tropsch synthesis, material corrosion testing, examination of coal pretreatment, and more. The HPFBG promises to reliably generate clean, high-pressure syngas directly from a variety of solid feeds for any number of potential applications. Syngas from the HPFBG typically contains H_2, CO, CO_2, N_2, and CH_4, with an H_2 to CO ratio of 2 to 1. Nitrogen and methane are typically near 5 %.

The HPFBG is capable of feeding up to 9.0 kg/hr (20 lb/hr) of pulverized coal or biomass at pressures up to 70 bar absolute (1000 psig). The externally heated bed is initially charged from an independent hopper with silica sand or, in the case of high-alkali fuels, an appropriate fluidization media. Independent mass flow controllers meter the flow of nitrogen, oxygen, steam, and recycled syngas into the bottom of the fluid bed. Various safety interlocks prevent the inadvertent flow of pure oxygen into the bed or of reverse flow into the coal feeder. Recycled syngas is injected several inches above the bottom distributor plate, which prevents direct combustion of syngas with oxygen entering at the bottom of the bed.

After a review of available alloys, Haynes 556® was selected as the material most suitable for fabrication of the high-temperature, high-pressure system as well as for all of the reactor nozzles and the cyclone. The reactor was designed with the capability to operate at the following maximum operating pressures:

- 70 bar (1000 psig) at operational temperatures of 843°C (1550°F)
- 45.8 bar (650 psig) at an operational temperature of 917°C (1650°F)
- 21.7 bar (300 psig) at an operational temperature of 1018°C (1800°F)

Figure 3.9. Lower Bed Section of the HPFBG.

The 2500-pound 316H stainless steel flanged connections at the top and bottom of the reactor are limited to somewhat lower maximum operating temperatures but do not greatly impact the operation of the gasifier, as they are generally cooler than the reactor bed itself. Sixteen thermocouple ports are spaced every 10 to13 cm (4 to 5 inches) up the bed to monitor for loss of fluidization, solids agglomeration, and localized combustion zones.

Coal is fed from a pressurized K-Tron® loss-in-weight feeder that provides online measurement of coal feed rate at pressures up to 70 bar (1000 psig). This system allows instantaneous measurement of the fuel feed rate to the gasification system. The feed system electronic controls are interfaced to a data acquisition system that allows for local or remote computer control of the fuel feed rate. Above the main feed hopper is the fuel charge hopper. The fuel charge hopper is manually charged with fuel through the top valve while at atmospheric pressure. It is then sealed and pressurized. Finally, the fuel feed material is transferred by gravity feed to the weigh hopper inside through the lower dual-valve system. The entire feed system pressure vessel is on a movable platform to allow easy transition from the HPFBG to the EFG.

Coal feed from the K-Tron system drops through a long section of vertical tubing and is then pushed quickly into the fluid bed through a downward-angled feed auger. Syngas exiting the fluid bed passes through a cyclone before flowing into a transport reactor that uses regenerable sorbent to remove sulfur from the syngas stream. The syngas then passes through a hot candle filter to remove fine particulate. The syngas, still hot and pressurized, is then routed through a series of water-cooled condensers to remove volatile organics and moisture. The clean, dry syngas exiting the condensers is then recycled through a compressor to the bottom of the HPFBG, and a portion is vented through a control valve to maintain system pressure. The syngas exiting the system passes through a Coriolis meter and a dry gas meter for mass balance. A slipstream of this depressurized, dry gas is also fed to a LGA and a GC for online analysis of major gas components and for low-level (ppb) analysis of sulfur species. In addition, operators can

periodically sample syngas from various points throughout the system using Dräger tubes for H_2S and other trace gases to verify low-level chromatograph data.

3.6 Warm-gas Conditioning and Sampling Port Description

The membrane test skid is installed at the back end of the warm syngas conditioning train. Referring to Figure 3.10, syngas flows from right to left, from the filter, through Fixed Beds 1–6, and then to the membranes. The particulate filter provides near absolute filtration. As part of this project, a series of six fixed beds were installed (Figure 36). Fixed Beds 1 and 2 are loaded with regenerable zinc-based RVS-1 sulfur sorbent. These are used in an alternating manner so that one can be regenerated while the other is in service. Sample Port A is located downstream of these two fixed beds to look for H_2S breakthrough using Dräger short-term measurement tubes.

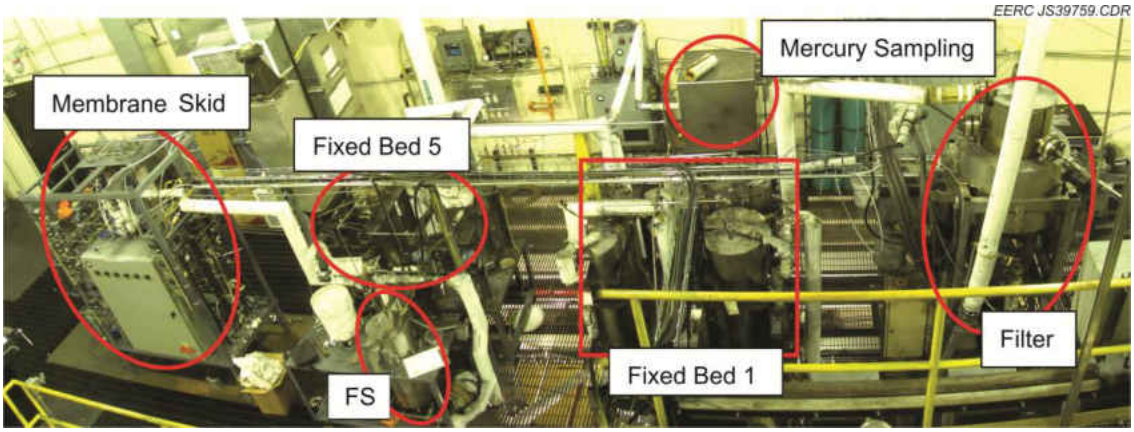

Figure 3.10. Warm-gas Conditioning Train.

Fixed Bed 3 contains iron-based ShiftMax 120 high-temperature shift catalyst used to increase the hydrogen concentration in the syngas. Fixed Bed 4 contains nonregenerable zinc-based Actisorb S2 sulfur sorbent and serves as a guard bed in the event either Fixed Bed 1 or Fixed Bed 2 has breakthrough or if the ShiftMax 120 in Fixed Bed 3 sheds sulfur. Sample Port B is located downstream of Fixed Bed 4 for drawing

samples through Dräger short-term measurement tubes and for continuous mercury monitoring.

Fixed Bed 5 contains two materials. The first is Actisorb Cl_2, a chlorine sorbent. The second layer in Fixed Bed 5 is a copper based low-temperature shift catalyst, ShiftMax 240. Fixed Bed 6 contains Arsine sorbent used for mercury control. Sample Port C is located downstream of Bed 6 and is used for Dräger tubes, trace metal sampling, and provides gas for the Varian GC and LGA-039 gas analyzers.

Figure 3.11 shows overall layout of the fixed beds and the membrane sampling plan for the test system. For the first test run, the Varian GC and the LGA 39 were connected to Sample Port C, but were switched with the Yokogawa GC and LGA 35 toward the end of the run and for the remainder of the test runs. The Varian GC and LGA 35 were then used for the remainder of the tests to sample the raffinate and permeate from each membrane. Sample Port A was used for taking Dräger tube samples at the bulk desulfurization (RVS-1) outlet to monitor for sulfur breakthrough. Table 3.3 shows the sampling plan for warm-gas cleanup and hydrogen separation membranes when tested on syngas from either gasifier.

3.7 Coal Properties

Antelope fuel from Wyoming was used for all of the testing in this program. The fuel was shipped in a large truckload and stored in a coal bunker. A small portion of the truckload was used for the testing. The preparation process for the fuel was different for each of the gasification systems.

Fuel for the EFG was first spread out and air-dried in the coal preparation facility. Then it was sized to approximately 10 mesh and dried in a rotary furnace. The fuel was

dried at 82°C (180°F) and for a residence time of 20–30 minutes to a moisture level of approximately 10%. Next, it was pulverized to 200 mesh before being loaded and sealed

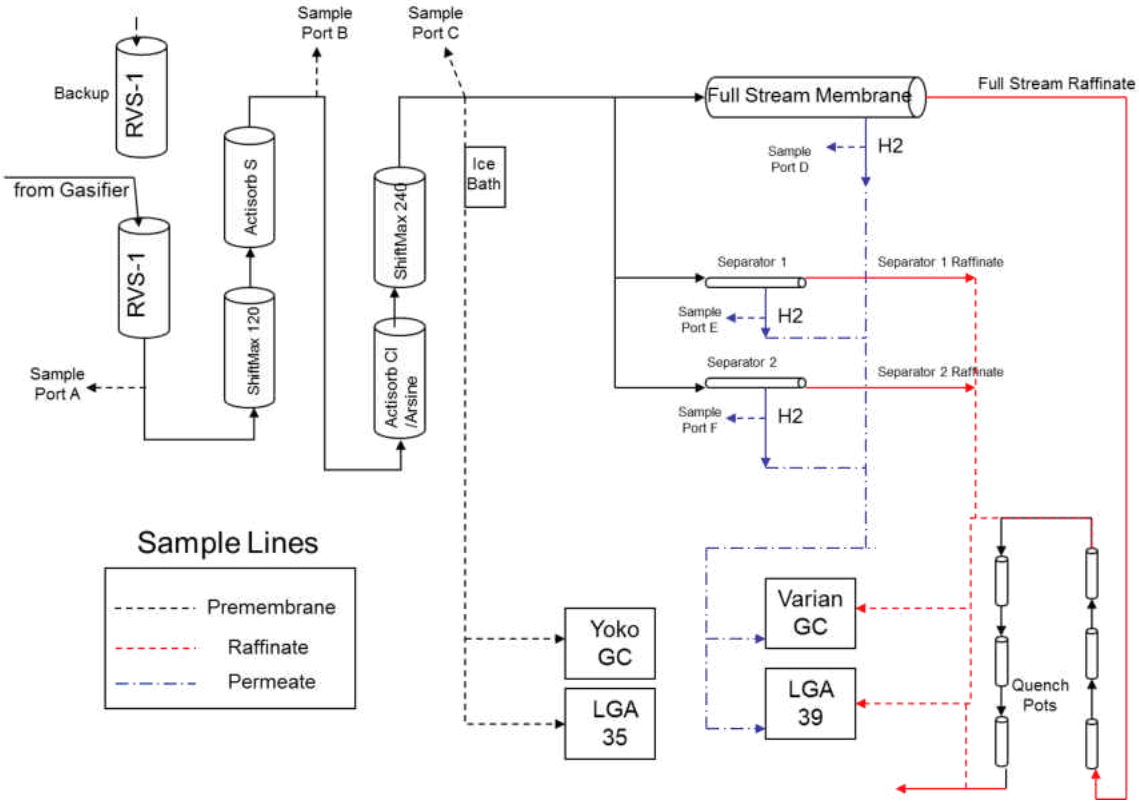

Figure 3.11. Membrane Sampling Plan.

Table 3.3. Warm-gas Cleanup and Membrane Sampling Plan

	Analyzers	Dräger Tubes					
Sample Port/Location	Bulk Gas Comp.	H_2S	NH_3	HCN	HCl	Hg	Gas Bag
Sample Port A	None	Hourly	None	None	None	None	None
Sample Port B	None	None	None	None	None	None	None
Sample Port C	Continuous	Hourly (cold)	1x/shift (hot)	1x/shift (hot)	Hourly (hot)	TBD	1x/shift
Sample Port D	Intermittent	1x/shift	None	None	None	None	1x/ shift
Sample Port E	Intermittent	1x/shift	None	None	None	None	1x/ shift
Sample Port F	Intermittent	1x/shift	None	None	None	None	1x/ shift
FS Raffinate	Continuous	1x/shift	1x/shift	1x/shift	1x/shift	1x/shift	1x/ day
SS1 Raffinate	Intermittent	1x/shift	1x/shift	1x/shift	1x/shift	1x/shift	1x/ day
SS2 Raffinate	Intermittent	1x/shift	1x/shift	1x/shift	1x/shift	1x/shift	1x/ day
LGA 35	Continuous	Continuous	N/A	N/A	N/A	N/A	N/A
LGA 39	Continuous	Continuous	N/A	N/A	N/A	N/A	N/A
Yokogawa	Continuous	Continuous	N/A	N/A	N/A	N/A	N/A
Varian	Continuous	Continuous	N/A	N/A	N/A	N/A	N/A

in lined drums. Moisture levels of less than 13% are required for the firing of subbituminous coals in the EFG. Coal for the FBG was spread out and air-dried to about 20% and then sized to 10 mesh. Table 3.4 shows the proximate, ultimate, and heating value analysis for coal fired on the EFG. The as-received analysis represents the moisture level as fired in the gasifier. The Antelope coal was relatively high in volatile matter which contributes to high reactivity. Ash and sulfur contents were both very low, and as-fired heating value was about 10,000 Btu/lb. Table 3.5 shows the analysis of fuel run on the FBG, which was very similar in composition. As expected, the moisture level was higher than the fuel run on the EFG, coming in at about 24%.

Table 3.4. Proximate/Ultimate Analysis of Antelope Coal Run on the EFG

	As-Det.	As-Recd.	Dry	Dry/Ash-Free
Proximate Analysis, wt%				
Moisture	5.19	12.59	N/A	N/A
Volatile Matter	37.48	34.56	39.53	42.66
Fixed Carbon, ind.	50.38	46.45	53.14	57.34
Ash	6.95	6.41	7.33	N/A
Ultimate Analysis, wt%				
Hydrogen	5.00	5.48	4.66	5.03
Carbon	65.68	60.56	69.28	74.76
Nitrogen	0.95	0.87	1.00	1.08
Sulfur	0.44	0.41	0.46	0.50
Oxygen, ind.	20.98	26.27	17.27	18.63
Ash	6.95	6.41	7.33	N/A
Heating Value, Btu/lb	11,180	10,308	11,792	12,725

As-received hydrogen not including hydrogen from moisture 4.07%.
As-received oxygen not including oxygen from moisture 15.09%.

Table 3.6 shows an elemental ash analysis of Antelope coal. Approximately two-thirds of the inorganics contained in the coal are Si, Al, and Ca. Sodium and potassium are known to be able to report to the vapor phase during gasification, and could potentially

reach membrane surfaces. Table 3.7 displays the concentration of trace components in Antelope coal. Mercury and chlorine are both very low for this fuel at 0.06 and 6 ppm respectively. Arsenic and selenium are of interest because they can remain in the vapor phase throughout the warm gas cleanup train and reach the hot gas filter vessel.

Table 3.5. Proximate/Ultimate Analysis of Antelope Coal Run on the HPFBG

	As-Det.	As-Recd.	Dry	Dry/Ash Free
Proximate Analysis, wt%				
Moisture	11.38	24.41	N/A	N/A
Volatile Matter	34.07	29.06	38.44	40.63
Fixed Carbon, ind.	49.77	42.45	56.16	59.37
Ash	4.79	4.08	5.40	N/A
Ultimate Analysis, wt%				
Hydrogen	5.44	6.28	4.70	4.97
Carbon	61.63	52.57	69.54	73.51
Nitrogen	4.79	4.08	5.40	5.71
Sulfur	0.35	0.30	0.39	0.42
Oxygen, ind.	23.01	32.69	14.57	15.40
Ash	4.79	4.08	5.40	N/A
Heating Value, Btu/lb	10,340	8820	11,668	12,334

As-received hydrogen not including hydrogen from moisture 3.55%.
As-received oxygen not including oxygen from moisture 11.01%.

Table 3.6 Elemental Ash Analysis of Antelope Coal

Ash Analysis, elemental oxide, wt%	
SiO_2	36.8
Al_2O_3	16.9
Fe_2O_3	6.1
TiO_2	1.0
P_2O_5	2.1
CaO	17.3
MgO	5.7
Na_2O	2.1
K_2O	0.5
SO_3	10.5
Total	99.0

Table 3.7 Trace Contaminant Analysis of Antelope Coal

Coal Analysis, dry basis, ppmw	
Cl	6.00
Hg	0.06
As	1.94
Be	0.29
Cd	0.08
Co	1.71
Cr	5.65
Mn	16.5
Ni	11.0
Pb	2.26
Sb	0.18
Se	1.72

CHAPTER 4

RESULTS OF TEST RUNS

Six weeks of testing were planned for exposing the membranes to coal-derived syngas. Table 4.1 shows the summary test plan for the 6 weeks of testing. Initial tests were planned to occur under lower-pressure conditions on the FBG and EFG. Higher-pressure tests were planned to be performed on the FBG later in the run. Tolerance to sulfur and other contaminants was planned for later in the testing because the poisoning may be irreversible. The goal for each of the runs was to expose all three of the membranes simultaneously to syngas for as long as possible. The slipstream membranes operate up to 200 and 300 psi, so more testing was planned at the lower pressure to maximize the exposure for each membrane to syngas. The test plan also called for operation at 500 psi on the FS membrane. This run condition was ultimately abandoned because of a leak that developed in the membrane.

Table 4.1. Overall Test Plan

Test Period	Gasifier	Fuel Source	Operating Pressure, psi	Sulfur Removal	Duration, hr
Week 1	HPFBG	PRB	200	<20 ppb	50–100
Week 2	EFG	PRB	200	<20 ppb	50–100
Week 3	EFG	PRB	200	<20 ppb	50–100
Week 4	HPFBG	PRB	200	<20 ppb	50–100
Week 5	HPFBG	PRB	300	<20 ppb	50–100
Week 6	HPFBG	PRB	500	<20 ppm	50–100

Table 4.2 shows the planned test conditions for the hydrogen separation membranes. These conditions represent Test Condition 1 and 2A from the NETL test protocol issued by the US DOE (56). Early tests were focused on hitting Test Condition

1. The original plan called for hitting Test Condition 2A, but problems with the membranes ultimately prevented this test condition from being tested. The general test plan and operating strategy for each of the weeks, shown in Table 4.3, was to bring the warm gas cleanup equipment and membranes on-line one at a time, and then to hold at that condition for as long as possible.

Table 4.2. Expected Membrane Test Conditions

	Test 1	Test 2A
Feed Gas Composition (before correction for addition of He)		
H_2, %	50.0	50.0
CO, %	<1.0	1.0
CO_2, %	30.0	30.0
H_2O, %	19.0	19.0
H_2S, %	0.000	0.002
N_2, %	<5	
Sweep Gas Inlet Composition, %	None	100
Total Feed Pressure, psia	200	200
H_2 Feed Partial Pressure, psia	100	100
Total Sweep Pressure, psig	None	<30
$(P_{H2S}/P_{H2})_{Feed}$	0.00E+00	4.00E-05
Temperature, °F	400–950	300–600

4.1 Week 1 Testing – HPFBG

Testing in Week 1 was performed on the HPFBG. The testing was focused on understanding the required operational parameters for the gasification, gas cleanup, and hydrogen separation operations. Testing occurred at 200 psi so that all three membranes could be evaluated simultaneously.

4.1.1 Test Plan

The test plan and operational parameters for the Week 1 testing are shown in Table 4.4. The basic strategy for the testing was to produce syngas with a high hydrogen

Table 4.3. General Operational Strategy for Weeks 1 – 6

Test Condition	RVS-1	High-Temp. WGS Bed	Sulfur Packed Bed	Chlorine Guard/ Mercury Sorbent	Low-Temp. WGS Bed	FS Membrane	SS1 Membrane	SS2 Membrane	Duration, hr*
1	Bypassed	Bypassed	Bypassed	Bypassed	Bypassed	Bypassed	Bypassed	Bypassed	4
2	On	Bypassed	Bypassed	Bypassed	Bypassed	Bypassed	Bypassed	Bypassed	4
3	On	On	On	Bypassed	Bypassed	Bypassed	Bypassed	Bypassed	4
4	On	On	On	On	Bypassed	Bypassed	Bypassed	Bypassed	4
5	On	On	On	On	On	Bypassed	Bypassed	Bypassed	4
6	On	On	On	On	On	On	Bypassed	Bypassed	2
7	On	On	On	On	On	On	On	Bypassed	2
8	On	On	On	On	On	On	On	On	54
9	On	On	On	On	On	On	On	Bypassed	1
10	On	On	On	On	On	On	Bypassed	Bypassed	1
11	On	On	On	Bypassed	Bypassed	Bypassed	Bypassed	Bypassed	2
12	On	Bypassed	Bypassed	Bypassed	Bypassed	Bypassed	Bypassed	Bypassed	2
13	Off	Bypassed	Bypassed	Bypassed	Bypassed	Bypassed	Bypassed	Bypassed	2
								*Total	86

Table 4.4. Planned Gasifier Operating Conditions

		Time, hr	Coal Feed, lb/hr	Oper. Temp., °F	Fluid. Velocity, ft/sec	H_2O/Coal Wt Ratio	Steam Flow, g/hr	O_2 to C Molar Ratio	O_2 Flow, scfh	N_2 Flow for AB, scfh	Recycle or N_2 Flow Rate, scfh	Total Gas Flow, scfh
Start-Up*	AB	2	10	1550	0.9	0.35	1589	0.4	63.2	300.8	112.0	607.0
Operation	OB	All Week	10	1550	0.9	1.4	6356	0.4	63.2	0.0	186.4	601.7

* Establish consistent operation with the gasifier for 2 hr, then transition to the oxygen-blown setting.

content, with a goal of achieving 50% hydrogen in the syngas. Additionally, test conditions must be such that the gasifier operation is consistent and smooth. In a small-scale system, it can be difficult to achieve both high hydrogen content and reasonable carbon conversion because the heat loss per unit area is high and greater amounts of CO_2 must be produced to make up for the lost heat. As this test and follow-on runs progressed, it was shown to be very difficult to produce gas with 50% hydrogen and maintain consistent gasifier operation. Therefore, the hydrogen content was typically in the upper 30% to low 40% range for most of the tests performed.

4.1.2 Gasifier Operations and Operating Data

Operational data for the FBG is shown in Table 4.5. The gasifier was started on December 13, 2010, at 16:13. Much of the first day was spent working out some issues with fluidization of the lower portion of the bed and avoiding temperature spikes and bed agglomeration. Because of the temperature issue, 100 to 150 scfh of nitrogen was used for the testing to ensure good mixing at the gasifier's inlet distributor plate and to avoid temperature spikes in the system. This, combined with other nitrogen purges, resulted in a syngas stream containing about 40% nitrogen for the duration of the testing. As will be presented later, nitrogen was able to be eliminated in future runs on the FBG. The main gasifier bed was typically run near 816°C (1500°F). The gasifier also has an extended freeboard section that was recently added for a separate project. This extension was run close to 704°C (1300°F) for the testing. The temperatures for the gas cleanup equipment ranged anywhere from near 480°C (900°F) at the filter vessel inlet to approximately 200°C (400°F) for the low-temperature shift catalyst. The temperature of the syngas decreased as it moved through each of the gas cleanup operations. The syngas was then

cooled and condensed in the quench pots from temperatures near 260°C (500°F), down to approximately 16°C (60°F) for syngas transitioning to the recycle syngas compressor.

Coal feed rate ranged nominally from 8 to 10 lb/hour throughout the HPFBG test. On December 15, the syngas compressor failed, but the test was continued and run without recycle syngas. To compensate for the additional nitrogen that had to be added to maintain fluidization, coal feed rate was increased to produce more syngas. Average coal feed rate during that time period was close to 13 lb/hr. Oxygen rates were held fairly low, and steam rates were kept fairly high during the test runs to compensate for the temperature excursions that were experienced at the bottom of the fluid bed. Product gas production rate was significantly higher when the compressor was offline because nitrogen was input into the system as a replacement for recycle gas. Closure, which is a calculation of the gas input rates vs. rate of gas leaving the system, was always over 100%. This indicates significant syngas production from the fuel. Also, hydrogen separated in the membranes is not counted toward the rate of gas leaving the system.

System pressure was originally set at 200 psi because that is the maximum operation temperature of one of the membranes. However, significant pressure drop was observed through the fixed beds, such that the pressure was down near 160 psi before entering the membranes. To compensate for the pressure loss, the gasifier pressure was slowly increased through the test run so that the hydrogen partial pressure to the membranes was maximized. By the end of the run, the gasifier was operating at 220 psi.

4.1.3 Warm-gas Cleanup Results

The syngas composition is highly dependent on the warm-gas cleanup systems in operation. Data were collected as each of the warm-gas cleanup systems was brought

Table 4.5. Operational Data for Week 1 (HPFBG)

	Pre-membrane	Membrane Online	Membrane Online No Recycle	Membrane Online
Start Date	12/15/2010	12/15/2010	12/15/2010	12/16/2010
Start Time	8:50	11:30	21:50	7:00
End Date	12/15/2010	12/15/2010	12/16/2010	12/17/2010
End Time	10:06	20:20	5:00	8:00
FBG Temp., °F				
O_2/Steam Inlet	701	680	692	653
Recycle Inlet	91	92	92	87
Lower Reactor Bed	1511	1532	1584	1542
Upper Reactor Bed	1414	1470	1526	1487
Lower Freeboard	1334	1439	1448	1464
Upper Freeboard	1521	1528	1549	1521
Reactor Extension	1264	1274	1271	1279
Cyclone Exit	987	991	994	984
Filter Vessel Temp., °F				
FV Inlet	877	883	824	893
FV Outlet	701	723	721	727
Packed Bed Temps., °F				
Bulk Sulfur Removal	602	607	610	611
High-Temperature Shift Catalyst	466	502	557	552
Sulfur Polishing	413	448	519	511
Chlorine Guard, Mercury Control	376	386	431	429
Low-Temperature Shift Catalyst	395	398	393	388
Quench Pot Temp., °F				
West Pot 1 Inlet	366	363	432	485
West Pot 3 Outlet	91	83	81	82
East Pot 1 Inlet	89	82	81	82
East Pot 3 Outlet	57	60	63	62
Flows				
Coal Feed Rate, lb/hr	7.8	8.3	12.8	10.0
Primary Nitrogen, scfh	115	154	115	154
Oxygen, scfh	54	50	78	50
Steam, lb/hr	11.5	11.5	9.2	11.4
Recycle Syngas, lb/hr	7.7	5.8	9.7*	6.4
Nitrogen Purge, scfh	9.1	7.9	6.1	5.9
Product Gas, scfh	283	314	654	293
Closure, %	159	149	187	140
Pressure, psi				
EFG Top	200	209	220	221
EFG Bottom	199	208	219	219
Filter Vessel	196	205	216	216
Quench Pot	159	165	163	167
Recycle Gas Surge Tank	798	798	283	800

* Recycle gas was nitrogen during this test period.

online during the FBG test and are presented in Table 4.6. Gas bag samples, GC, and LGA instrumentation were utilized to determine bulk and trace syngas analyte concentrations. The data presented in Table 4.6 are a combination of both LGA and GC data. Operational difficulties with the gasifier resulted in the addition of nitrogen to the system to aid in fluidization, which led to significant levels of nitrogen in the syngas. The bulk desulfurizer reduced the H_2S syngas concentration from 700 to 0.27 ppmv. This represents a H_2S reduction of 99.96% across the desulfurizer bed. When the high-temperature shift catalyst was brought online, the CO values decreased from 9.9 to 1.73 mol%. The H_2/CO ratio increased from about 3 to approximately 21 when the syngas reached equilibrium. When the sulfur polishing bed was turned on, the H_2S concentration decreased to levels below the LGA detection limit. Dräger tube data show that the H_2S concentrations decreased to less than 20 ppb. The main syngas constituents remained constant when the chlorine guard/mercury control bed was brought online, while the mercury and chlorine values decreased to 1.30 μg/dNm^3 and less than 1 ppm, respectively.

Throughout the Week 1 test period, the major and trace syngas species were monitored using the LGA and GC instruments. Figure 4.1 plots the syngas species for the duration of the Week 1 test period. The data remained fairly steady throughout the test period. The drop in the CO concentration and subsequent rise in the H_2 and CO_2 concentrations correspond to the WGS catalyst being brought online. The methane and H_2S levels remained low throughout the test period.

Mercury data were collected to measure the mercury concentrations at the Port C sampling location, which is after the mercury control column and before the hydrogen

Table 4.6. Week 1 Syngas Composition (HPFBG)

Sample Point	H_2, mol%	CO, mol%	CO_2, mol%	N_2, mol%	CH_4, mol%	H_2S, ppmv	H_2/CO Ratio
Bulk Desulfurizer Inlet RVS-1, Bed 1	23.62	9.85	19.57	40.23	1.44	700	2.40
Bulk Desulfurizer Outlet RVS-1, Bed 1	28.75	9.9	25.3	29.63	1.65	0.27	2.90
High-Temperature Shift Catalyst Outlet, Bed 3	30.35	1.73	24.93	37.36	1.24	0.27	17.54
Sulfur Polishing Bed Outlet, Bed 4	29.88	1.38	24.16	38.41	1.2	0.22	21.65
Chlorine Guard/Mercury Control Outlet, Bed 5	28.65	1.35	24.95	39.11	1.17	ND*	21.22
Low-Temperature Shift Catalyst Outlet, Bed 6	29.38	1.44	29.31	33.63	1.16	ND	20.40

* Not detected.

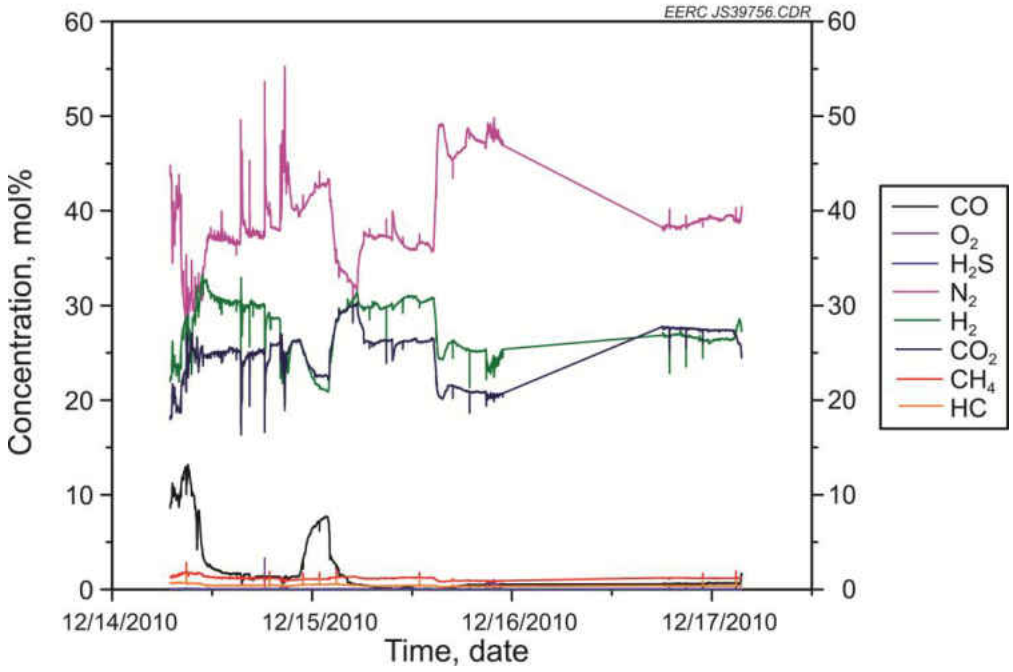

Figure 4.1. Week 1 Syngas Data.

separation membranes. Sampling at this location determines the effectiveness of the mercury control column and measures the mercury concentrations that are seen by the hydrogen separation membranes. Mercury concentrations were determined by syngas sampling using sorbent traps. The samples were collected using OhioLumex sorbent traps and analyzed using an OhioLumex RA915+ mercury analyzer. This instrument utilizes a

pyrolysis technique followed by Zeeman atomic absorption detection. Table 4.7 displays the sorbent trap data for Week 1. Based on the coal feed rate and coal mercury concentration, the calculated inlet mercury concentration was approximately 19.97 $\mu g/dNm^3$. This corresponded to a mercury removal of 93% at the outlet of the mercury control bed.

Table 4.7. Week 1 Mercury Sorbent Trap Data

Sample Time	Sample Location	Hg Concentration, $\mu g/dNm^3$
12/15/2010 11:15	Port C (cold side)	1.38
12/16/2010 10:40	Port C (cold side)	1.43
12/17/2010 8:55	Port C (cold side)	1.09
Average		1.30

Dräger tubes were used to measure the concentration of low level contaminants and species that were not monitored by the online gas analyzers. Species measured include low-level sulfur, NH_3, HCN, and HCl. H_2S was measured by running the syngas sample through an ice bath before going into the Dräger tube. The other species were measured hot. The results averaged over the entire week for each species are shown in Table 4.8. Dräger tubes indicated that H_2S averaged 0.11 ppm for the test run. Ammonia was approximately 2700 ppm for the run, HCN was 0.06 ppm, and HCl averaged 3.5 ppm.

Table 4.8. Dräger Tube Results Summary for Week 1

	Cold-Side Sampling		Sample Port C Hot Side		
	Sample Port A H_2S	Sample Port C H_2S	NH_3	HCN	HCl
Concentration, ppm	0.19	0.11	2700	0.06	3.5

The concentration of the syngas contaminants after the warm gas cleanup train was very low in week 1, and this trend continued during the remaining testing. These results show that commercially available warm gas cleanup equipment can achieve the

same removal efficiency as Rectisol for many of the impurities. Testing by Guazzone et. al. has shown that contaminants such as sulfur, sodium, and arsenic can contaminate a membrane surface, but these tests were performed on coupons placed in front of the warm gas cleanup beds (47). This work intends to complement those findings by understanding whether those contaminants will be observed on the membrane surface after warm gas cleanup techniques are employed.

4.1.4 Membrane Results and Performance

The membranes were brought online at about noon on December 15. Initially, no flux was observed across any of the membranes. This was expected since there is typically a conditioning period that must occur before hydrogen separation can begin. The first period that was considered steady-state production started at 00:00 on December 16. Figure 4.2 shows the hydrogen production across the FS membrane from December 16 through shutdown on the morning of December 17. The data represent a smoothed average over a 10-minute time period. At 05:00 on December 16, the syngas compressor went offline, but the gasifier was continued to be run in air-blown mode, and membrane syngas exposure continued. The compressor was brought back online at 10:00. Over Steady-State Period 2, the flux across the membrane increased significantly as expected. The flux was then relatively steady, averaging near 50 scfh for the remainder of the run.

SS1 membrane, as shown in Figure 4.3, started to achieve flux near the same time that the FS membrane's performance started to improve, but the flux was not maintained for the duration of the run. At the time it was unknown if the membrane had been poisoned after a few hours of exposure. Subsequent testing showed it was not poisoned and the reason for the loss of flux was more likely related to measurement difficulties

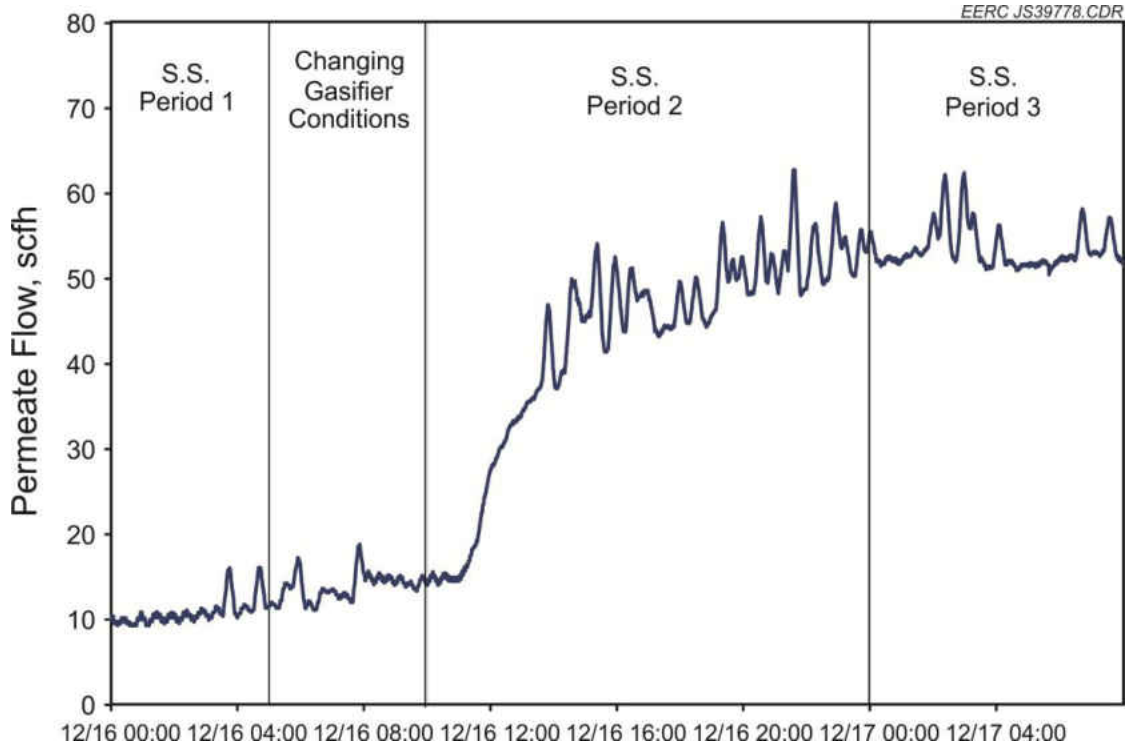

Figure 4.2. FS Membrane Permeate Flow Rate during Week 1 (S.S. Period 1 = Steady-State Period 1).

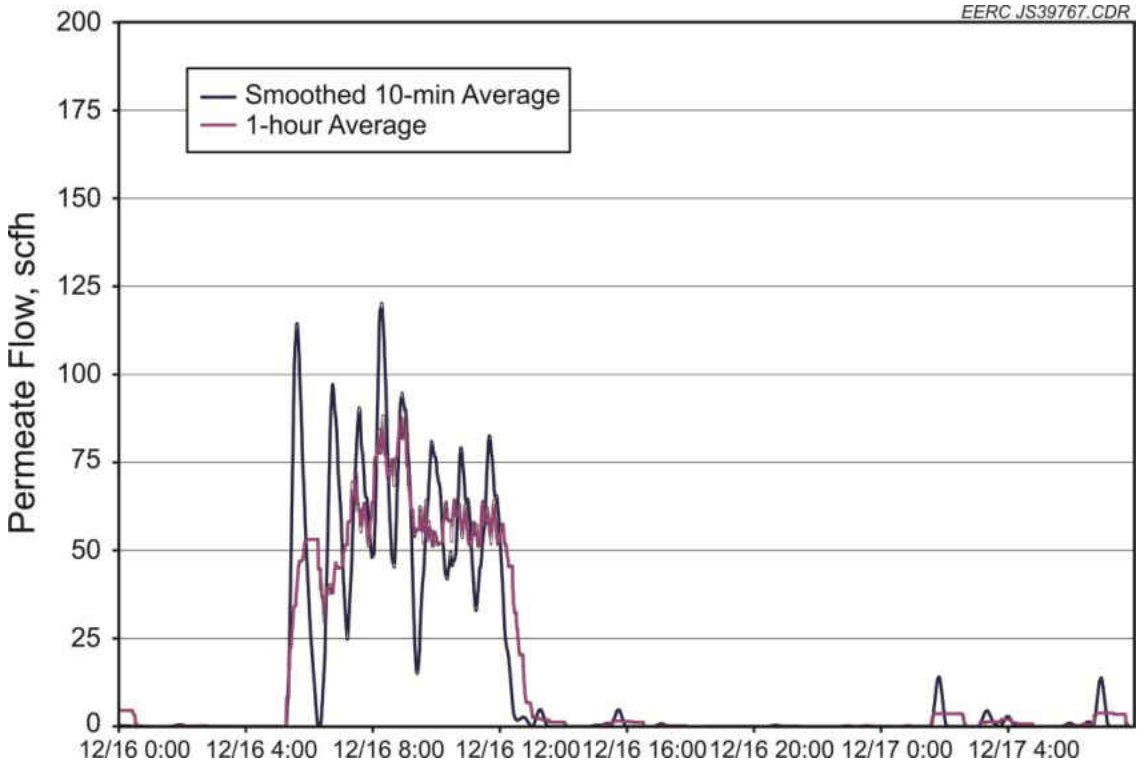

Figure 4.3. SS1 Membrane Flux Rates during Week 1.

with the permeate flow rate. The permeate stream gas meter was slightly oversized for the flux being achieved. The SS2 membrane, shown in Figure 4.4, was shown to have similar issues with measurement. Starting with Week 4, a Gilibrator™ was used to measure the flows coming off of the permeate side of the membranes so accurate flux measurements could be made.

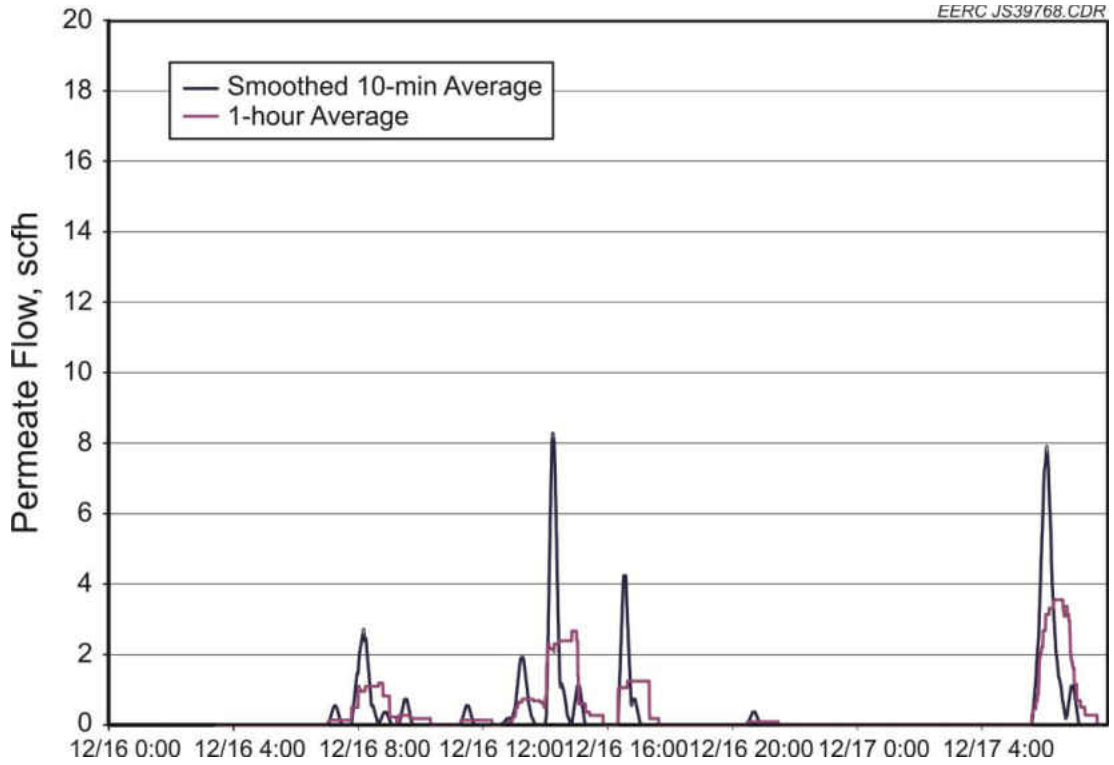

Figure 4.4. SS2 Membrane Flux Rates during Week 1.

Tables 4.9–4.11 list the performance data for the three membranes during the steady-state periods identified. Despite the fact that partial pressure differential across the FS membrane decreased as the run progressed, the hydrogen flux increased significantly after the conditioning period was complete. The inlet temperature on SS1 membrane dropped significantly, which may explain the loss of flux later in the run. The membrane temperature itself was still kept high throughout the run. A small amount of hydrogen

flux was observed on SS2 membrane after the inlet temperature was increased to over 316°C (600°F) and the membrane temperature brought above 450°C (850°F).

Table 4.9. FS Membrane Performance Data during Week 1

	S.S. Period 1	S.S. Period 2	S.S. Period 3
	12/16/10 00:00–05:00	12/16/10 10:00–24:00	12/17/10 00:00–08:00
Heater Temperature, °F	550	642	650
Membrane Inlet, °F	519	576	590
Permeate Inlet, °F	526	588	602
Permeate Exit, °F	77	75	73
Syngas Inlet, °F	629	669	547
Syngas Inlet Pressure, psi	169	172	173
Permeate Pressure, in. H_2O	7	10	11
Flux, scfh/ft^2	0.8	3.0	3.8
H_2 Inlet, mol%	24.7	27.8	26.6
Wet H_2 Inlet, mol%	20.7	19.6	18.3
Raffinate H_2, mol%	24.1	22.9	20.5
Inlet H_2, scfh	224	156	155
Raffinate H_2, scfh	208	82	78
Permeate H_2, scfh	11	43	54
H_2 Balance, %	97.5	80.5	85.2
Hydrogen Recovery, %	4.9	27.0	34.8
Theoretical Max Recovery, %	66.6	64.8	62.0
Partial Pressure Differential, psi	23.1	21.4	19.3

Hydrogen mass balance was between 80.5% and 97.5% for the FS membrane, indicating that there was some measurement error. Recovery rate hit almost 35% during the last test period, which was over half of the theoretical maximum recovery rate based on partial pressure differential. The hydrogen mass balance was better for the slipstream membranes, but the hydrogen recovery rates as measured were low.

One important point to note is that the actual hydrogen concentration in the gas stream is impacted significantly from the amount of moisture in the syngas. It is very important to quantify the moisture leaving the system because the gas analyzers measure the streams on a dry basis. The wet-basis hydrogen is shown to be significantly lower

than the dry basis. This has a significant influence on the partial pressure differential, flux rates, and theoretical maximum recovery.

Table 4.10. SS1 Membrane Performance Data during Week 1

	S.S. Period 1	S.S. Period 2	S.S. Period 3
	12/16/10 00:00–05:00	12/16/10 10:00–24:00	12/17/10 03:12–08:00
Membrane Temperature, °F	758	744	730
Membrane Inlet, °F	720	740	352
Permeate Inlet, °F	124	121	99
Permeate Exit, °F	77	74	73
Raffinate Inlet, °F	344	459	393
Raffinate Exit, °F	78	75	74
Syngas Inlet, °F	629	669	547
Syngas Inlet Pressure, psi	169	172	173
Permeate Pressure, in. H_2O	9	8	4
Raffinate Exit Pressure, in. H_2O	42.4	46	40
Raffinate Flow Rate, scfh	8.8	13	11
Flux, scfh/ft^2	0.007	1.2	0.16
H_2 Inlet, mol%	24.7	27.8	26.4
Wet H_2 Inlet, mol%	19.9	17.5	16.3
Raffinate H_2, mol%	26.0	26.0	26.0
Inlet H_2, scfh	2.1	3.4	4.0
Raffinate H_2, scfh	2.2	3.2	3.9
Permeate H_2, scfh	0.0001	0.020	0.0026
H_2 Balance, %	105.1	93.6	98.4
Hydrogen Recovery, %	0.005	0.624	0.065
Theoretical Max Recovery, %	66.7	64.8	60.9
Partial Pressure Differential, psi	23.0	21.5	18.7

Hydrogen flow across the membranes was investigated by plotting the membrane inlet and raffinate hydrogen concentrations for the Week 1 test period. The difference between the two concentrations reflects the amount of hydrogen that passes through the membrane. Figure 4.5 plots the membrane inlet and raffinate hydrogen concentrations for the Week 1 test period. At first, the inlet and raffinate hydrogen concentrations are similar which indicates that little to no hydrogen is flowing through the membrane because of membrane conditioning in the syngas environment. After the membrane is conditioned, the raffinate hydrogen concentration decreases, which indicates that there is

hydrogen flow across the membrane. At the end of the test run, there is a difference of approximately 8 mol% in hydrogen concentration across the membrane.

Table 4.11. SS2 Membrane Performance Data during Week 1

	S.S. Period 1	S.S. Period 2	S.S. Period 3
	12/16/10	12/16/10	12/17/10
	00:00–05:00	10:00–24:00	03:12–08:00
Membrane Temperature, °F	852	883	867
Membrane Inlet, °F	323	358	621.6
Permeate Inlet, °F	86	86	81.8
Permeate Exit, °F	78	75	73.5
Raffinate Inlet, °F	307	355	406.3
Raffinate Exit, °F	79	76	74
Syngas Inlet, °F	629	669	546.6
Syngas Inlet Pressure, psi	169	172	173.4
Permeate Pressure, in. H_2O	2	3	2
Permeate Flow Rate, scfh	0	0.0003	0.0032
Raffinate Exit Pressure, in. H_2O	45	47	38.4
Raffinate Flow Rate, scfh	7	9	7.7
Flux, scfh/ft^2	0.000	0.019	0.044
H_2 Inlet, mol %	24.7	27.8	26.4
Wet H_2 Inlet, mol%	19.9	17.5	16.3
Raffinate H_2, mol%	26.6	26.6	25.9
Inlet H_2, scfh	1.8	2.4	3.0
Raffinate H_2, scfh	1.9	2.3	2.9
Permeate H_2, scfh	0.000	0.000	0.001
H_2 Balance, %	107.8	95.8	98.0
Hydrogen Recovery, %	0.000	0.016	0.029
Theoretical Max Recovery, %	65.9	63.6	58.5
Partial Pressure Differential, psi	30.6	29.0	26.1

Table 4.12 displays the permeate and raffinate syngas data for each of the membranes tested. These data were predominantly collected via gas bag sampling. The FS membrane provided excellent permeate hydrogen purity of 99.995 mol%. The only impurity detected was CO at a concentration of 0.005 mol%. The SS1 membrane also displayed a very good permeate hydrogen purity of 99.24 mol%. During the Week 1 testing, the SS2 membrane had little to no flux measured through the membrane which accounts for the low permeate hydrogen concentration. The FS and SS1 raffinate

concentrations were similar in composition other than the FS raffinate had a lower hydrogen concentration. The lower hydrogen concentration was due to the higher hydrogen flux through the FS membrane.

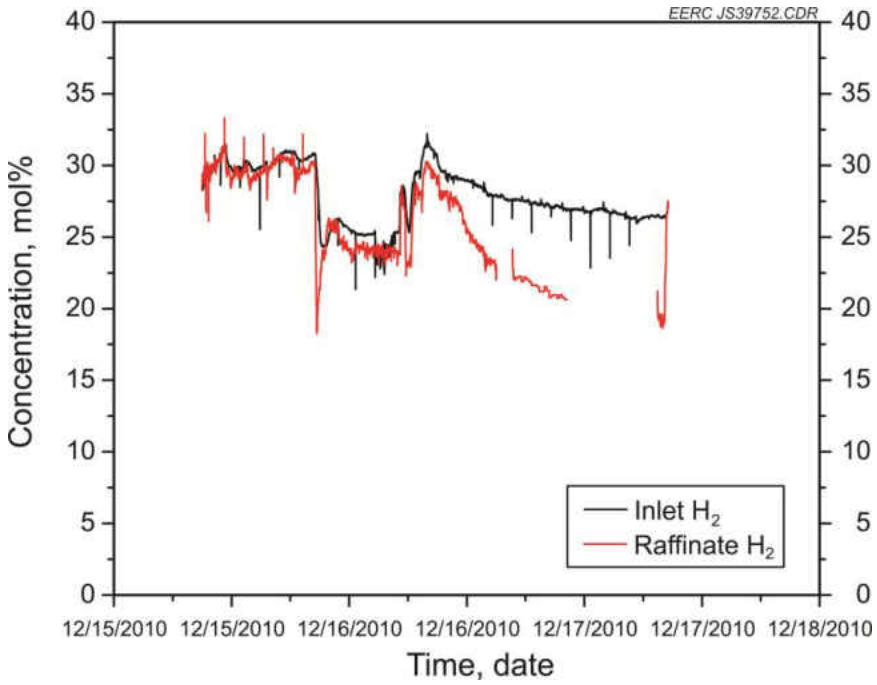

Figure 4.5. Week 1 FS Membrane Inlet and Raffinate Concentration Data.

Table 4.12. Week 1 Membrane Permeate and Raffinate Syngas Data

Membrane	H_2, mol%	CO, mol%	CO_2, mol%	N_2, mol%	CH_4, mol%	H_2S, ppmv
FS Permeate	99.995	0.005	ND	ND	ND	ND
FS Raffinate	21.16	0.72	30.81	41.48	2.41	ND
SS1 Permeate	99.24	ND	0.18	0.48	0.1	ND
SS1 Raffinate	25.97	0.73	29.24	39.02	2.21	ND
SS2 Permeate	32.3	0.66	22.96	40.07	1.74	ND
SS2 Raffinate	26.62	0.73	28.91	38.56	2.22	ND

4.2 Week 2 Testing – EFG

Week 2 testing occurred on the EFG. Unfortunately, only a few hours of data were obtained on the membranes because of a slag plug in the EFG furnace tube. Some

of the operating data are presented here, but the membranes did not reach steady state; therefore, the membrane performance data are deferred to a more successful test run.

4.2.1 Test Plan

The warm gas cleanup operational strategy for week 2 was the same as the previous week's plan, and can be found in Table 4.3. The goal was to get the gasifier into a steady-state condition, bring on the fixed beds, verify the levels of contaminants, and then bring the membranes online. Test conditions for the gasifier were set such that the system would run smoothly while trying to maximize hydrogen production. The actual system set points were developed based on an earlier run with the Antelope Mine coal.

4.2.2 Gasifier Operations and Operating Data

Coal feed to the gasifier started at 12:41 on January 3, 2011. The gasifier operating data are shown in Table 4.13. The coal feed rate was ramped to approximately 8 lb/hr, and then the fixed beds were brought online. The first membrane was brought online at 23:15, but was taken offline at 00:37 the next day because of a high CO alarm in the building. While attempting to troubleshoot the potential leak (which turned out to be in the thermal oxidizer, not the membrane), the operator increased steam in the system to try to carry more heat to the back end of the system and to increase WGS. Unfortunately, this change cooled the furnace tube to the point where slag started to deposit at the bottom of the tube and eventually it plugged off. The system was shutdown at 03:30 because of excessively high differential pressure across the furnace tube. Upon depressurization and removal of the slag pot, it was found that the furnace tube was plugged.

Temperatures in the system during the short-duration test run reached a maximum of 1477°C (2690°F). The heated zone thermocouples actually measure the temperature just outside the furnace tube; therefore, the internal tube temperature is unknown. It typically takes about 1 day of coal feed for the entire system to reach its operating temperature. Zones 3 and 4 of the furnace indicate a lower temperature than Zones 1 and 2, but this is known to be due to a purge flow that reduces the temperature measurement in these areas. The furnace tube itself is known to be hotter, because if the purge flows are shut off, the thermocouples in Zones 3 and 4 will read very close to those in Zones 1 and 2. By the time the gas reaches the quench zone, it is down in the 760°C (1400°F) range, with no water quench online. The drop in temperature is simply due to heat loss through the walls. Temperature at the gasifier exit is in the 204°C (400°F) range, and this temperature drop is due to heat loss in the gasifier and some of the cooler purge gas recombining with the syngas.

The filter vessel was run between 370° and 427°C (700° and 800°F) during this test run, although there were some localized measurements in the filter vessel in the 204°C (400°F) range. Upon system start-up, the rate of ash deposition in the filter vessel is significant. However, as the gasifier is transitioned into steady state, the rate of ash buildup decreases significantly because of high carbon conversion and lower gas velocities. The low gas velocities cause more ash to settle into the slag pot and less to reach the filter vessel. On average, the candle filter needs to be pulsed once every few hours during an EFG run. This is compared to twice an hour for an FBG run.

The warm gas-cleanup packed beds were run in a similar manner to the previous weeks testing, with temperatures ranging from just over 316°C (600°F) to just under 204°C

(400°F). The quench pots cooled the gas from near 500°C (500°F) to 12°C (54°F). Slightly cooler gas temperatures were able to be obtained than the previous week simply due to the fact that the cooling water comes into the building colder in January than in December.

Coal feed rate was intended to be about 8 lb/hr but averaged closer to 9.0 lb/hr. This difference may be attributed to the fact that the scale span is adjusted based on operating pressure because of the impact of pressure on the load cells. The required scale span tends to change from run to run and is a potential source of measurement error. The oxygen rates were held steady at 115 scfh, and the steam rates were held near 6.6 lb/hr for most of the run, except during the period previously mentioned when the rate was increased. Nitrogen purge rates for this run were significant and caused, in part, to thermal management issues observed with the gasifier. These high purge rates do have a significant impact on the gas composition and ultimately reduce the hydrogen partial pressure at the membranes. No water quench was used for this run; instead, the purge gas was routed so that it combined with the syngas in the quench zone. This eliminated the need for a water quench and prevented any issues with wet deposition at the exit of the gasifier, but also reduced the amount of water available for the WGS reaction. Closure was around 150% when the membranes were offline, indicating significant gas production. The closure was reduced when the membranes were online because the hydrogen permeate does not travel through the main system gas meter and is not counted toward the closure calculation. Gasifier pressure was set at 230 psi for this test run. Significant pressure drop occurs through the fixed beds so that the pressure at the system exit (and hydrogen separation membranes) was just under 200 psi.

Table 4.13. Gasifier Operation Data for Week 2 (EFG)

	Premembrane	FS Online	FS Offline
Start Date	1/3/2011	1/3/2011	1/4/2011
Start Time	21:07	23:15	2:30
End Date	1/3/2011	1/4/2011	1/4/2011
End Time	22:18	0:37	3:30
EFG Temp., °F			
O_2/Steam Inlet	651	651	643
Recycle Inlet	361	400	394
Top Outside of Furnace Tube	1614	1640	1786
Zone 1	2465	2487	2554
Zone 2	2634	2655	2690
Zone 3	2376	2399	2409
Zone 4	1716	1734	1672
Post Quench	1415	1446	1350
EFG Outlet	472	445	418
Filter Vessel Temp., °F			
FV Inlet	729	726	736
FV Outlet	774	774	783
Packed Bed Temp., °F			
Bulk Sulfur Removal	610	617	616
High-Temperature Shift Catalyst	618	617	602
Sulfur Polishing	519	519	511
Chlorine Guard, Mercury Control	398	405	414
Low-Temperature Shift Catalyst	365	404	408
Quench Pot Temp., °F			
West Pot 1 Inlet	541	451	489
West Pot 3 Outlet	68	65	72
East Pot 1 Inlet	69	66	72
East Pot 3 Outlet	54	54	54
Flows			
Coal Feed Rate, lb/hr	9.0	9.4	8.4
Oxygen, scfh	115	115	115
Steam, lb/hr	6.6	6.7	9.7
Recycle Gas, lb/hr	7.9	10.3	9.8
Nitrogen Purge, scfh	239	213	213
Quench Flow, lb/hr	0	0	0
Product Gas, scfh	539	415	486
Closure, %	146	118	154
Pressure, psig			
EFG Top	230	230	228
EFG Bottom	230	230	228
Filter Vessel	227	227	225
Quench Pot	196	196	199
Recycle Gas Surge Tank	800	800	800

4.2.3 Warm-gas Cleanup Results

The Week 2 syngas data are limited because of the short test period on the EFG. Data were collected as each of the warm gas cleanup systems was brought online during the EFG test and are presented in Table 4.14. Gas bag samples, GC, and LGA instrumentation were utilized to determine bulk and trace syngas analyte concentrations. The bulk desulfurizer reduced the H_2S syngas concentration from 260 ppmv to below the LGA detection limit. When the high-temperature shift catalyst was brought online, the CO concentration decreased by approximately 3%, and the hydrogen and CO_2 concentrations increased by approximately 2%. The H_2/CO ratio remained fairly low and reached a maximum of 8.27. This is much lower than the H_2/CO ratio presented in Week 1. The difference is due to the different designs and operating conditions of the FBG and EFG gasifiers. The sulfur polishing bed further decreased the sulfur concentration down to 0.154 ppmv after all of the warm-gas cleanup systems were brought online. This represents a sulfur removal of 99.94%. The major syngas species remained consistent when the chlorine guard/mercury control bed was brought online.

During the Week 2 test period, the major and trace syngas species were monitored using the LGA and GC instruments to provide continuous real-time data. Figure 4.6 plots the syngas composition for the Week 2 test period. During the steady-state periods, the syngas composition remained fairly consistent. The drop in the CO concentration and increase in H_2 and CO_2 concentrations occurred when the WGS catalyst was brought online. The trace species remained consistently low throughout the test period which shows that the cleanup beds were able to maintain their functionality throughout the test period.

Table 4.14. Week 2 Syngas Composition (EFG)

Sample Point	H_2, mol%	CO, mol%	CO_2, mol%	N_2, mol%	CH_4, mol%	H_2S, ppmv	H_2/CO Ratio
Bulk Desulfurizer Inlet RVS-1, Bed 1	15.21	16.74	9.43	56.2	ND	260	0.91
Bulk Desulfurizer Outlet RVS-1, Bed 1	16.69	12.86	11.88	56.22	ND	ND	1.30
High-Temp. Shift Catalyst Outlet, Bed 3	18.65	9.25	13.68	56.03	ND	ND	2.02
Sulfur Polishing Bed Outlet, Bed 4	27.56	7.55	21.58	41.01	ND	0.262	3.65
Chlorine Guard/ Mercury Control Outlet, Bed 5	27.98	6.02	24.63	28.8	ND	0.161	4.65
Low-Temp. Shift Catalyst Outlet, Bed 6	30.09	3.64	28.18	35.65	ND	0.154	8.27

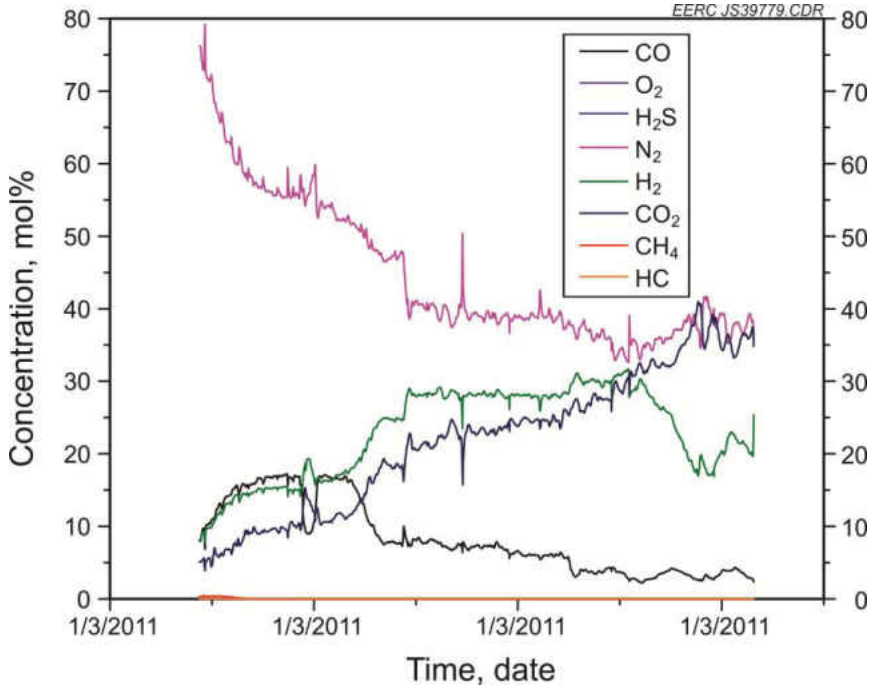

Figure 4.6. Week 2 Syngas Data.

4.2.4 Membrane Results and Performance

Even though this was a very short duration test because of gasifier operational issues, good flux rates were achieved on the full-scale membrane. Figure 4.7 shows that flux rates exceeded100 scfh for a period of time. As shown in Table 4.15, the hydrogen

mass balance was over 100% during this time period, but recovery rates stayed well under the theoretical maximum. Average partial pressure differential was 41 psi for the run, up significantly from the previous run. This was due to higher hydrogen concentration and slightly higher static pressures at the membranes for this run. The slipstream units did not go online for this short test run.

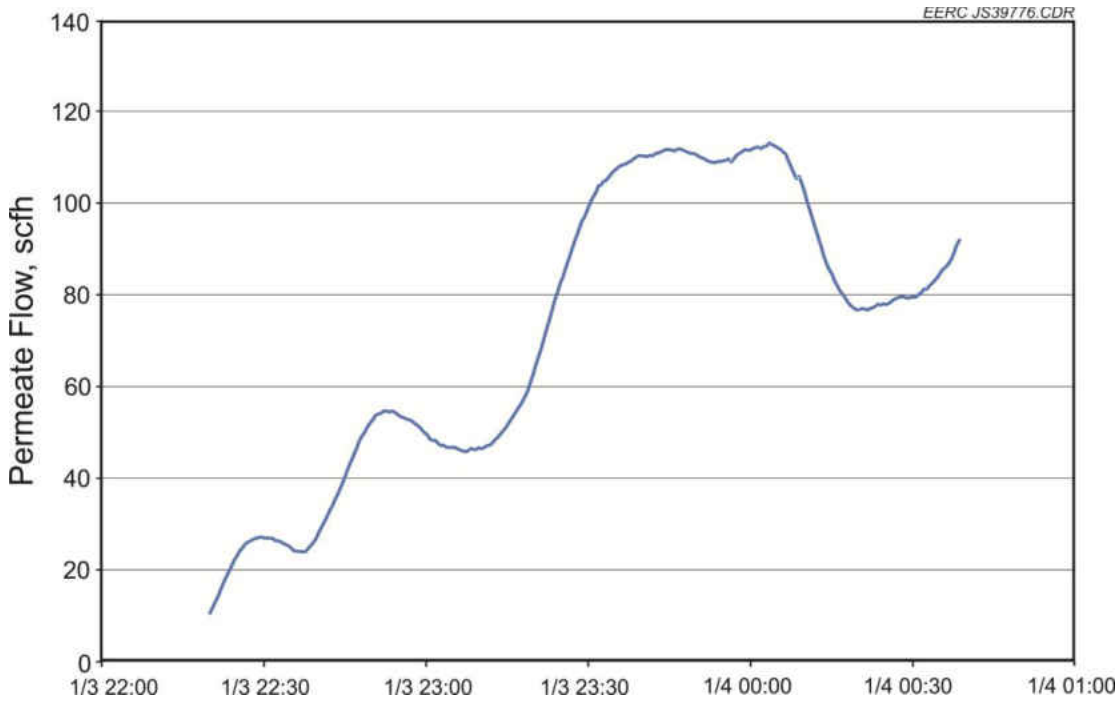

Figure 4.7. FS Membrane Permeate Flow for Week 2.

Hydrogen flow across the membranes was investigated by plotting the membrane inlet and raffinate hydrogen concentrations for the Week 2 test period, as shown in Figure 4.8. For most of this test period, the syngas was not being sent to the membrane. The decrease in raffinate hydrogen concentration at the very end of the test period is when the hydrogen membrane was brought online. The inlet hydrogen remained consistent in the 30–32 mol% range, and the raffinate hydrogen concentration decreased to 20–22 mol%, which demonstrates flux through the membrane.

Table 4.15. FS Membrane Performance Data for Week 2

	1/3/10 22:20 – 1/4/10 00:38
Heater Temperature, °F	612
Membrane Inlet, °F	643
Permeate Inlet, °F	628
Permeate Exit, °F	72
Syngas Inlet, °F	325
Syngas Inlet Pressure, psi	201
Permeate Pressure, in. H_2O	11
Flux, scfh/ft^2	4.0
H_2 Inlet, mol%	29.5
Wet H_2 Inlet, mol%	25.9
Raffinate H_2, mol%	23.0
Inlet H_2, scfh	226.4
Raffinate H_2, scfh	134.6
Permeate H_2, scfh	55.6
H_2 Balance, %	84.4
Hydrogen Recovery, %	24.1
Theoretical Max Recovery, %	79.0
Partial Pressure Differential	40.8

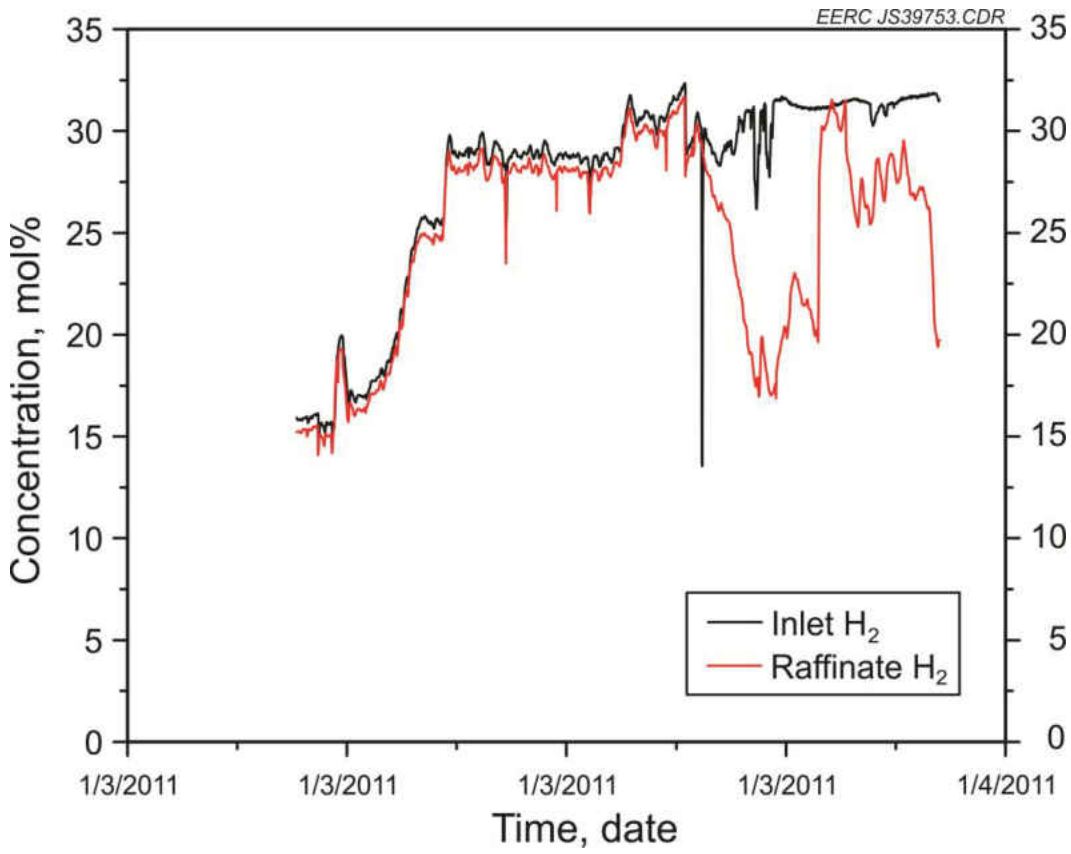

Figure 4.8. Week 2 FS Membrane Inlet and Raffinate Concentration Data.

Because of the short Week 2 test period, limited permeate and raffinate syngas data were collected when the membranes were operational. Table 4.16 presents the FS membrane data. The SS1 and SS2 membranes were not online during the short test period. Gas bag data collected on the FS permeate side show that the hydrogen stream had a purity of 99.99%. CO was the only detected impurity at a concentration of 0.01%. The raffinate data were collected using the GC data and are comparable to the inlet data except for the lower hydrogen concentration because of hydrogen flux through the FS membrane.

Table 4.16. Week 2 Membrane Permeate and Raffinate Syngas Data

Membrane	H_2, mol%	CO, mol%	CO_2, mol%	N_2, mol%	CH_4, mol%	H_2S, ppmv
FS Permeate	99.99	0.01	ND	ND	ND	ND
FS Raffinate	22.84	3.58	32.96	38.21	0.0028	0.163
SS1 Permeate	–	–	–	–	–	–
SS1 Raffinate	–	–	–	–	–	–
SS2 Permeate	–	–	–	–	–	–
SS2 Raffinate	–	–	–	–	–	–

4.3 Week 3 Testing - EFG

Testing in Week 3 was intended to pick up where Week 2 left off with the EFG. Flame temperature calculations for the fuel in the EFG were performed to help understand optimal operating conditions to prevent slag buildup in the tube. Unfortunately these conditions also result in less overall hydrogen production, because more carbon and hydrogen are burned to generate process heat. Steady-state hydrogen separation data were achieved during this test run.

4.3.1 Test Plan

The test plan again called for establishing steady-state operation with the gasifier, bringing on the fixed beds, verifying the contaminant levels, and then sending syngas to

the membranes, as shown in Table 4.3. The goal was to come as close as possible to Test Condition 1 as specified by the DOE membrane test protocol (56). Challenges to reach the 50% hydrogen criteria include attempting to increase the furnace temperature and the high purge rates required for thermal management of the gasifier.

4.3.2 Gasifier Operations and Operating Data

Coal feed to the EFG was started at 09:08 on January 10, 2011. All of the fixed beds were online by 16:02, and flow was established to all of the membranes by 16:45. The run appeared to progress smoothly for the next couple of days with very few operational issues. During the evening of January 12, a differential pressure increase was observed in the furnace tube area, and the system was shut down by 00:22 on January 13. After depressurizing and removing the slag pot, it was found that a large deposit had built up, not in the furnace tube but rather just below the tube. This deposit is thought to have been the result of routing the purge gas into the quench zone to control temperatures. It is possible that the flow of purge gas into this area was simply too high and caused freezing of the slag at the bottom of the tube. Operational data for Week 3 is shown in Table 4.17.

Gasifier temperatures for this run were just over 1482°C (2700°F) in Zones 1 and 2 and were just below 980°C (1800°F) in Zone 4. The higher operating temperature also resulted in higher post quench and EFG outlet temperature during the run. The temperature at the EFG outlet was as high as 346°C (654°F) by the end of the run. Filter vessel inlet temperatures were slightly lower than the previous run, but the gas still reached 370°C (700°F) at the outlet of the heated vessel.

Temperatures in the fixed beds were similar to the previous runs. It should be noted that sulfur breakthrough of about 3 ppm was observed at the outlet of Fixed Bed 1

Table 4.17. Gasifier Operational Data for Week 3 (EFG)

	Pre-membrane	Membrane Online	Membrane Online	Membrane Online
Start Date	1/10/2011	1/10/2011	1/11/2011	1/12/2011
Start Time	15:00	16:10	0:00	0:00
End Date	1/10/2011	1/10/2011	1/11/2011	1/12/2011
End Time	16:10	23:59	23:59	23:59
EFG Temp., °F				
O_2/Steam Inlet	608	608	607	607
Recycle Inlet	322	327	338	322
Top Outside of Furnace Tube	1913	1875	1756	1588
Zone 1	2710	2710	2708	2707
Zone 2	2705	2706	2706	2707
Zone 3	2527	2532	2539	2542
Zone 4	1757	1770	1790	1791
Post Quench	1529	1546	1579	1531
EFG Outlet	552	578	626	654
Filter Vessel Temp., °F				
FV Inlet	595	587	575	573
FV Outlet	730	734	730	662
Packed Bed Temp., °F				
Bulk Sulfur Removal	575	577	570	547
High-Temperature Shift Catalyst	594	601	607	608
Sulfur Polishing	519	564	571	573
Chlorine Guard, Mercury Control	372	459	474	475
Low Temperature Shift Catalyst	330	370	375	376
Quench Pot Temp., °F				
West Pot 1 Inlet	436	475	470	467
West Pot 3 Outlet	67	66	67	66
East Pot 1 Inlet	68	67	68	67
East Pot 3 Outlet	52	52	53	53
Flows				
Coal Feed Rate, lb/hr	9.2	9.9	10.1	10.3
Oxygen, scfh	127	127	127	127
Steam, lb/hr	6.6	6.6	6.6	6.6
Recycle Gas, lb/hr	7.6	8.3	9.0	8.4
Nitrogen Purge, scfh	284	284	284	284
Quench Flow, lb/hr	NA*	NA	NA	NA
Product Gas, scfh	616	468	429	427
Closure, %	150	110	100	99
Pressure, psig				
EFG Top	235	233	233	233
EFG Bottom	235	233	233	233
Filter Vessel	232	230	229	227
Quench Pot	203	195	199	203
Recycle Gas Surge Tank	800	800	800	800

* Not available.

on January 11 and that Fixed Bed 2 was then brought online. No sulfur was observed after the polishing bed, and details for the gas analysis will be presented later in this section. Fixed Bed 1 was regenerated with air and nitrogen after it was taken offline. The low-temperature shift catalyst was operated fairly cool at the start of the run, but the temperature was brought up to near 190°C (375°F) during the remainder of the run. The quench pots cooled the gas from near 230°C (450°F) to as low as 11°C (52°F). The cooler temperature as compared to the last run is again due to the cooling of city water in the winter in North Dakota.

Coal feed rate was set at 8 lb/hr but, according to the feeder scale, ranged from 9.2 to 10.3 lb/hr for the test run. Oxygen was higher than the previous run at 127 scfh, and steam remained consistent at 6.6 lb/hr. Nitrogen purge was high at 284 scfh throughout the run. The high nitrogen purge rate is indicative of deteriorating refractory in the gasifier upper zones and points toward the need for a refractory repour. Purge gas was used instead of water to quench the hot gas leaving the reactor. Closure was near 100% during membrane operations and is the result of gas production rate minus gas separation in the membranes and any leaks in the system.

Gasifier pressure was maintained near 233 psi during the test run so that the pressure at the membranes was close to 200 psi. Pressure in the quench pot location ranged from 195 to 203 psi.

4.3.3 Warm-gas Cleanup Results

The EFG gasifier ran very well during the Week 3 test period and obtained consistent syngas to the membranes. Table 4.18 displays the syngas data as each of the warm-gas cleanup systems was brought online. GC and LGA data were utilized to

determine bulk and trace syngas analyte concentrations across the warm-gas cleanup system. The bulk desulfurizer was able to achieve a sulfur removal of 99.63% and decreased H_2S concentrations from 340 to 1.256 ppmv. The high-temperature WGS catalyst performed well during this test period. When it was brought online, the CO concentration decreased from 20 to 8.75 mol% while increasing both the hydrogen and CO_2 concentrations by 7 and 8 mol %, respectively. When brought online, the sulfur polishing bed further decreased the H_2S concentration from 1.256 to 0.146 ppmv. This resulted in a total sulfur removal of 99.96%. The chlorine guard/mercury control bed was able to reduce the chlorine concentration to below detectable levels using Dräger tubes. Mercury concentrations were reduced to an average concentration of 0.27 $\mu g/dNm^3$, which is a mercury reduction of approximately 98%. The low-temperature shift catalyst was able to further reduce CO concentrations to 2.43 mol% when it was brought online.

Table 4.18. Week 3 Syngas Composition (EFG)

Sample Point	H_2, mol%	CO, mol%	CO_2, mol%	N_2, mol%	CH_4, mol%	H_2S, ppmv	H_2/CO Ratio
Bulk Desulfurizer Inlet RVS-1, Bed 1	18.46	20.2	11.52	47.49	ND	340	0.91
Bulk Desulfurizer Outlet RVS-1, Bed 1	18.55	20.77	11.83	46.44	ND	1.256	0.89
High-Temp. Shift Catalyst Outlet, Bed 3	25.91	8.75	20.16	42.91	ND	1.256	2.96
Sulfur Polishing Bed Outlet, Bed 4	25.76	6.15	22.59	43.06	ND	0.146	4.19
Chlorine Guard/Mercury Control Outlet, Bed 5	24.34	4.74	23.44	45.68	ND	0.146	5.14
Low-Temp. Shift Catalyst Outlet, Bed 6	22.25	2.43	29.28	43.92	ND	0.146	9.16

Figure 4.9 displays the continuous syngas data for the Week 3 test on the EFG. The data represent the equilibrated syngas conditions after all of the warm-gas cleanup beds were online. The syngas concentrations remained very consistent throughout the test

period. The initial decrease in CO and subsequent increases in CO_2 and H_2 concentrations are due to the low-temperature WGS catalyst being brought online. The trace syngas species remained low throughout the test period.

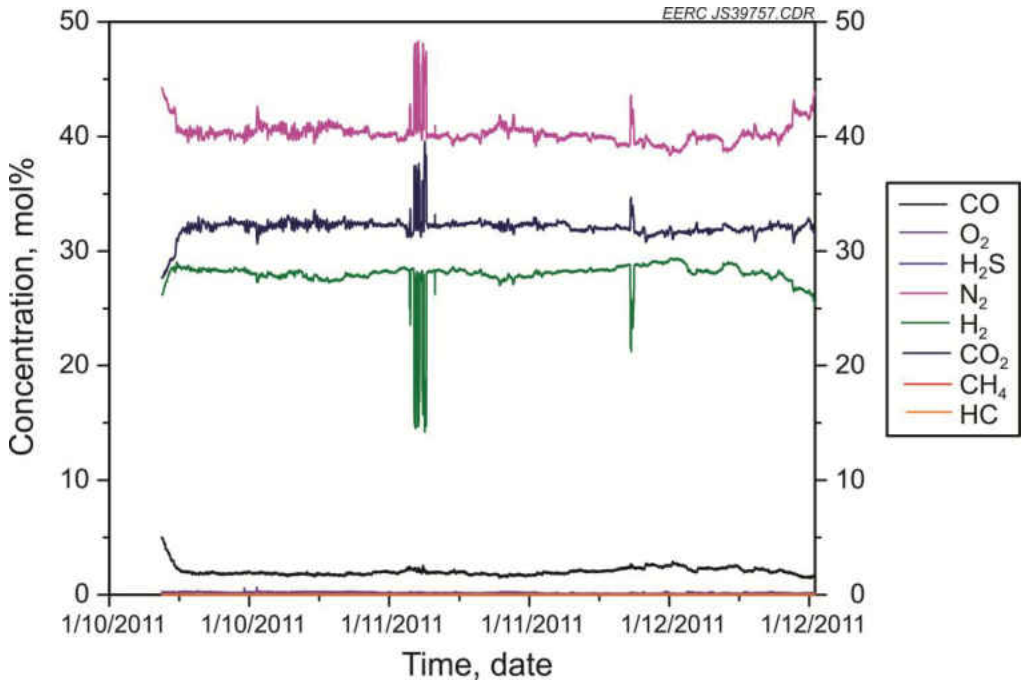

Figure 4.9. Week 3 Syngas Data.

Mercury data were collected to measure the mercury concentrations at the Port C sampling location, which is after the mercury control column and before the hydrogen separation membranes. Sampling at this location determines the effectiveness of the mercury control column and measures the mercury concentrations that are seen by the hydrogen separation membranes. Mercury concentrations were determined by syngas sampling using sorbent traps. The results of the analysis are shown in Table 4.19. The two traps that were collected during steady-state conditions showed low mercury concentrations of 0.49 and 0.06 µg/dNm^3, with an average of 0.27 µg/dNm^3. This shows that the mercury control bed was working effectively and maintained low mercury concentrations during the test period.

Dräger tube samples were again taken for this run. The average concentration of the species measured with Dräger tubes is shown in Table 4.20. The contamination levels were significantly lower for this test than for the previous run on the FBG.

Table 4.19. Week 3 Mercury Sorbent Trap Data

Sample Time	Sample Location	Hg Concentration, μg/dNm^3
1/11/2011 14:12	Port C (cold side)	0.49
1/12/2011 14:03	Port C (cold side)	0.06
Average		0.27

Table 4.20. Dräger Tube Results Summary for Week 3

	Cold-Side Sampling		Sample Port C Hot Side		
	Sample Port A H_2S	Sample Port C H_2S	NH_3	HCN	HCl
Concentration, ppm	0.09	0.07	71	ND	ND

4.3.4 Membrane Results and Performance

Approximately 56 hours of continuous run time was achieved on all three membranes during the Week 3 test run. The EFG provided a very steady stream of syngas until it was shut down on December 13 because of a slag deposit on the bottom of the furnace tube. Figure 4.10 shows that flux rates near 100 scfh were achieved for the duration of the run on the FS membrane. The conditioning achieved in the previous week appeared to hold for this week's run as there was virtually no conditioning period. Issues with consistent flow measurement issues continued on the slipstream membranes, as shown in Figures 4.11 and 4.12. SS1 membrane produced near 100 sccm near the end of the run, and SS2 membrane produced 20–30 sccm toward the end. The measurements are considered suspect, and a Gilibrator was used in subsequent runs to measure the flow.

Table 4.21 shows that almost 40% of the incoming hydrogen was recovered in the FS membrane at a partial pressure differential near 40 psi. This is approximately half of the theoretical maximum recovery at this pressure. Hydrogen mass balance was low,

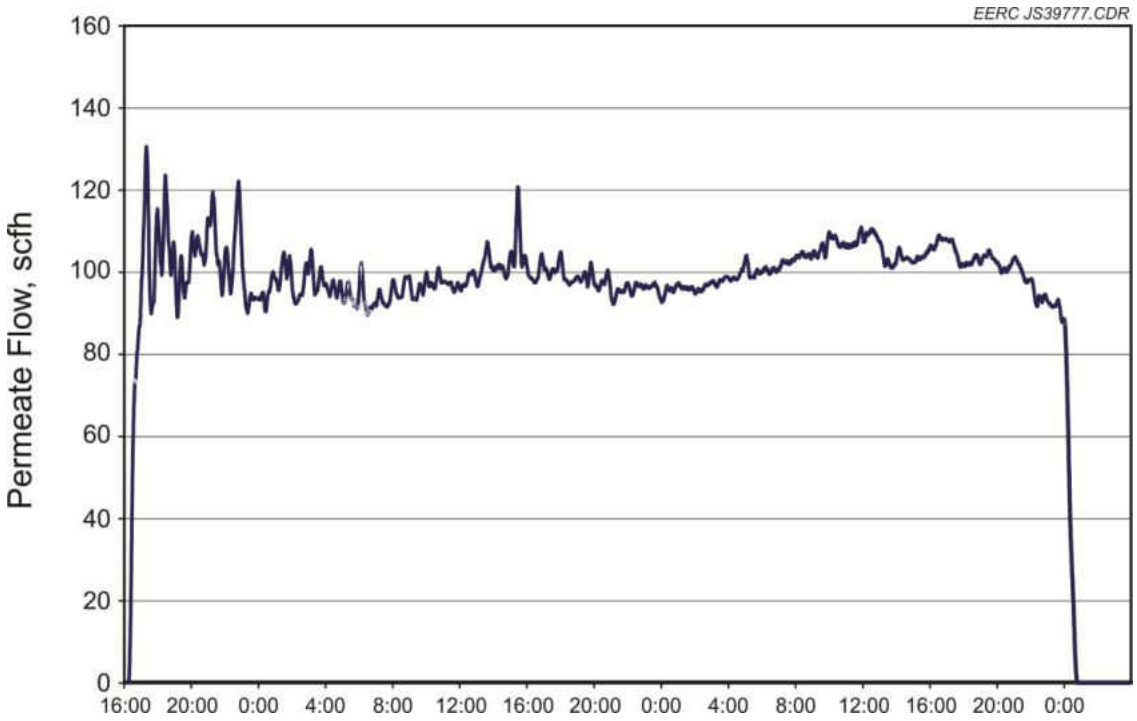

Figure 4.10. FS Membrane Permeate Flow Rate for Week 3.

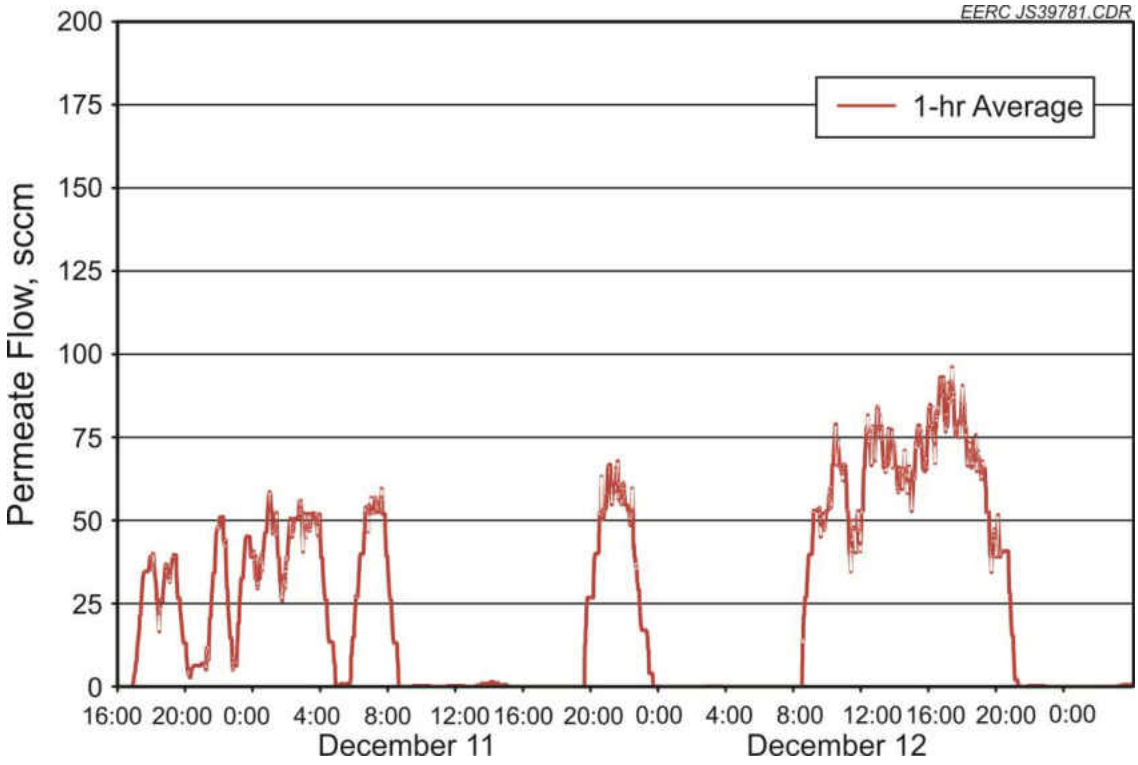

Figure 4.11. SS1 Membrane Permeate Flow Rate for Week 3.

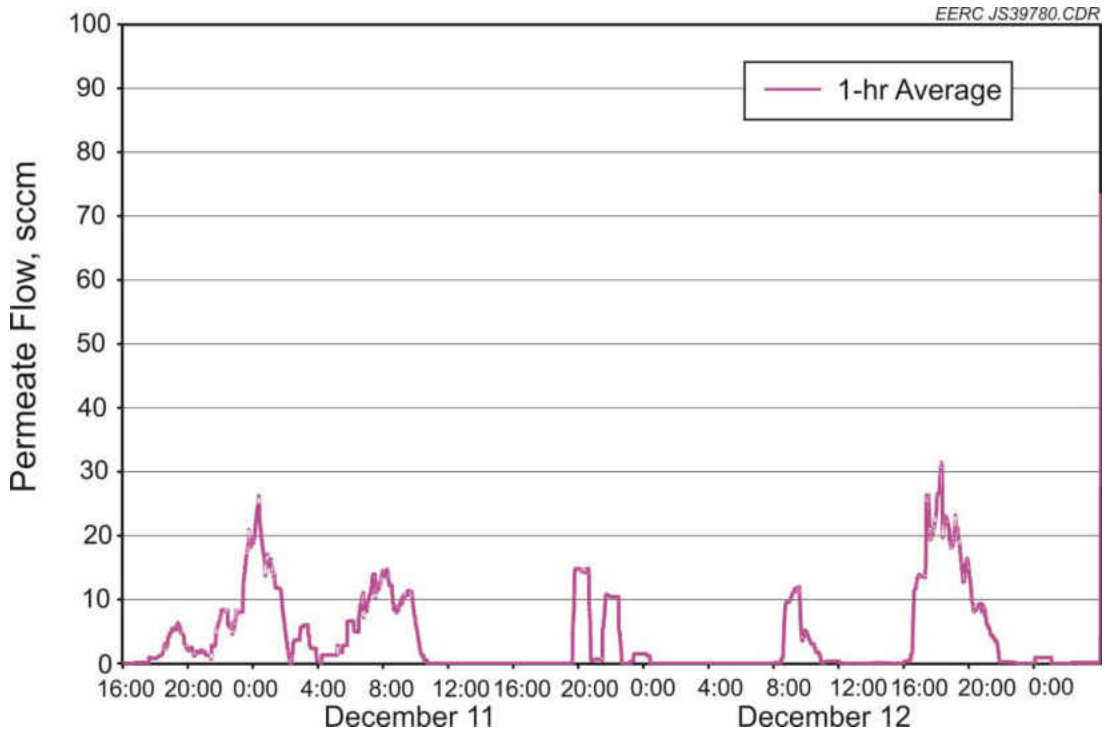

Figure 4.12. SS2 Membrane Permeate Flow Rate for Week 3.

Table 4.21. FS Membrane Performance Data for Week 3

	S.S. Period 1	S.S. Period 2	S.S. Period 3
	1/10 18:00 – 00:00	1/11 00:00 – 23:59	1/12 00:00 – 23:59
Heater Temperature, °F	650	650	650
Membrane Inlet, °F	589	587	587
Permeate Inlet, °F	601	600	600
Permeate Exit, °F	71	73	74
Syngas Inlet, °F	641	683	687
Syngas Inlet Pressure, psi	200	203	207
Permeate Pressure, in. H_2O	17	19	20
Flux, scfh/ft^2	7.4	7.0	7.3
H_2 Inlet, mol%	28.3	27.6	28.1
Wet H_2 Inlet, mol%	26.3	25.6	26.2
Raffinate H_2, mol%	15.9	14.5	13.9
Inlet H_2, scfh	273.0	256.9	260.7
Raffinate H_2, scfh	95.4	83.6	78.6
Permeate H_2, scfh	103.4	97.7	101.6
H_2 Balance, %	72.8	70.7	69.1
Hydrogen Recovery, %	37.8	38.1	39.0
Theoretical Max Recovery, %	79.3	78.7	80.0
Partial Pressure Differential, psi	41.0	40.2	42.7

averaging near 70% for the duration of the run. Table 4.22 shows very low recovery rates for SS1 membrane, but comparable flux rates to the FS membrane. The mass balance was good for this membrane. Table 4.23 shows low flux rates for SS2 membrane, but as stated earlier, the measurements are suspect and were reevaluated during the next run.

Table 4.22. SS1 Membrane Performance Data for Week 3

	S.S. Period 1	S.S. Period 2	S.S. Period 3
	1/10 18:00 – 00:00	1/11 00:00 – 23:59	1/12 00:00 – 23:59
Membrane Temperature, °F	752	739	738
Membrane Inlet, °F	795	781	770
Permeate Inlet, °F	131	139	142
Permeate Exit, °F	73	74	75
Raffinate Inlet, °F	401	537	549
Raffinate Exit, °F	74	75	76
Syngas Inlet, °F	645	683	687
Syngas Inlet Pressure, psi	200	203	207
Permeate Pressure, in. H_2O	13	12	14
Permeate Flow Rate, sccm	24	19	33
Raffinate Exit Pressure, in. H_2O	51	63	64
Raffinate Flow Rate, scfh	11	27	27
Flux, scfh/ft^2	3.1	2.5	4.3
H_2 Inlet, mol%	28.3	27.6	28.1
Wet H_2 Inlet, mol%	26.3	25.6	26.2
Raffinate H_2, mol%	25.8	25.9	26.0
Inlet H_2, scfh	3.2	7.4	7.6
Raffinate H_2, scfh	2.9	6.9	7.0
Permeate H_2, scfh	0.1	0.0	0.1
H_2 Balance, %	91.4	94.7	92.6
Hydrogen Recovery, %	1.6	0.8	1.1
Theoretical Max Recovery, %	79.4	78.6	80.0
Partial Pressure Differential, psi	41.2	40.4	42.9

Hydrogen flow across the membranes was investigated by plotting the membrane inlet and raffinate hydrogen concentrations for the Week 3 test period. Figure 4.13 plots the inlet and raffinate hydrogen concentrations across the three hydrogen membranes. The start of the data in Figure 4.13 coincides with the FS membrane being brought online. The raffinate hydrogen concentration quickly decreases which indicates hydrogen

flux through the membrane. The inlet hydrogen concentration remained consistent at approximately 27 mol% for the duration of the test period. The raffinate concentration reached equilibrium at approximately 15 mol%. This shows approximately a 12 mol% hydrogen flux through the membranes.

Table 4.23. SS2 Membrane Performance Data for Week 3

	S.S. Period 1	S.S. Period 2	S.S. Period 3
	1/10 18:00 – 00:00	1/11 00:00 – 23:59	1/12 00:00 – 23:59
Membrane Temperature, °F	879	871	892
Membrane Inlet, °F	699	726	796
Permeate Inlet, °F	86	89	90
Permeate Exit, °F	74	75	76
Raffinate Inlet, °F	441	514	565
Raffinate Exit, °F	74	75	76
Syngas Inlet, °F	641	683	687
Syngas Inlet Pressure, psi	200	203	207
Permeate Pressure, in. H_2O	11	11	13
Permeate Flow Rate, sccm	6	4	4
Raffinate Exit Pressure, in. H_2O	53	60	62
Raffinate Flow Rate, scfh	9	15	19
Flux, scfh/ft^2	0.31	0.21	0.20
H_2 Inlet, mol%	28.3	27.6	28.1
Wet H_2 Inlet, mol%	26.3	25.6	26.2
Raffinate H_2, mol%	27.2	26.6	26.4
Inlet H_2, scfh	2.6	4.3	5.4
Raffinate H_2, scfh	2.5	4.1	5.1
Permeate H_2, scfh H	0.006	0.004	0.004
H_2 Balance, %	96.1	97.0	93.8
Hydrogen Recovery, %	0.22	0.12	0.12
Theoretical Max Recovery, %	79.3	78.7	80.0
Partial Pressure Differential, psi	49.7	49.0	50.9

Table 4.24 displays the raffinate and permeate gas bag data for each of the hydrogen separation membranes tested during Week 3. The FS membrane had a hydrogen purity of 99.00 mol%, with only CO and nitrogen impurities present at concentrations of 0.99 and 0.01 mol%, respectively. The FS raffinate concentration from the gas bag data was slightly higher than the continuous sampling data but also shows

significant hydrogen flux through the FS membrane. The nitrogen present may be from air in-leakage during sampling or analysis.

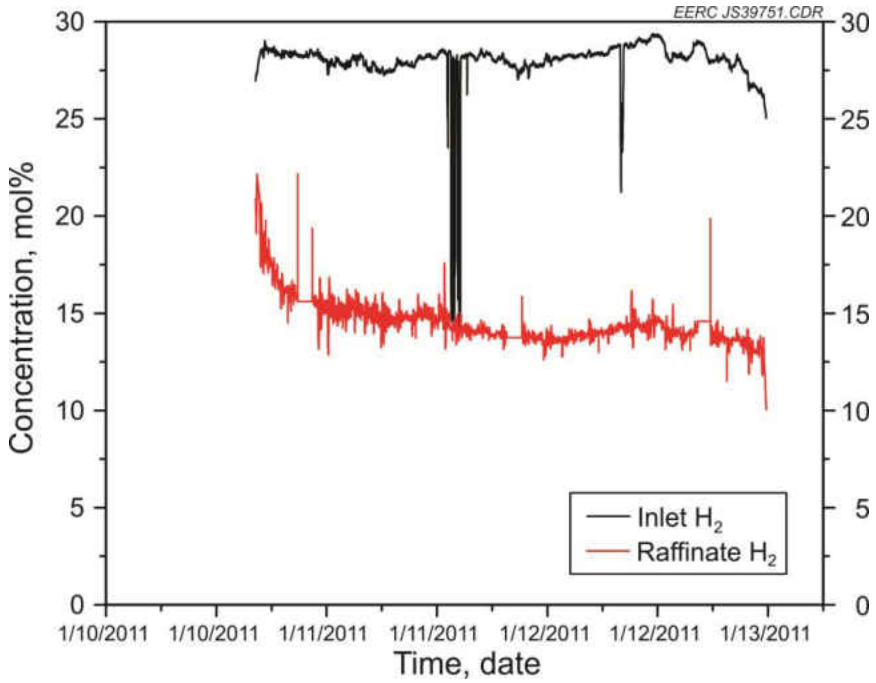

Figure 4.13. Week 3 FS Membrane Inlet and Raffinate Concentration Data.

Table 4.24. Week 3 Membrane Permeate and Raffinate Syngas Data

Membrane	H_2, mol%	CO, mol%	CO_2, mol%	N_2, mol%	CH_4, mol%	H_2S, ppmv
FS Permeate	99.00	0.01	ND	0.99	ND	<0.02
FS Raffinate	21.13	2.29	32.32	44.26	0.01	0.07
SS1 Permeate	99.02	0.02	0.01	0.96	ND	0.04
SS1 Raffinate	27.43	2.61	29.78	40.17	0.01	0.07
SS2 Permeate	40.78	1.6	20.93	36.69	0.01	0.07
SS2 Raffinate	28.18	2.63	29.5	39.68	0.01	0.07

The SS1 membrane also performed well during the Week 3 test run. The SS1 membrane permeate concentration was 99.02 mol%. The three impurities present in the permeate were CO, CO_2, and N_2 and concentrations of 0.02, 0.01 and 0.96 mol%, respectively. The SS1 raffinate hydrogen concentration of 27.43 mol% is similar to the

inlet concentration which indicates that the hydrogen recovery is fairly low through the membrane, but the hydrogen that does flow through has high purity.

The SS2 membrane also exhibited low hydrogen flux and a hydrogen purity only about 15 mol% higher than the inlet concentration. The permeate hydrogen concentration was only 40.78 mol% with high CO_2 and N_2 concentrations present. The permeate hydrogen concentration for this run was significantly higher than the previous run, and the difference in hydrogen concentration from the raffinate does indicate selective hydrogen transport.

4.4 Week 4 Testing – HPFBG

Testing for Week 4 was moved back to the HPFBG. The goal of this test was to get as much run time on the membranes as possible with coal-derived syngas. A new distributor plate was also used for this test to try and avoid the lower bed temperature excursions that were observed in the previous run on the HPFBG.

4.4.1 Test Plan

The target for this test was Condition 1 from the DOE test protocol (56). The gasifier was again intended to be run in a manner that allowed for consistent operation and high hydrogen production. The warm gas cleanup train was operated as shown in Table 4.3. One of the problems encountered during this run was that one of the filter vessel heaters stopped working. This made it difficult to inject high steam rates into the gasifier and, in turn, limited the amount of hydrogen that could be produced.

4.4.2 Gasifier Operations and Operating Data

Coal feed was started at 03:30 on January 24, 2011. System operation went relatively smooth, and all of the fixed beds were online by 14:36, and the membranes

were online by 15:35. The system ran well into the next day, but then a leak in the coal delivery auger packing developed near midday, and the system had to be shutdown at 11:45. The entire system had to be shut down to fix the problem, and all of the membranes were not online until 01:40 on January 26. The system ran well for the rest of the week with the exception of a brief upset on January 27 that caused the membranes to be offline for about an hour. The system was then shut down in a controlled manner on the morning of January 28. Gasifier operations data are shown in Table 4.25.

The lower fluidized bed was run near 843°C (1550°F) for the duration of the test run. An additional oxygen/steam superheater was brought online midweek which increased the temperature of the lower bed. The freeboard section of the reactor was run between 795° and 824°C (1463 and 1515°F), and the reactor extension was run at a lower temperature earlier in the week but a higher temperature later in the week. The heaters in that section were increased to try to carry more heat to the filter vessel, which had one heater out. As can be seen by the filter vessel temperatures, a significant increase in temperature was observed later in the week.

The fixed beds were run in a similar manner as the previous weeks testing. Bulk Desulfurization Bed 2 was used originally, but breakthrough occurred so Bed 1 was brought online midweek. Bed 1 was not fully regenerated; therefore, breakthrough was observed after a couple of days, and Bed 2 was brought online again on the evening of January 27. Despite these upsets, no sulfur was detected at the polishing bed outlet, and these results will be discussed in more detail in the next section.

Coal feed rate ranged from approximately 9 to 11 lb/hr during the test run according to the feeder scale measurement. Primary nitrogen was not used for the test;

Table 4.25. Gasifier Operations Data for Week 4 (HPFBG)

	Pre-membrane	Membrane Online	Pre-membrane	Membrane Online	Membrane Online
Start Date	1/24/2011	1/24/2011	1/25/2011	1/26/2011	1/27/2011
Start Time	12:00	18:00	22:30	4:00	18:30
End Date	1/24/2011	1/25/2011	1/26/2011	1/27/2011	1/28/2011
End Time	15:00	11:45	1:15	15:15	7:40
FBG Temp., °F					
O_2/Steam Inlet	380	382	397	653	678
Recycle Inlet	547	562	563	579	535
Lower Reactor Bed	1541	1548	1549	1576	1571
Upper Reactor Bed	1490	1495	1497	1520	1506
Lower Freeboard	1464	1463	1466	1480	1470
Upper Freeboard	1499	1510	1515	1517	1511
Reactor Extension	1307	1304	1309	1325	1431
Cyclone Exit	1001	1012	1026	1041	1132
Filter Vessel Temp., °F					
FV Inlet	553	557	516	789	836
FV Outlet	690	663	658	686	685
Packed Bed Temp., °F					
Bulk Sulfur Removal	562	571	591	605	589
High-Temperature Shift Catalyst	615	628	616	623	624
Sulfur Polishing	504	520	502	515	522
Chlorine Guard, Mercury Control	382	415	408	422	427
Low-Temperature Shift Catalyst	428	385	332	393	396
Quench Pot Temp., °F					
West Pot 1 Inlet	448	469	480	484	484
West Pot 3 Outlet	86	83	103	94	78
East Pot 1 Inlet	84	82	100	92	78
East Pot 3 Outlet	54	57	56	57	55
Flows					
Coal Feed Rate, lb/hr	9.5	9.7	11.3	9.1	11.2
Primary Nitrogen, scfh	0	0	0	0	0
Oxygen, scfh	90	90	80	76	85
Steam, lb/hr	17	17	16	17	17
Recycle Gas, lb/hr	11	13	10	15	10
Nitrogen Purge, scfh	6	7	6	11	11
Product Gas, scfh	280	101	222	75	114
Closure, %	241	87	192	65	93
Pressure, psi					
HPFBG Top	231	228	229	228	227
HPFBG Bottom	229	226	227	226	225
Filter Vessel	227	224	221	223	222
Quench Pot	216	209	209	207	201
Recycle Gas Surge Tank	800	800	800	800	846

therefore, steam and recycle gas rates were kept high to ensure adequate bed velocity. Nitrogen purge rates were kept to a minimum, which resulted in very low nitrogen content in the syngas. Closure dropped significantly during hydrogen separation testing, which indicates good hydrogen production rates but was also caused by the significant leak in the coal delivery auger packing.

Pressure was maintained at 230 psi in the gasifier, and dropped to just above 200 psi in the quench pot location. The pressure into the membrane was throttled to just below 200 psi.

4.4.3 Warm-gas Cleanup Results

Table 4.26 displays the syngas composition for the Week 4 test period. The syngas composition is different than the Week 2 and 3 test runs because the Week 4 test run was conducted on the FBG. GC and LGA data were utilized to determine bulk and trace syngas analyte concentrations across the warm-gas cleanup system. When the bulk desulfurizer was brought online, the sulfur concentrations decreased from 430 ppmv to below Dräger tube detection limits. A significant increase in hydrogen and CO_2 concentration was observed when the high-temperature WGS catalyst was brought online. The hydrogen and CO_2 concentrations increased by 16 and 12 mol%, respectively, and the CO concentration decreased by 3 mol%. The sulfur polishing bed further decreased the sulfur concentration to 0.609 ppmv, which yielded a total sulfur removal of 99.86%. After the chlorine guard/mercury control bed was brought online, the chlorine concentrations were reduced to below Dräger tube detection levels. The mercury concentration was slightly higher than the other test runs with an average concentration

of 5.35 µg/dNm^3. The low-temperature WGS catalyst increased the hydrogen and CO_2 concentrations by 1–2 mol% and decreased the CO concentration by 3 mol%.

Table 4.26. Week 4 Syngas Composition (HPFBG)

Sample Point	H_2, mol%	CO, mol%	CO_2, mol%	N_2, mol%	CH_4, mol%	H_2S, ppmv	H_2/CO Ratio
Bulk Desulfurizer Inlet RVS-1, Bed 1	26.6	7.34	14.1	50.87	2.49	430	3.62
Bulk Desulfurizer Outlet RVS-1, Bed 1	22.48	9.28	25.03	45.57	3.25	ND	2.42
High Temp Shift Catalyst Outlet, Bed 3	38.81	6.11	37.02	2.09	6.36	ND	6.35
Sulfur Polishing Bed Outlet, Bed 4	34.81	3.31	34.97	21.86	4.97	0.609	10.52
Chlorine Guard/Mercury Control Outlet, Bed 5	34.92	4.27	34.59	21.7	5.00	0.558	8.18
Low Temp Shift Catalyst Outlet, Bed 6	36.54	1.06	35.42	20.7	4.74	0.675	34.47

Figure 4.14 plots the steady-state syngas composition data after the warm-gas cleanup systems are online. The data are fairly constant except for a brief system upset on January 27, 2011. The steady syngas mainly comprised hydrogen and CO_2. The step change in syngas concentrations January 27, 2011, was due to a coal feed rate increase. The trace syngas constituents remained low during the test period and showed little deviation during the steady-state conditions.

Mercury data were collected to measure the mercury concentrations at the Port C sampling location, which is after the mercury control column and before the hydrogen separation membranes. Sampling at this location determines the effectiveness of the mercury control column and measures the mercury concentrations that are seen by the hydrogen separation membranes. Mercury concentrations were determined by syngas sampling using sorbent traps.

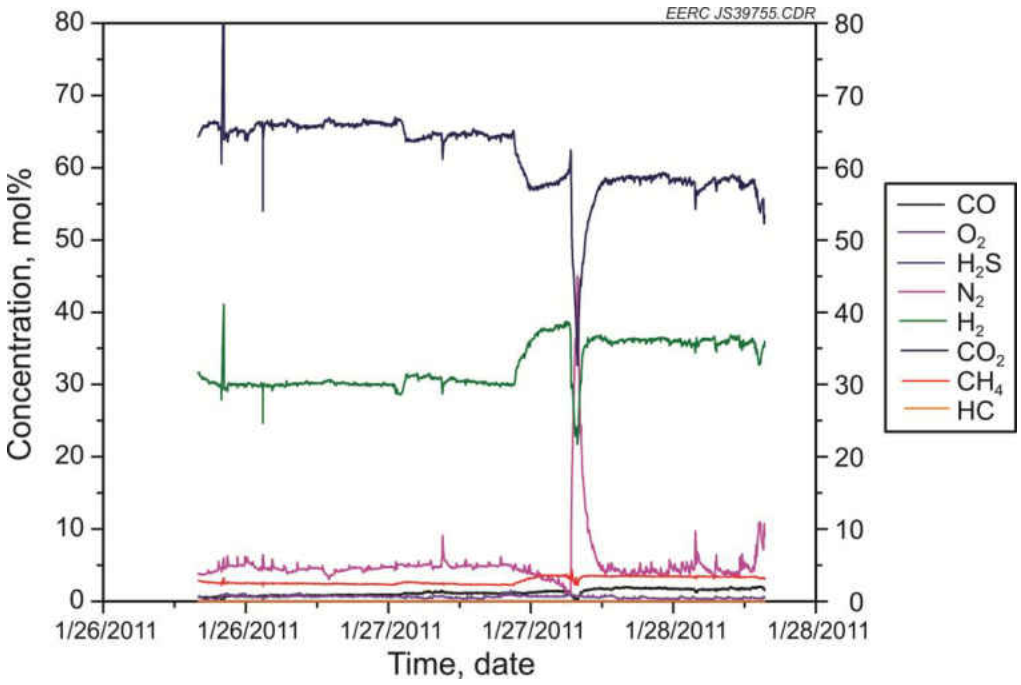

Figure 4.14. Week 4 Syngas Data.

Table 4.27 displays the mercury sorbent trap data for the Week 4 test period. The sorbent traps collected during steady-state conditions showed higher mercury concentrations than previously observed, and a mercury removal of 73.2% was observed based on these data.

In addition to mercury data, trace element data were collected at the Port C sampling location using a multielement sorbent trap (ME-ST) method. The method is currently being developed under the EERC's Center for Air Toxic Metals® Program to serve as an alternative to U.S. Environmental Protection Agency (EPA) Method 29. The ME-ST method collects the trace elements of interest on a sorbent trap and is later analyzed using a proprietary process. The ME-ST data collected during the Week 4 test period are presented in Table 4.28. Of the hazardous air pollution (HAP) elements analyzed, Sb, Be, and Se were not detected above the detection limit of the method. As, Cd, Cr, Co, Pb, Mn, Hg, and Ni were present in the samples at various concentrations. Cr,

Mn, and Ni were present at the highest concentrations. The concentration of the detected trace elements ranged from 0.40 μg/dNm^3 for Cd to 191.6 μg/dNm^3 for Ni. Elements contained in stainless steel such as nickel may not be derived from the coal, but none the less have the potential to impact membrane performance if they are deposited on the surface.

Average removal efficiency of the trace elements was calculated based on the concentration of the elements in Antelope coal, coal feed rate, and syngas flow rate. Syngas flow rate was estimated from the permeate flow, product gas flow, and recycle syngas flow. Coal feed rates were taken as an average during the sampling times. Trace element removal across the warm gas cleanup train was shown to be greater than 90% for all of the detected elements. Mercury and chromium had the lowest removals at 93% and 92% respectively. These data indicate that the warm gas cleanup train is capable of removing more than 90% of the trace metals from the syngas stream.

Table 4.27. Week 4 Mercury Sorbent Trap Data

Sample Time	Sample Location	Hg Concentration, μg/dNm^3
1/25/2011 10:37	Port C (cold side)	3.68
1/26/2011 11:14	Port C (cold side)	4.64
1/27/2011 14:41	Port C (cold side)	7.73
Average		5.35

Table 4.28. Week 4 Trace Element Data (Sample Port C)

	μg/dNm^3										
Sample Time	Sb	As	Be	Cd	Cr	Co	Pb	Mn	Hg	Ni	Se
1/26/2011 9:32	ND	13.2	ND	0.36	276.2	5.9	3.9	237.8	1.0	284.5	ND
1/26/2011 15:41	ND	12.8	ND	0.62	76.8	3.5	3.6	32.5	0.6	55.4	ND
1/27/2011 9:23	ND	13.5	ND	0.35	89.7	3.3	3.7	52.9	2.2	235.0	ND
Average	ND	13.2	ND	0.40	147.6	4.2	3.8	107.7	1.3	191.6	ND
Removal Eff. %	NA	97.9	NA	98.4	92.1	99.2	99.5	98.0	93.0	94.7	ND

Dräger tube samples were also collected through the week to monitor trace species, and the average through the week is shown in Table 4.29. Sample Port A indicated higher readings than previous weeks because some sulfur breakthrough had

occurred in the first fixed bed and the secondary bed was brought online. H_2S at Sample Port C was very low for the week. Ammonia levels were similar to previous weeks on the FBG, and HCN and HCl were very low.

Table 4.29. Dräger Tube Results Summary for Week 4

	Cold-Side Sampling		Sample Port C Hot Side		
	Sample Port A H_2S	Sample Port C H_2S	NH_3	HCN	HCl
Concentration, ppm	0.41	0.01	2000	ND	0.17

4.4.4 Membrane Results and Performance

Figure 4.15 shows the variable membrane performance during Week 4, which was caused by variation in the gasifier operation, and system downtime. The most consistent flux was achieved toward the end of the run during Steady-State Period 3. Lower partial pressure differential was observed for this run, resulting in lower average flux rates for the FS membrane than in previous runs.

A Gilibrator for low flow measurement was used for the slipstream membranes during this run. Figure 4.16 shows that the gas meter was not capable of detecting flow during the run, but the Gilibrator indicated an average flow rate near 200 sccm during the latter half of the test. The Gilibrator also indicated that the SS2 membrane flux was significantly higher than what was indicated by the gas meter. Figure 4.17 shows that flux averaged near 140 sccm during the early part of the run and near 120 sccm during the latter part of the run.

Table 4.30 shows that hydrogen recovery was near 48% during Steady-State Period 1 on the FS membrane. This is good recovery considering the partial pressure differential was only 28.2 psi and the maximum recovery possible was 70.6%. The hydrogen balance was again somewhat low for this run.

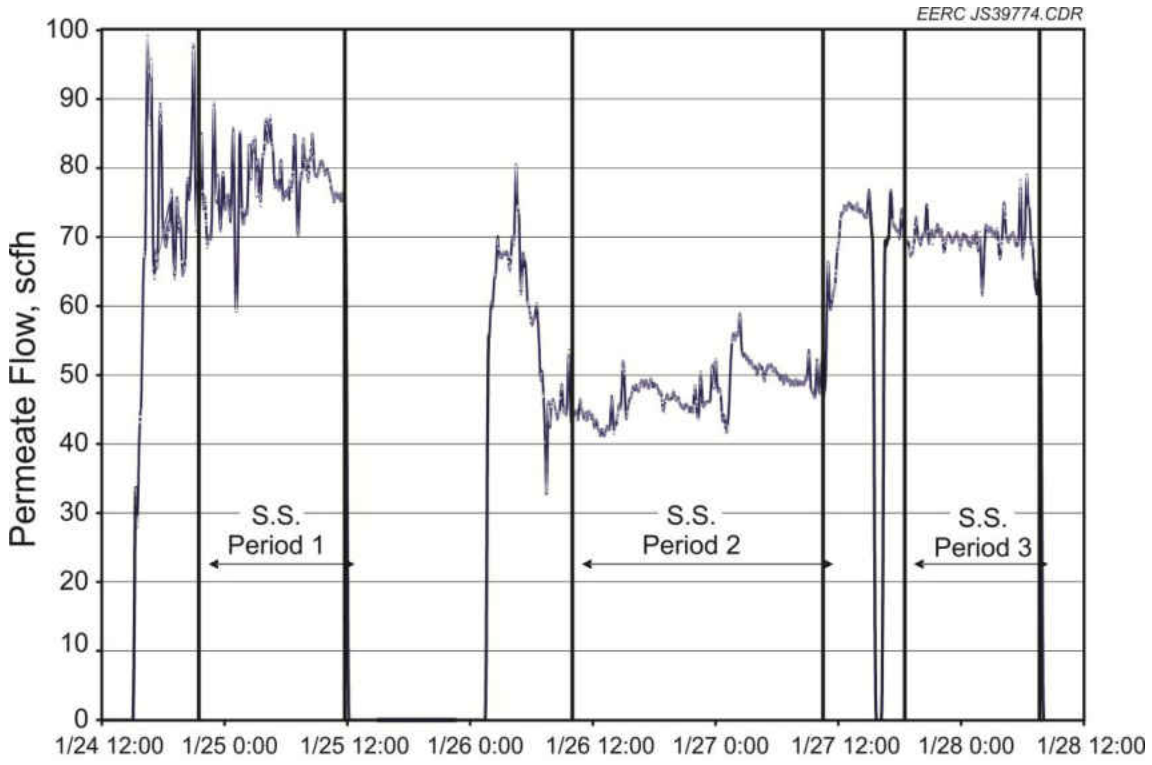

Figure 4.15. FS Membrane Permeate Flow Rate during Week 4.

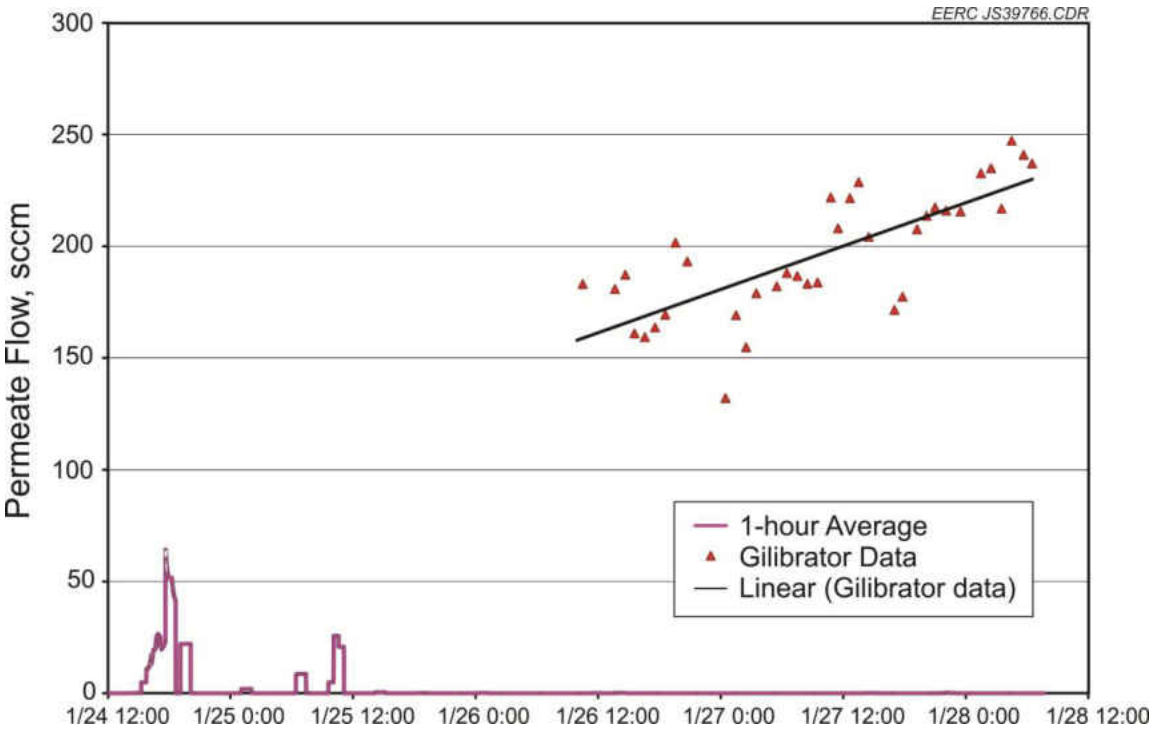

Figure 4.16. SS1 Membrane Permeate Flow Rate during Week 4.

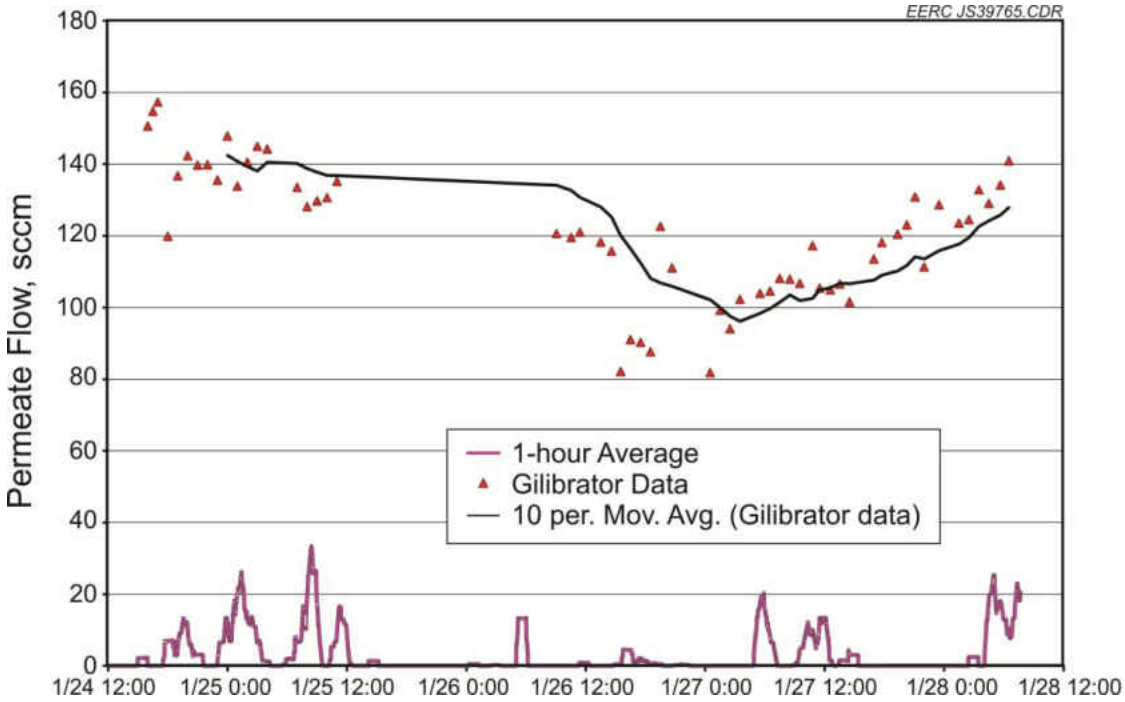

Figure 4.17. SS2 Membrane Permeate Flow for Week 4.

Table 4.30. FS Membrane Performance Data for Week 4

	S.S. Period 1	S.S. Period 2	S.S. Period 3
	1/24 17:30 – 1/25 10:30	1/26 10:00 – 1/27 10:30	1/27 18:30 – 1/28 07:40
Membrane Heater, °F	650	650	650
Membrane Inlet, °F	578	593	595
Permeate Inlet, °F	593	605	606
Permeate Exit, °F	74	79	78
Syngas Inlet, °F	717	698	703
Syngas Inlet Pressure, psi	212	211	210
Permeate Pressure, in. H_2O	16.8	13.8	15.3
Flux, scfh/ft^2	5.5	3.4	5.0
H_2 Inlet, mol%	30.2	30.2	35.9
Wet H_2 Inlet, mol%	19.2	15.7	18.6
Raffinate H_2, mol%	24.1	18.4	21.0
Inlet H_2, scfh	176.2	139.0	159.1
Raffinate H_2, scfh	77.9	55.5	52.1
Permeate H_2, scfh	77.1	47.8	69.8
H_2 Balance, %	89.3	75.4	76.8
Hydrogen Recovery, %	47.6	36.9	44.2
Theoretical Max Recovery, %	70.6	62.4	69.0
Partial Pressure Differential, psi	28.2	20.3	26.7

Table 4.31 shows the flux rates achieved in SS1 membrane, using first the dry gas meter and then the Gilibrator for Periods 2 and 3. The flux rates measured with the Gilibrator are very good. Hydrogen recovery rates are still very low, indicating the incoming feed rates may have been too high. The flux rate measurements were also greatly improved for the SS2 membrane using the Gilibrator, as shown in Table 4.32. However, hydrogen purity was low for the SS2 membrane, so it is unclear how much of the gas is derived from flux in the membrane or from a potential leak.

Table 4.31. SS1 Membrane Performance Data for Week 4

	S.S. Period 1	S.S. Period 2	S.S. Period 3
	1/24 21:30 – 1/25 11:45	1/26 10:00 – 1/27 10:30	1/27 18:30 – 1/28 07:40
Membrane Temperature, °F	731	729	729
Membrane Inlet, °F	688	683	686
Permeate Inlet, °F	141	139	143
Permeate Exit, °F	75	80	79
Raffinate Inlet, °F	613	615	633
Raffinate Exit, °F	76	80	79
Syngas Inlet, °F	716	698	703
Syngas Inlet Pressure, psi	212	211	211
Permeate Pressure, in. H_2O	10.6	9.3	11.5
Permeate Flow Rate, sccm	6.3	178*	217*
Raffinate Exit Pressure, in. H_2O	62.7	60.4	62.1
Raffinate Flow Rate, scfh	28.7	27.8	30.9
Flux, scfh/ft^2	0.8	23.4*	28.5*
H_2 Inlet, mol%	30.1	30.2	35.9
Wet H_2 Inlet, mol%	19.1	15.7	18.8
Raffinate H_2, mol%	37.1	30.0	35.1
Inlet H_2, scfh	8.7	8.8	11.5
Raffinate H_2, scfh	10.6	8.3	10.8
Permeate H_2, scfh	0.01	0.38*	0.46*
H_2 Balance, %	123.6	99.3	97.9
Hydrogen Recovery, %	0.1	5.3	4.0
Theoretical Max Recovery, %	70.4	62.2	69.6
Partial Pressure Differential, psi	28.3	20.5	27.2

* Denotes data obtained from Gilibrator measurements.

Hydrogen flow across the membranes was investigated by plotting the membrane inlet and raffinate hydrogen concentrations for the Week 4 test period. Figure 4.18 plots

the inlet and raffinate hydrogen concentrations across the FS membrane. The difference between the inlet and raffinate hydrogen concentration remained consistent throughout the test period, which indicates consistent hydrogen flux through the membranes. On average, approximately 13 mol% of hydrogen was able to pass through the membrane.

Table 4.32. SS2 Membrane Performance Data for Week 4

	S.S. Period 1	S.S. Period 2	S.S. Period 3
	1/24 21:30 – 1/25 11:45	1/26 10:00 – 1/27 10:30	1/27 18:30 – 1/28 07:40
Membrane Temperature, °F	853	871	873
Membrane Inlet, °F	763	720	726
Permeate Inlet, °F	92	99	98
Permeate Exit, °F	76	81	80
Raffinate Inlet, °F	614	499	489
Raffinate Exit, °F	76	81	80
Syngas Inlet, °F	716	698	703
Syngas Inlet Pressure, psi	212	211	211
Permeate Pressure, in. H_2O	9.2	6.8	8.4
Permeate Flow Rate, sccm	137.8*	104.2*	127.1*
Raffinate Exit Pressure, in. H_2O	61.5	50.9	51.5
Raffinate Flow Rate, scfh	21.5	6.9	6.6
Flux, scfh /ft^2	7.6*	6.1*	11.8*
H_2 Inlet, mol%	30.1	30.2	35.9
Wet H_2 Inlet, mol%	19.1	15.7	18.8
Raffinate H_2, mol%	32.3	30.0	30.2
Inlet H_2, scfh	6.6	2.2	2.6
Raffinate H_2, scfh	6.9	2.1	2.0
Permeate H_2, scfh	0.15*	0.12*	0.23*
H_2 Balance, %	107.3	99.3	85.5
Hydrogen Recovery, %	2.3	5.5	9.1
Theoretical Max Recovery, %	70.5	62.4	69.8
Partial Pressure Differential, psi	35.7	27.4	29.5

* Denotes data obtained from Gilibrator measurements.

The data presented in Table 4.33 show that hydrogen flux was different for each of the membranes tested. The FS membrane had a very high hydrogen flux for this test period because the raffinate hydrogen concentration was only 6.95 mol%. The purity of the FS permeate was also very high with a hydrogen purity of 99.94 mol% with only CO_2 and N_2 impurities present at concentrations of 0.05 and 0.01 mol%. Because of the high

hydrogen flux through the membrane, the raffinate stream was predominantly CO_2, with a concentration of 78.85 mol%.

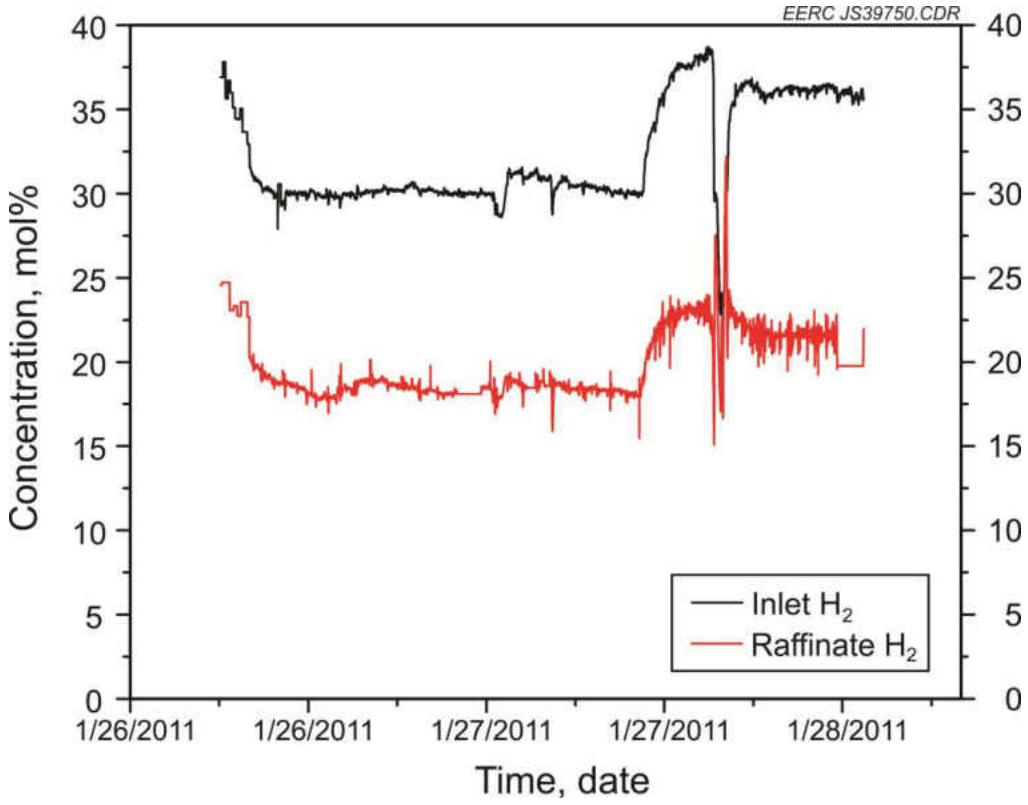

Figure 4.18. Week 4 FS Membrane Inlet and Raffinate Concentration Data.

Table 4.33. Week 4 Membrane Permeate and Raffinate Syngas Data

Membrane	H_2, mol%	CO, mol%	CO_2, mol%	N_2, mol%	CH_4, mol%	H_2S, ppmv
FS Permeate	99.94	ND	0.05	0.01	ND	<0.020
FS Raffinate	6.95	4.26	78.85	ND	9.61	0.654
SS1 Permeate	97.68	0.12	1.52	0.56	0.11	<0.020
SS1 Raffinate	34.03	1.38	57.97	1.56	4.98	0.652
SS2 Permeate	59.74	0.86	34.59	2.24	2.48	0.685
SS2 Raffinate	31.18	1.5	60.47	1.19	5.45	0.656

The SS1 membrane also had a fairly high hydrogen purity during the Week 4 test period with a purity of 97.68 mol%. The other syngas species present included CO, CO_2, N_2, and methane. The flux was fairly low through the SS1 membrane with a raffinate concentration that was similar to the inlet hydrogen concentration.

The SS2 membrane had low hydrogen flux but saw an increase in hydrogen purity compared to the Week 3 data. The permeate hydrogen purity increased to 59.7 mol%, which is a 19 mol% increase in hydrogen purity compared to the Week 3 data. The main impurity present was CO_2 at a concentration of 34.59 mol%.

4.5 Week 5 Testing – HPFBG

Testing in Week 5 occurred on the FBG, with the operational strategy presented in Table 4.3. This time, the system pressure was increased to just over 300 psi in order to try to get more flux through the membranes. This change also required that SS2 membrane was taken offline, because it was only capable of operation up to 200 psi.

4.5.1 Test Plan

The test plan was very similar to the test plan for the previous weeks, with the exception of the increased pressure in the system. This increased pressure did result in some operational changes for the FBG to maintain a velocity of approximately 0.9 ft/sec. The modified run conditions are shown in Table 4.34. The warm gas cleanup strategy followed the protocol in Table 4.3. The main goal of the run was to get the fixed beds online and achieve as many run hours as possible on each of the hydrogen separation membranes.

Table 4.34. Planned Run Conditions for Week 5 Testing

	Type *	Time, h	Coal Feed Rate, lb/hr	Temp., °C	Fluid. Velocity, ft/sec	H_2O/ Coal Wt Ratio	Steam Flow, g/hr	O_2 to C molar ratio	O_2 Flow, scfh	N_2 Flow for AB, scfh	Recycle or Nitrogen Flow Rate, scfh
Start-Up	AB	5	11	843	0.9	0.4	1998	0.6	104	496	186.5
Operation	OB	100	11	843	0.9	1.3	6492	0.6	104	0	474.3

*AB = air-blown and OB = oxygen blown.

4.5.2 Gasifier Operations and Operating Data

Coal feed for the Week 5 test started on January 30, 2011, at 22:30. All of the fixed beds were online by 08:30 on January 31, and flow to the membranes started at

12:30 that day. The system ran well until 07:30 the next day, when it was taken down because of a coal feed delivery auger packing leak. The system was repaired, and the membranes were brought back online at 19:00 on February 1. The system was again shut down the following morning because the auger packing was still leaking. After an extensive repair, the system was brought back online again at 18:00 on February 2 and ran for the rest of the week without significant issues. The gasifier operating data are shown in Table 4.35.

Reactor temperatures were held near 843°C (1550°F) in the lower fluid-bed section and mainly between 760° and 816°C (1400° and 1500°F) in the rest of the reactor. Filter vessel temperatures were over 316°C (600°F) at the outlet. The fixed-bed reactors were held at similar set points as the previous runs. The backup fixed bed for bulk desulfurization was brought online February 3. No detectable sulfur breakthrough was observed from the polishing bed.

Coal feed rate was slightly higher for this run than previous tests because the increase in pressure also requires the gasifier to be run with a higher standard volumetric flow to maintain bed velocity. The recycle rate was also increased significantly to maintain bed velocities. Product gas was significantly reduced while the membranes were online because of significant flux.

Gasifier pressure was held steady near 310 psi throughout the run. Pressure at the quench pots (and the membranes) was in the 280 to 290 psi range.

4.5.3 Warm-gas Cleanup Results

Table 4.36 displays the syngas composition for the Week 5 test period as each of the warm-gas cleanup systems are brought online. The syngas composition is very similar

Table 4.35. Gasifier Operating Data for Week 5 (HPFBG)

	Pre-membrane	Membrane Online	Pre-membrane	Membrane Online	Pre-membrane	Membrane Online
Start Date	1/31/2011	1/31/2011	2/1/2011	2/1/2011	2/2/2011	2/2/2011
Start Time	8:30	14:00	17:30	19:30	17:50	21:00
End Date	1/31/2011	2/1/2011	2/1/2011	2/2/2011	2/2/2011	2/4/2011
End Time	12:00	7:00	18:45	6:50	19:30	8:00
FBG Temp., °F						
O_2/Steam Inlet	685	686	686	685	670	684
Recycle Inlet	592	592	608	603	607	603
Lower Reactor Bed	1543	1541	1502	1541	1576	1578
Upper Reactor Bed	1486	1485	1404	1456	1503	1504
Lower Freeboard	1457	1458	1393	1444	1471	1457
Upper Freeboard	1467	1476	1435	1469	1487	1477
Reactor Extension	1437	1439	1428	1438	1432	1433
Cyclone Exit	1169	1172	1152	1158	1142	1153
Filter Vessel Temp., °F						
FV Inlet	827	889	853	875	869	859
FV Outlet	636	655	677	691	687	686
Packed Bed Temp., °F						
Bulk Sulfur Removal	606	616	616	630	615	617
High-Temperature Shift Catalyst	577	580	591	608	586	634
Sulfur Polishing	540	544	535	576	512	579
Chlorine Guard, Mercury Control	450	460	420	478	443	481
Low-Temperature Shift Catalyst	400	411	372	413	441	413
Quench Pot Temp., °F						
West Pot 1 Inlet	500	506	486	504	454	506
West Pot 3 Outlet	120	117	116	111	109	119
East Pot 1 Inlet	117	113	112	108	106	115
East Pot 3 Outlet	55	57	55	56	61	58
Flows						
Coal Feed Rate, lb/hr	11.1	10.9	11.2	11.0	11.0	11.4
Primary Nitrogen, scfh	0	0	0	0	0	0
Oxygen, scfh	92	92	92	92	92	91
Steam, lb/hr	16	16	16	16	16	17
Recycle Gas, lb/hr	29	36	25	30	21	26
Nitrogen Purge, scfh	0	0	0	0	0	0
Product Gas, scfh	177	71	172	91	211	126
Closure, %	162	61	148	75	185	104
Pressure, psig						
FBG Top	311	311	312	312	311	311
FBG Bottom	309	309	309	309	309	309
Filter Vessel	305	305	306	305	306	305
Quench Pot	282	279	286	283	290	283
Recycle Gas Surge Tank	800	800	800	800	800	800

Table 4.36. Week 5 Syngas Composition (HPFBG)

Sample Point	H_2, mol%	CO, mol%	CO_2, mol%	N_2, mol%	CH_4, mol%	H_2S, ppmv	H_2/CO Ratio
Bulk Desulfurizer Inlet RVS-1, Bed 1	27.3	17.56	40.93	6.16	2.8	1200	1.55
Bulk Desulfurizer Outlet RVS-1, Bed 1	27.25	18.43	42.71	3.32	2.89	2.172	1.48
High-Temp. Shift Catalyst Outlet, Bed 3	33.33	8.96	48.36	0.85	2.95	2.172	3.72
Sulfur Polishing Bed Outlet, Bed 4	32.64	8.32	47.97	2.51	2.97	0.175	3.92
Chlorine Guard/Mercury Control Outlet, Bed 5	33.08	7.76	48.76	1.79	2.95	0.158	4.26
Low-Temp. Shift Catalyst Outlet, Bed 6	35.86	3.82	51.87	1.32	2.93	0.158	9.39

to the Week 4 syngas composition and utilized the same FBG. GC and LGA data were utilized to determine bulk and trace syngas analyte concentrations across the warm-gas cleanup system. When the bulk desulfurizer was brought online, the sulfur concentrations decreased from 1200 to 2.172 ppmv, which is a removal of 99.82%. The high-temperature WGS catalyst yielded a 9 mol% decrease in CO concentration and a 6 mol% increase in H_2 and CO_2 concentrations. The H_2/CO ratio increased from approximately 1.5 to 4 when the shift catalyst was brought online. The sulfur polishing bed further reduced the H_2S concentration down to 0.175 ppmv, which yields a total sulfur removal of 99.99% across the two sulfur beds. After the chlorine guard/mercury control bed was brought online, the chlorine concentrations were reduced to below Dräger tube detection levels. The mercury concentration was slightly higher than previous runs, with an average concentration of 2.90 $\mu g/dNm^3$. The low-temperature WGS catalyst increased the H_2 and CO_2 concentrations by 3 mol% and decreased the CO concentration by 4 mol%.

Figure 4.19 plots the steady-state syngas composition data for the Week 5 test period. The data set is limited because of two system upsets that occurred during the

middle of the test period. The trace syngas constituents remained consistently low throughout the test period, which indicates that the warm-gas cleanup system maintained consistent removals throughout the test period. The H_2 and CO_2 concentrations exhibited some variation over the course of the test period, but stayed within a 5 mol% range.

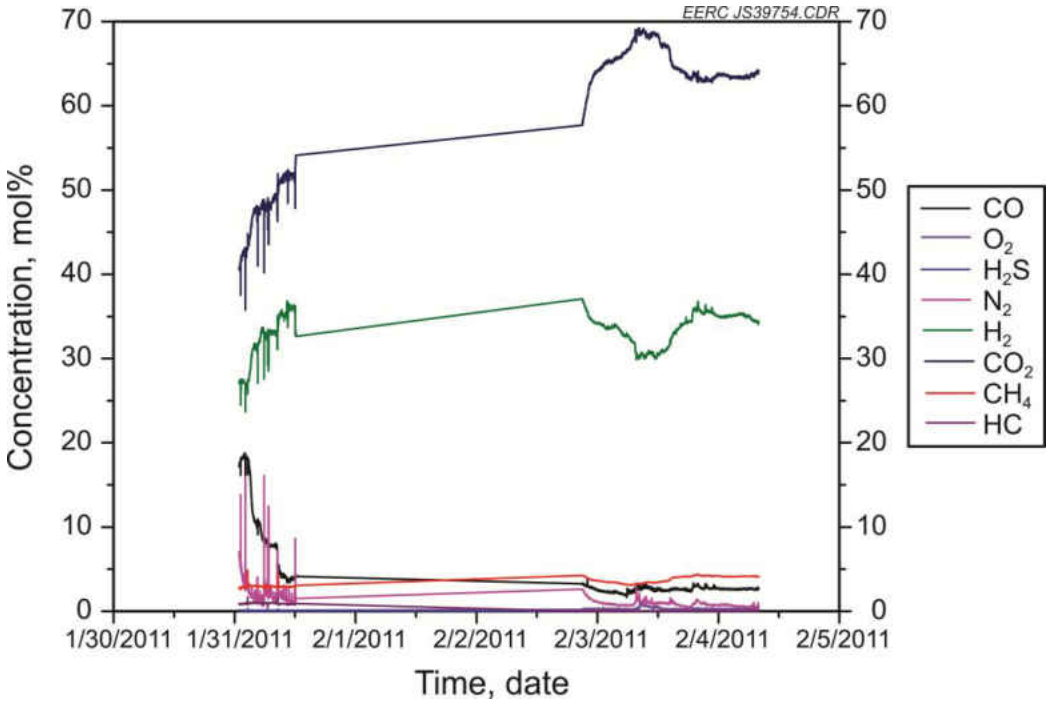

Figure 4.19. Week 5 Syngas Data.

Mercury data were collected to measure the mercury concentrations at the Port C sampling location, after the mercury control column and before the hydrogen separation membranes. Sampling here determined the effectiveness of the mercury control column and measured the mercury concentrations seen by the hydrogen separation membranes. Mercury concentrations were determined by syngas sampling using sorbent traps.

Table 4.37 displays the mercury sorbent trap data for the Week 5 test period. The Week 5 mercury sorbent trap data yielded a mercury removal that was more consistent with Week 2 and Week 3 testing and had an average mercury removal of 85.5%.

Trace element data were also collected at sample port C during the Week 5 test period using the ME-ST sampling technique. Table 4.38 displays the trace element data for the Week 5 test period. Of the HAP elements analyzed, Sb, Be, and Se were not detected above the detection limit of the method. As, Cd, Cr, Co, Pb, Mn, Hg, and Ni were present in the samples at various concentrations. The concentrations of the trace elements were similar to the Week 4 data, with the exception of Mn remaining low for all of the sampling times.

Average removal efficiency of the trace elements was calculated based on the concentration of the elements in Antelope coal, coal feed rate, and syngas flow rate. Syngas flow rate was estimated from the permeate flow, product gas flow, and recycle syngas flow. Coal feed rates were taken as an average during the sampling times. Trace element removal across the warm gas cleanup train was shown to be greater than 90% for all of the detected elements. Mercury, nickel and chromium had the lowest removals, and it is likely that the nickel is derived from the stainless steel tubing. These data indicate that the warm gas cleanup train is capable of removing more than 90% of the trace metals from the syngas stream.

Table 4.37. Week 5 Mercury Sorbent Trap Data

Sample Time	Sample Location	Hg Concentration, µg/dNm^3
1/31/2011 10:30	Port C (cold side)	1.74
2/3/2011 10:48	Port C (cold side)	3.33
2/4/2011 7:32	Port C (cold side)	3.64
Average		2.90

Table 4.38. Week 5 Trace Element Data (Sample Port C)

	µg/dNm^3										
Sample Time	Sb	As	Be	Cd	Cr	Co	Pb	Mn	Hg	Ni	Se
1/31/2011 12:30	ND	12.2	ND	0.35	74.8	2.1	3.5	15.8	1.0	103.7	ND
2/3/2011 12:48	ND	13.5	ND	0.39	76.4	2.1	3.9	17.5	1.2	374.4	ND
2/4/2011 9:32	ND	14.3	ND	0.49	86.7	2.1	4.3	19.4	0.9	228.0	ND
Average	ND	13.3	ND	0.4	79.3	2.1	3.9	17.6	1.1	235.4	ND
Removal Eff. %	NA	96.9	NA	97.6	93.7	99.4	99.2	99.5	91.8	90.4	NA

Dräger tube samples were taken at Sample Ports A and C, and the average results for the week are shown in Table 4.39. Results were similar to the previous week's testing.

Table 4.39. Dräger Tube Results Summary for Week 5

	Cold-Side Sampling		Sample Port C Hot Side		
	Sample Port A H_2S	Sample Port C H_2S	NH_3	HCN	HCl
Concentration, ppm	0.16	0.18	1000	ND	ND

4.5.4 Membrane Results and Performance

The FBG was run at 300 psi for Week 5 testing. SS2 membrane was not used because it was only rated for operation at 200 psi. Flux rates for the FS membrane were near 80 scfh during the steady-state periods, as shown in Figure 4.20. Control issues with the gasifier resulted in two down periods for this week's testing. Partial pressure differential was over 50 psi during Steady- State Period 3, so it is not immediately clear why flux rates were not higher. It is possible that some level of contamination was beginning to impact membrane performance.

Figure 4.21 shows that SS1 membrane may have experienced a slight degradation in performance over the course of the run, despite increasing partial pressure differential. The 1-hour average data plot refers to the measurements taken with the gas meter, and the data are compared to the Gilibrator measurements. The plot also shows that there is significant variation with the Gilibrator measurement technique.

Table 4.40 shows that flux rates were down significantly for this run on the FS membrane despite the increase in partial pressure differential over Week 4. The reduced flux rates may have been caused by increased CO concentrations over the previous run. CO is not considered a poison for this membrane, but can reduce flow rates above concentrations of 2%, as stated by the manufacturer. The average CO concentration at the

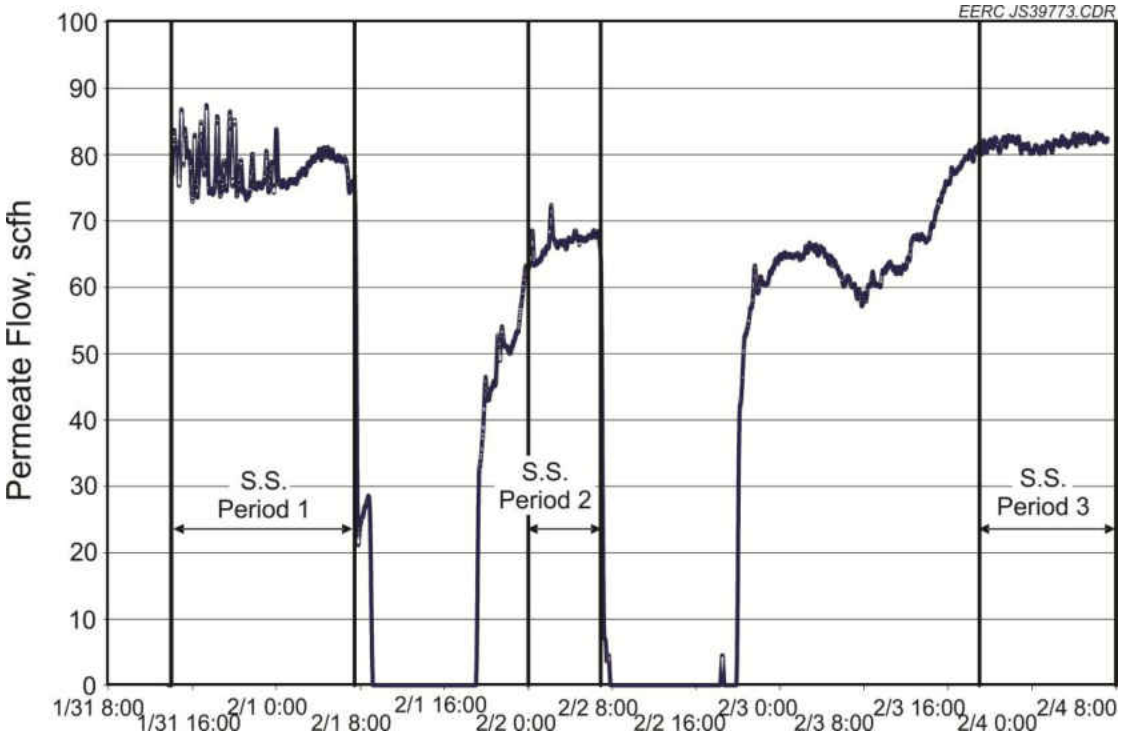

Figure 4.20. FS Membrane Permeate Flow Rate during Week 5.

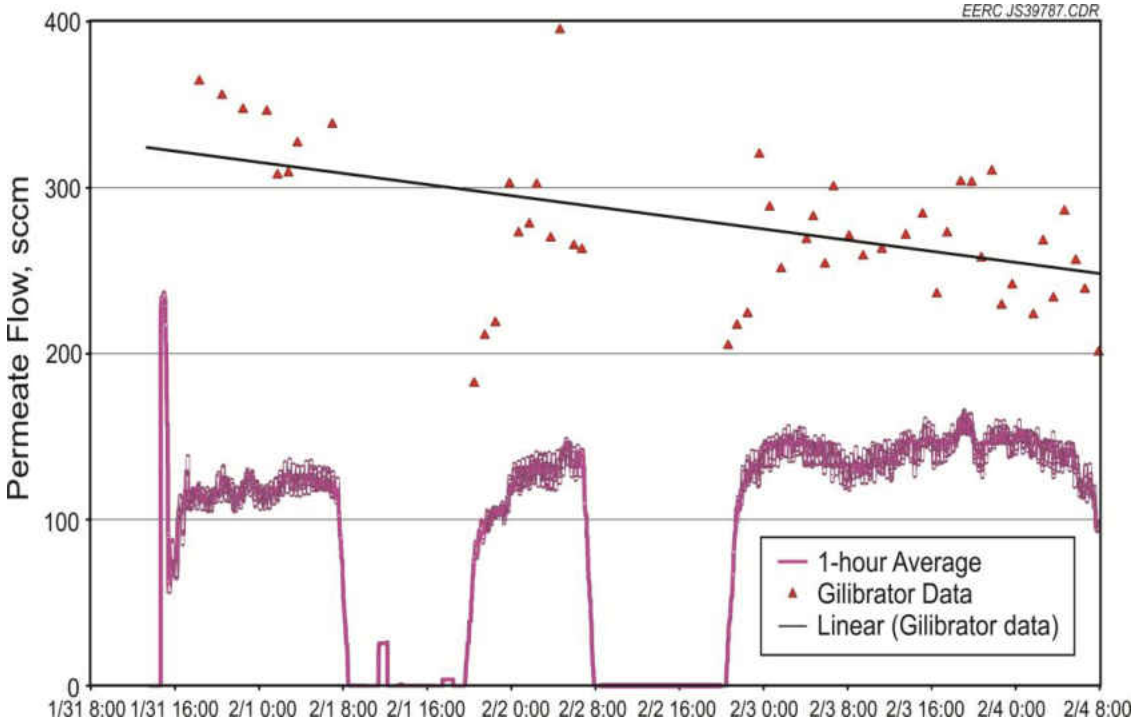

Figure 4.21. SS1 Membrane Permeate Flow Rate during Week 5.

Table 4.40. FS Membrane Performance Data for Week 5

	S.S. Period 1	S.S. Period 2	S.S. Period 3
	1/31 14:00 – 2/1 07:28	2/2 00:00 – 06:54	2/3 19:00 – 2/4 08:00
Membrane Heater, °F	650	650	650
Membrane Inlet, °F	573	574	577
Permeate Inlet, °F	584	585	586
Permeate Exit, °F	78	81	80
Syngas Inlet, °F	680	685	550
Syngas Inlet Pressure, psi	284	287	286
Permeate Pressure, in. H_2O	18	17	15
Flux, scfh/ft^2	5.0	4.4	5.3
H_2 Inlet, mol%	29.3	30.8	34.8
Wet H_2 Inlet, mol%	19.8	20.3	22.8
Raffinate H_2, mol%	17.9	19.2	27.5
Inlet H_2, scfh	237.1	215.9	255.5
Raffinate H_2, scfh	102.7	95.4	141.9
Permeate H_2, scfh H	69.6	61.0	74.4
H_2 Balance, %	72.6	73.0	84.6
Hydrogen Recovery, %	29.4	28.4	29.1
Theoretical Max Recovery, %	81.4	81.6	84.2
Partial Pressure Differential, psi	45.6	47.1	54.9

membrane inlet during this run was about 2.5%. The average CO concentration during the previous run was about 1.5%. The higher CO concentration was likely caused from degradation of the low-temperature WGS catalyst over time. Unfortunately, a leak was also detected in the membrane which likely increased the measured flux rate over what it would have been without the leak. Flux rates were significantly higher for SS1 membrane than they were for the previous week, which can be attributed to the increase in partial pressure differential. The increase in CO concentration did not appear to have the same impact on this membrane as on the FS. Table 4.41 shows flux rates as high as 40 scfh/ft^2 of membrane area. However, the flux rate did drop throughout the week. A leak was also detected on this membrane during the run, which did not appear to be present in the previous weeks' test.

Table 4.41. SS1 Membrane Performance Data for Week 5

	S.S. Period 1	S.S. Period 2	S.S. Period 3
	1/31 14:00 – 2/1 07:28	2/2 00:00 – 06:54	2/3 19:00 – 2/4 08:00
Membrane Temperature, °F	727	726	759
Membrane Inlet, °F	686	686	735
Permeate Inlet, °F	139	130	124
Permeate Exit, °F	78	81	81
Raffinate Inlet, °F	646	652	369
Raffinate Exit, °F	77	79	82
Syngas Inlet, °F	680	684	550
Syngas Inlet Pressure, psi	284	287	286
Permeate Pressure, in. H_2O	12	19	18
Permeate Flow Rate, sccm*	338	293	255
Raffinate Exit Pressure, in. H_2O	71	71	46
Raffinate Flow Rate, scfh	40	44	5
Flux, scfh/ft^2*	40.6	36.2	33.1
H_2 Inlet, mol%	29.3	30.8	34.8
Wet H_2 Inlet, mol%	19.8	20.3	22.8
Raffinate H_2, mol%	25.7	27.9	31.6
Inlet H_2, scfh	12.4	14.0	2.4
Raffinate H_2, scfh	10.4	12.2	1.7
Permeate H_2, scfh *	0.7	0.6	0.5
H_2 Balance, %	88.4	91.0	93.5
Hydrogen Recovery, %	5.3	4.2	26.2
Theoretical Max Recovery, %	87.2	87.7	88.9
Partial Pressure Differential, psi	45.4	46.6	53.6

* Denotes data obtained from Gilibrator measurements.

Hydrogen flow across the membranes was investigated by plotting the membrane inlet and raffinate hydrogen concentrations for the Week 5 test period. Figure 4.22 plots the inlet and raffinate hydrogen concentrations for the FS membrane. The initial drop in the raffinate concentration for each period of data was when the membranes were brought online. The flux through the membrane was consistent through the test period and was approximately 10 mol%. As seen with the syngas data presented in Figure 4.22, the inlet and raffinate hydrogen concentrations vary because of changes in gasifier operation.

The permeate and raffinate data for the FS and SS1 membranes are presented in Table 4.42. The SS2 membrane was not operated during this test period. The FS

membrane developed a small leak during this period. This reduced the flux through the membrane and decreased the permeate purity. The FS permeate hydrogen purity was 91.2 mol%, which is much lower than previously observed because of the leak.

The SS1 membrane had a permeate purity of 96.28 mol%, which was slightly lower than the Week 4 data. The impurities present were CO, CO_2, N_2, and methane. The recovery across the membrane was low, with the raffinate hydrogen concentration being similar to the inlet hydrogen concentration.

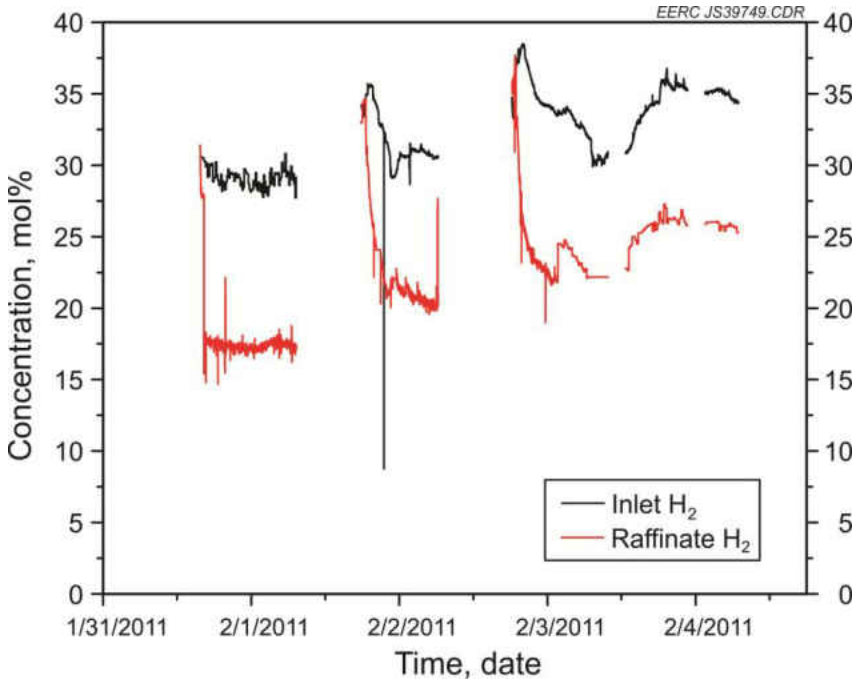

Figure 4.22. Week 5 FS Membrane Inlet and Raffinate Concentration Data.

Table 4.42. Week 5 Membrane Permeate and Raffinate Syngas Data

Membrane	H_2, mol%	CO, mol%	CO_2, mol%	N_2, mol%	CH_4, mol%	H_2S, ppmv
FS Permeate	91.2	0.44	7.8	ND	0.56	0.446
FS Raffinate	13.98	5.71	73.2	ND	7.02	0.580
SS1 Permeate	96.28	0.19	2.58	0.81	0.14	0.579
SS1 Raffinate	29.46	3.27	61.79	0.25	5.16	0.518
SS2 Permeate	–	–	–	–	–	–
SS2 Raffinate	–	–	–	–	–	–

4.6 Week 6 Testing – HPFBG

The original plan for Week 6 testing called for testing of the FS membrane only at approximately 500 psi. Changes were made to the fixed-bed setup because the low-temperature WGS catalyst and chlorine/mercury bed were only capable of running up to 300 psi. The low-temperature WGS catalyst, chlorine guard, and sulfur polishing beds were all combined in three layers in Fixed-Bed 4. This change was expected to increase the levels of chlorine and mercury to the hydrogen separation membranes but was not expected to have a significant impact on the sulfur levels.

Because of the significant leak observed during the previous test, it was decided to run the system at 200 psi and bring all three membranes online again. The changes were already made to the fixed beds before this decision was made, so the changes were kept in place for the run even though they were not technically needed for the pressure requirements. It was also thought that if the leak did not get worse during the run, the pressure may be ramped up to 500 psi.

4.6.1 Test Plan

As stated above, the original test plan called for running only the FS membrane at 500 psi. This was abandoned because of a significant leak, and all three membranes were run at 200 psi. Another goal for this run was to increase the hydrogen content of the syngas and provide as much syngas exposure as possible to the membranes. Because of the changes in the fixed-bed setup, more contaminants were expected to reach the membrane units. The operational strategy still called for brining on the fixed beds as shown in Table 4.3, with the exception of combining three sorbents into one fixed bed.

4.6.2 Gasifier Operations and Operating Data

Coal feed was started at 00:36 on February 14, 2011. The fixed beds were brought online by 12:37, and the membranes were all online by 20:00. Some delays were experienced in bringing on the membranes because of some temperature fluctuations in the fixed beds. The system ran well throughout the week, and no shutdowns were experienced. Pressure in gasifier was increased on February 17 to 300 psi in order to help determine the nature of the leak in the membrane. The system was taken offline at 05:40 on February 18, 2011. Gasifier operating data are shown in Table 4.43.

The operational set points were very similar to the previous week. The temperature of the lower bed was set near 843°C (1550°F), and the rest of the reactor was in the 760° and 816°C (1400° to 1500°F) range. Filter vessel temperatures were over 316°C (600°F) at the outlet. The fixed-bed reactors were held at similar set points as the previous runs. The last two beds were not used because of the planned high-pressure tests, and the chlorine guard and low-temperature WGS catalyst were combined into the sulfur polishing bed. The backup fixed bed for bulk desulfurization was brought online on February 16. No sulfur breakthrough was observed from the polishing bed.

Coal feed rate was similar to the previous runs at 200 psi, and feed rate was increased for the 300 psi test. Oxygen, recycle, and purge gas rates were also increased. Approximately 175 psi pressure was observed in the quench pots and membranes early in the test, and the pressure was increased to near 270 psi at the end of the run.

4.6.3 Warm-gas Cleanup Results

Table 4.44 displays the syngas composition for the Week 6 test period as each of the warm-gas cleanup systems are brought online. GC and LGA data were utilized to

Table 4.43. Gasifier Operating Data for Week 6 (HPFBG)

	Pre-membrane	Membrane Online	Membrane Online	Membrane Online	Membrane Online
Start Date	2/14/2011	2/14/2011	2/16/2011	2/17/2011	2/17/2011
Start Time	13:00	22:00	0:00	0:00	17:00
End Date	2/14/2011	2/15/2011	2/16/2011	2/17/2011	2/18/2011
End Time	18:00	23:59	23:59	14:30	5:40
FBG Temp., °F					
O_2/Steam Inlet	676	685	687	687	704
Recycle Inlet	645	677	674	675	725
Lower Reactor Bed	1540	1544	1550	1545	1548
Upper Reactor Bed	1470	1472	1474	1471	1475
Lower Freeboard	1441	1443	1443	1442	1446
Upper Freeboard	1442	1457	1458	1456	1447
Reactor Extension	1422	1419	1419	1416	1425
Cyclone Exit	1111	1114	1110	1108	1153
Filter Vessel Temp., °F					
FV Inlet	813	838	836	829	867
FV Outlet	655	663	662	659	685
Packed Bed Temp., °F					
Bulk Sulfur Removal	610	615	613	614	634
High-Temperature Shift Catalyst	654	651	646	650	661
Sulfur Polishing/Cl Guard/Low-Temp. Shift	456	452	450	457	498
Quench Pot Temp., °F					
West Pot 1 Inlet	399	452	450	452	469
West Pot 3 Outlet	93	84	85	88	109
East Pot 1 Inlet	91	82	83	86	105
East Pot 3 Outlet	59	58	57	56	56
Flows					
Coal Feed Rate, lb/hr	8.8	8.9	8.9	9.2	11.4
Primary Nitrogen, scfh	0	0	0	0	0
Oxygen, scfh	80	80	80	80	97
Steam, lb/hr	16	16	16	16	16
Recycle Gas, lb/hr	12	15	15	15	28
Nitrogen Purge, scfh	4	4	5	5	42
Product Gas, scfh	215	83	87	90	106
Closure, %	213	79	81	82	64
Pressure, psi					
EFG Top	201	201	201	201	301
EFG Bottom	199	199	199	199	299
Filter Vessel	196	196	196	196	295
Quench Pot	177	174	173	168	267
Recycle Gas Surge Tank	800	800	800	800	800

Table 4.44. Week 6 Syngas Composition (HPFBG)

Sample Point	H_2, mol %	CO, mol %	CO_2, mol %	N_2, mol %	CH_4, mol %	H_2S, ppmv	H_2/CO Ratio
Bulk Desulfurizer Inlet RVS-1, Bed 1	25.63	12.85	49.35	3.71	2.59	1100	1.99
Bulk Desulfurizer Outlet RVS-1, Bed 1	28.3	15.06	45.89	3.64	2.47	3.384	1.88
High-Temp. Shift Catalyst Outlet, Bed 3	35.49	2.77	52.03	3.02	2.25	3.384	12.81
Sulfur Polishing, Chlorine Guard, Low-Temp. Shift, Bed Outlet, Bed 4	38.46	0.33	53.98	3.16	2.17	0.754	116.55

determine bulk and trace syngas analyte concentrations across the warm-gas cleanup system. During this test period, the chlorine guard/mercury control bed and the low-temperature WGS catalyst beds were not used in order to change the syngas composition seen by the membranes. Some of the chlorine removal sorbent and the low-temperature WGS catalyst were added to the end of Bed 4. When the bulk desulfurizer was brought online, the sulfur concentrations decreased from 1100 to 3.4 ppmv, which is a removal of 99.7%. The high-temperature WGS catalyst performed well and decreased the CO concentration to 2.8 mol% and increased the H_2 and CO_2 concentrations by approximately 7 mol%. The sulfur polishing bed further reduced the H_2S concentration down to 0.7 ppmv, which yields a total sulfur removal of 99.9% across the two sulfur beds. The chlorine concentrations were reduced to below Dräger tube detection levels.

Figure 4.23 plots the continuous syngas composition data for the Week 4 test period. The drop in the CO concentration indicates when the high-temperature WGS catalyst was brought online. The trace syngas species remained low throughout the test period, which indicates that the warm-gas cleanup system maintained consistent removals for the test duration.

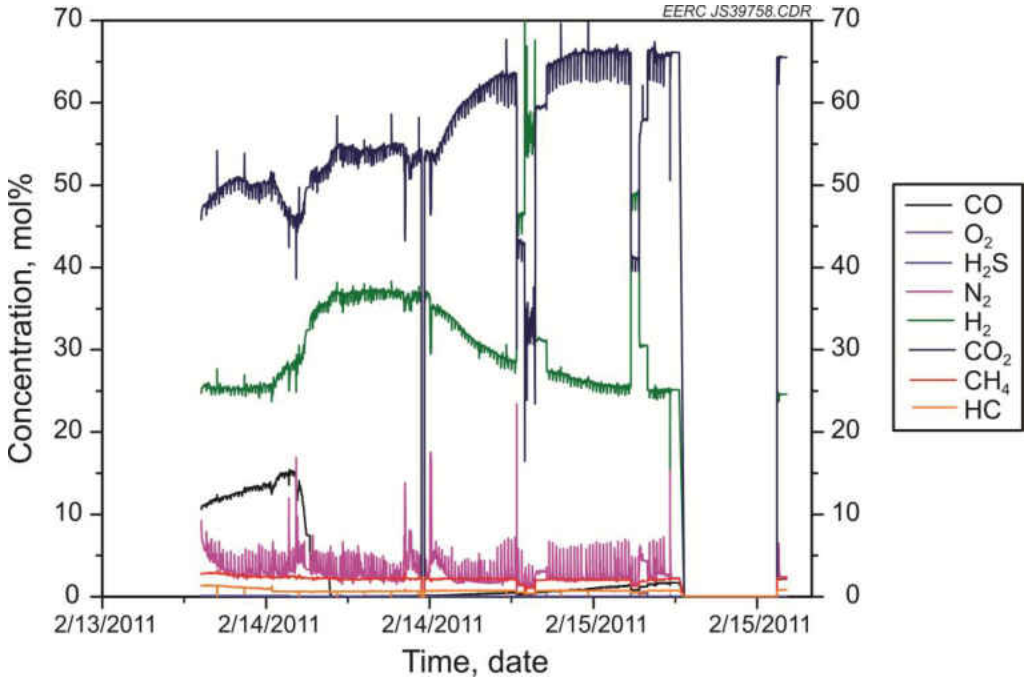

Figure 4.23. Week 6 Syngas Data.

Mercury data were collected to determine the mercury concentrations at the Port C sampling location, which is after the mercury control column and before the hydrogen separation membranes. Sampling at this location determines the effectiveness of the mercury control column and measures the mercury concentrations that are seen by the hydrogen separation membranes. Mercury concentrations were determined by syngas sampling using sorbent traps. Table 4.45 displays the mercury sorbent trap data for the Week 6 test period. The sorbent trap data are slightly higher than other test periods, with an average of 4.49 µg/dNm^3. This was expected though because the mercury control bed was not online during the test period. This also shows that the other beds, likely the low-temperature WGS catalyst bed, can also remove mercury.

Dräger tube samples were taken at Sample Ports A and C, and the average results for the week are shown in Table 4.46. Results were similar to the previous week's testing.

Table 4.45. Week 6 Mercury Sorbent Trap Data

Sample Time	Sample Location	Hg Concentration, μg/dNm^3
2/15/2011 9:38	Port C (cold side)	4.05
2/16/2011 10:40	Port C (cold side)	4.17
2/17/2011 9:57	Port C (cold side)	5.24
Average		4.49

Table 4.46. Dräger Tube Results Summary for Week 6

	Cold-Side Sampling		Sample Port C Hot Side		
	Sample Port A H_2S	Sample Port C H_2S	NH_3	HCN	HCl
Concentration, ppm	0.11	ND	1000	0.14	ND

4.6.4 Membrane Results and Performance

Permeate flow was high for the Week 6 test run, but unfortunately this was partially the result of a significant leak in the membrane. The original plan to run at 500 psi in the gasifier was abandoned because of this leak. Permeate flow averaged near 125 scfh for the initial part of the run, as shown in Figure 4.24. The pressure was increased in the gasifier to 300 psi toward the end of the run, and flux increased to 175 scfh.

SS1 membrane was also showing a leak based on the gas analysis of the permeate. The leak appeared to get worse toward the middle and end of the run, but flux likely also increased because the composition of the permeate did not deteriorate significantly from the start of the run. Figure 4.25 shows that permeate flow was near 600 sccm at the start of the run and approached 800 sccm at the end of the run when the pressure was increased. The permeate measurements were consistent at the gas meter, but the meter is not considered to be correctly calibrated at this flow rate.

Despite the fact that the permeate flow was higher, the hydrogen flux as reported in Table 4.47 was similar to other runs on the FS membrane, because the flux calculation considers the hydrogen concentration. Recovery rate was 38% for the run, but some of

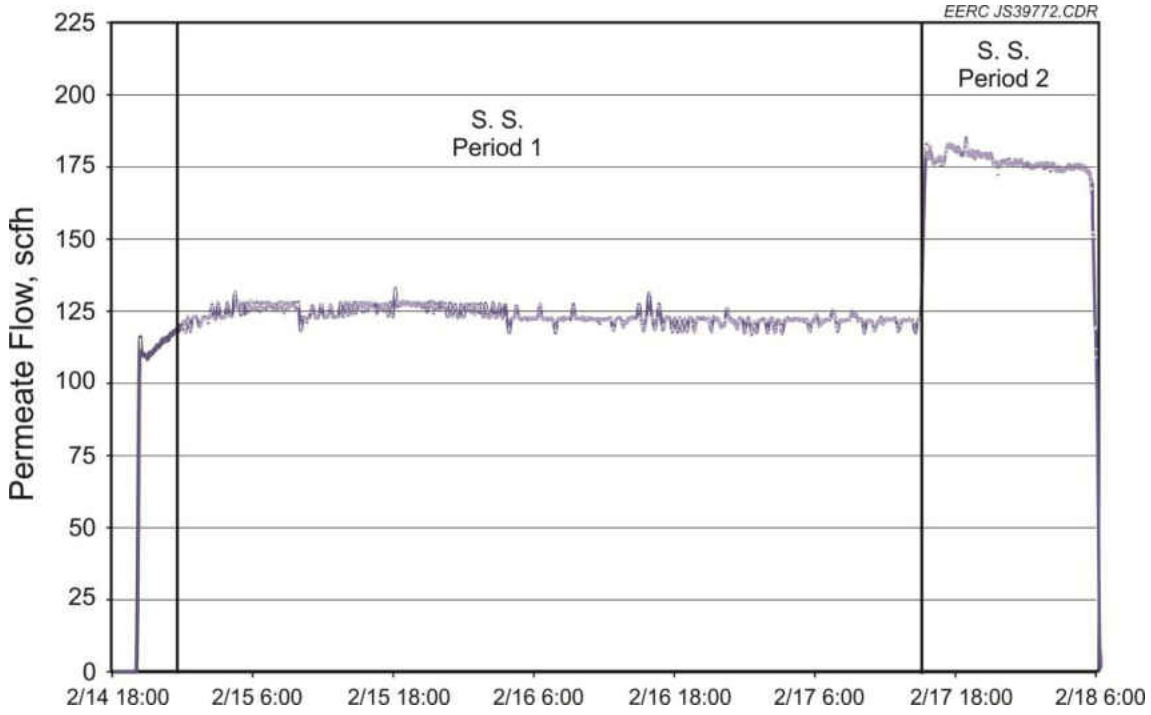

Figure 4.24. FS Membrane Permeate Flow Rate during Week 6.

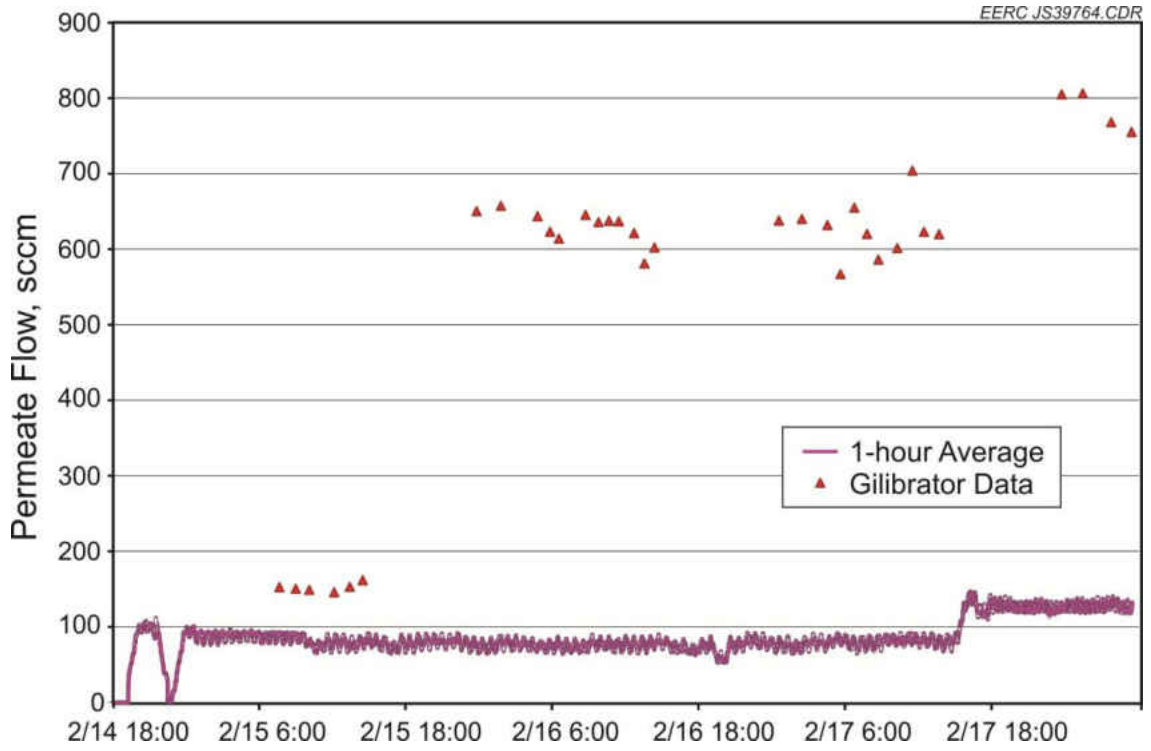

Figure 4.25. SS1 Membrane Permeate Flow Rate during Week 6.

Table 4.47. FS Membrane Performance Data for Week 6

	S.S. Period 1	S.S. Period 2
	2/14 23:00 – 2/17 14:35	2/17 15:30 – 2/18 05:28
Membrane Heater, °F	632	634
Membrane Inlet, °F	494	505
Permeate Inlet, °F	514	519
Permeate Exit, °F	74	75
Syngas Inlet, °F	588	593
Syngas Inlet Pressure, psi	177	272
Permeate Pressure, in. H_2O	22	31
Flux, scfh/ft^2	4.8	7
H_2 Inlet, mol%	37.4	31.8
Wet H_2 Inlet, mol%	23.2	22.6
Raffinate H_2, vol%	28.2	23.1
Inlet H_2, scfh	178.4	248.9
Raffinate H_2, scfh	83.2	112.6
Permeate H_2, scfh*	67.8	94.2
H_2 Balance, %	84.7	83.1
Hydrogen Recovery, %	38.0	37.9
Theoretical Max Recovery, %	85.4	90.4
Partial Pressure Differential, psi	35.9	56.2

the hydrogen recovered was through the leak in the membrane. Partial pressure differential was over 50 psi for Period 2, but recovery rates remained about the same. This is most likely due to the increased gas flows into the membrane and reduced residence time for separation.

Table 4.48 shows that a flux of 61 scfh/ft^2 was achieved with the slipstream membrane during Steady-State Period 2. This can be partially attributed to the leak, but hydrogen permeation must have also increased. Recovery rate was also much higher, near 24%. This is well below the theoretical maximum recovery of 87.7% during Period 2.

The inlet and raffinate hydrogen concentrations for the FS and SS1 membranes are presented in Figure 4.26. The initial drop in the raffinate concentration for each period of data was when the membranes were brought online. The flux through the membranes was consistent through the test period and was approximately 10 mol%. The

leak in the FS membrane grew larger during this test period and had a significant impact on the hydrogen flux through the membrane during this test period.

Table 4.48. SS1 Membrane Performance Data for Week 6

	S.S. Period 1	S.S. Period 2
	2/14 23:00 – 2/17 14:35	2/17 15:30 – 2/18 05:28
Membrane Temperature, °F	750	749
Membrane Inlet, °F	776	775
Permeate Inlet, °F	121	126
Permeate Exit, °F	76	78
Raffinate Inlet, °F	465	459
Raffinate Exit, °F	77	79
Syngas Inlet, °F	588	593
Syngas Inlet Pressure, psi	177	272
Permeate Pressure, in. H_2O	12	19
Permeate Flow Rate, sccm*	432	127
Raffinate Exit Pressure, in. H_2O	53	60
Raffinate Flow Rate, scfh	9	10
Flux, scfh/ft^2*	38.3	61.1
H_2 Inlet, mol%	37.4	31.8
Wet H_2 Inlet, mol%	23.2	22.6
Raffinate H_2, mol%	32.5	27.2
Inlet H_2, scfh	3.9	4.3
Raffinate H_2, scfh	2.9	2.8
Permeate H_2, scfh*	0.6	1.0
H_2 Balance, %	89.2	89.3
Hydrogen Recovery, %	15.8	24.1
Theoretical Max Recovery, %	81.9	87.7
Partial Pressure Differential, psi	34.2	54.3

* Denotes data obtained from Gilibrator measurements.

Table 4.49 displays the permeate and raffinate syngas data for the FS and SS1 membranes. The leak in the FS membrane became larger during this test period and significantly degraded the membrane's performance as seen by the very low hydrogen purity on permeate stream. The flux was also significantly reduced.

The purity of the SS1 membrane permeate stream also decreased during this test period likely due to a leak in the membrane. The permeate hydrogen purity decreased from approximately 98 mol% in the previous weeks to 67.53 mol% during the Week 6

test period. The recovery through the membrane was also low, which is consistent with the other weeks of testing.

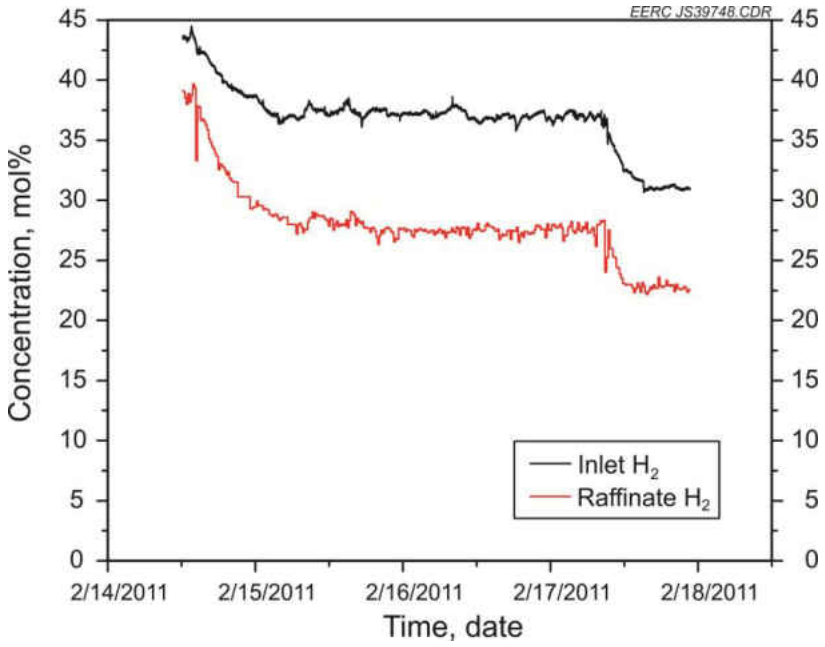

Figure 4.26. Week 6 FS Membrane Inlet and Raffinate Concentration Data.

Table 4.49. Week 6 Membrane Permeate and Raffinate Syngas Data

Membrane	H_2, mol%	CO, mol%	CO_2, mol%	N_2, mol%	CH_4, mol%	H_2S, ppmv
FS Permeate	53.8	1.38	39.83	2.12	2.87	ND
FS Raffinate	39.64	0.42	54.55	0.28	5.11	ND
SS1 Permeate	67.53	0.98	27.71	1.8	1.98	ND
SS1 Raffinate	31.83	1.96	55.72	6.14	4.34	ND
SS2 Permeate	–	–	–	–	–	–
SS2 Raffinate	–	–	–	–	–	–

4.7 Test Run Summary

Overall, approximately 331 hours of run time was accomplished on the gasifiers during the test campaign. With the simultaneous membrane skid capable of testing up to three membranes at once, an estimated 836 membrane-hours were accomplished during the program. On the fluid bed, 665 membrane-hours were accomplished, and 171 membrane-hours were completed on the EFG. The FS membrane was exposed to syngas

for 331 hours. SS1 membrane was exposed for 328 hours, and SS2 membrane was exposed for approximately 177 hours. Table 4.50 summarizes each of the test runs.

Table 4.50. Hydrogen Separation Membrane Run Summary

Run	Start Date	End Date	Membrane, Run, hr	Membranes Run	Notes
FBG012	12/13/2010	12/17/2010	46	3	First shakedown run
EFG031	1/3/2011	1/4/2011	3	1	Gasifier plugged
EFG032	1/10/2011	1/13/2011	56	3	Shutdown after 3 days due to plug
FBG013	1/24/2011	1/28/2011	75	3	Intermittent shutdowns
FBG014	1/31/2011	2/4/2011	67	2	Intermittent shutdowns
FBG015	2/14/2011	2/18/2011	84	2	Ran well

4.7.1 Hydrogen Purity

Figure 4.27 shows hydrogen purity from the permeate side of each membrane throughout the test campaign. The FS membrane had very high hydrogen purity during the initial weeks of the test period, with purities over 99.99%. The purity dropped off in Week 5 because of a leak in the membrane. The leak rate increased substantially in Week 6 and led to lower purity hydrogen in the permeate. The SS1 membrane also showed high purity, achieving 99.2% purity. Purity dropped off slightly during the week, with a potential leak noticed in Week 5 and a substantial leak found in Week 6. SS2 membrane did not achieve high hydrogen purity during the test run, but the hydrogen purity did improve through the course of the testing. The highest purity achieved was 60%.

4.7.2 Flux and Partial Pressure Differential

Figure 4.28 shows the performance of the FS membrane throughout the course of the run and compares it to the partial pressure differential of hydrogen for each point on the graph. The highest flux was achieved during the January EFG runs, despite the fact that partial pressure differential was higher for some of the membrane test runs later in

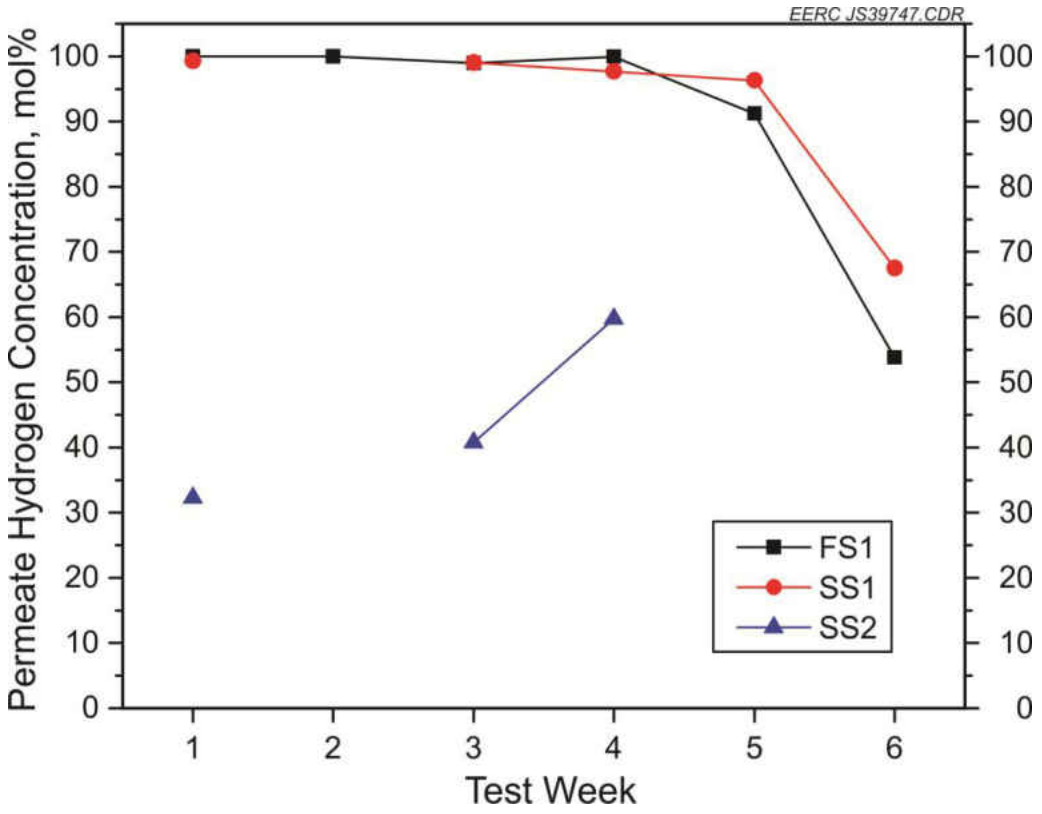

Figure 4.27. Membrane Hydrogen Permeate Concentrations for Each Test Week.

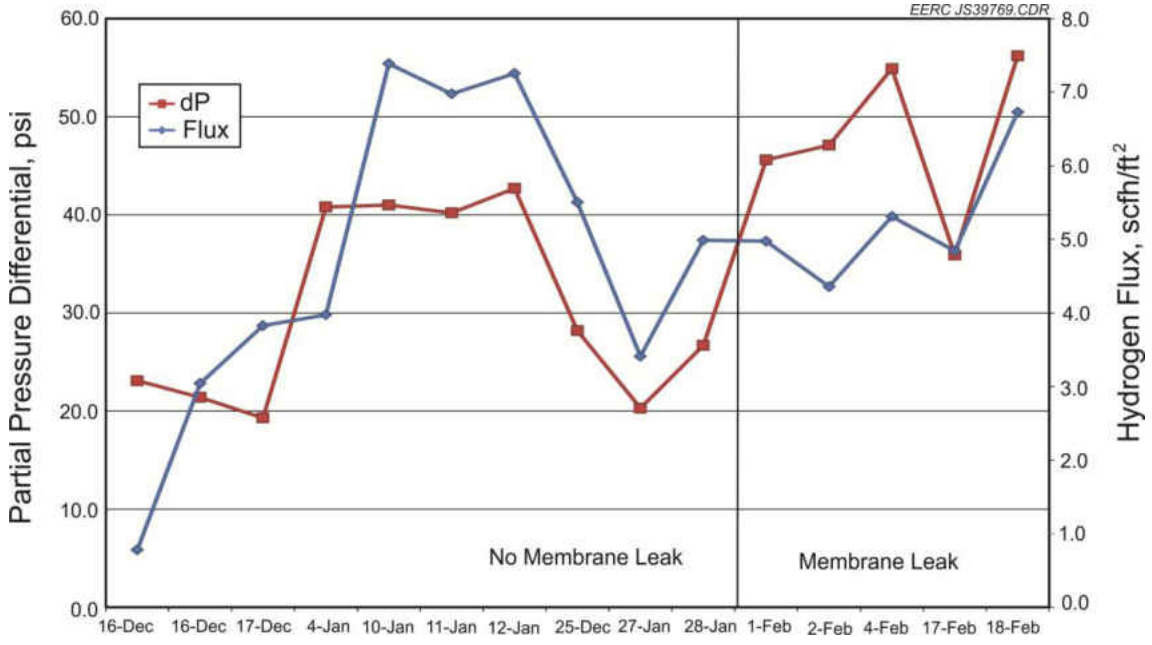

Figure 4.28. Hydrogen Flux across the FS Membrane during the Test Campaign.

the campaign. Also, a leak developed later in the test campaign that should have worked to increase flux for two reasons: 1) hydrogen is bypassing the membrane and penetrating to the permeate side through the leak and 2) the other syngas components leaking through the membrane act as a sweep gas to increase partial pressure differential across the membrane. Even with the leak and the increased partial pressure, flux was decreased from where it was earlier in the test campaign. This indicates that there may have been some performance degradation because of syngas contaminants, but more investigation would be necessary to verify.

Figure 4.29 shows the hydrogen flux across the SS1 membrane during the test campaign and compares to partial pressure differential. The one problem with this graph is that measurements earlier in the test campaign were performed with the gas meter, and later measurements were made with the Gilibrator. The gas meter measurements do show a correlation with partial pressure differential, even if the absolute value is not correct. With the Gilibrator measurements, the run during the first week of February actually showed decreasing flux with increasing partial pressure differential. The run the next week indicated increasing flux with increasing partial pressure differential. Unfortunately, the membrane also had a significant leak during this run, and the flux increase with increasing pressure could be attributed to the leak. These data might suggest some degradation because of contamination, but more investigation is required. It should be noted that the absolute value of the flux measurements was significantly higher on this membrane than on the FS membrane or SS2 membrane.

Figure 4.30 shows the hydrogen flux across SS2 membrane during the test runs when it was online. The gas meter was not capable of accurately measuring permeate

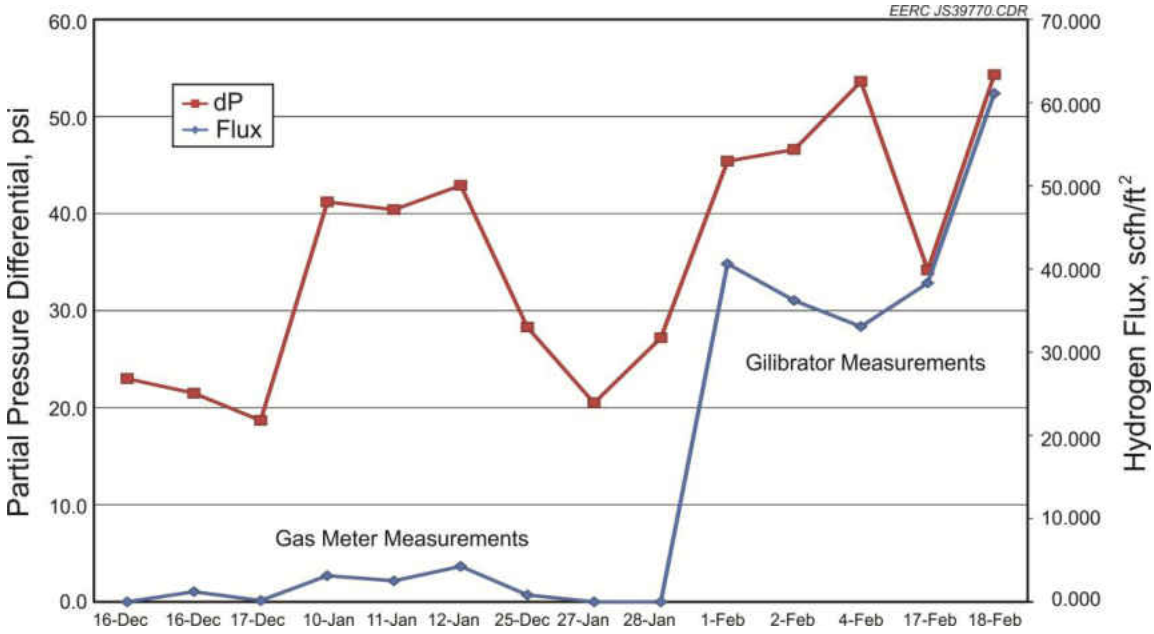

Figure 4.29. Hydrogen Flux across the SS1 Membrane during the Test Campaign.

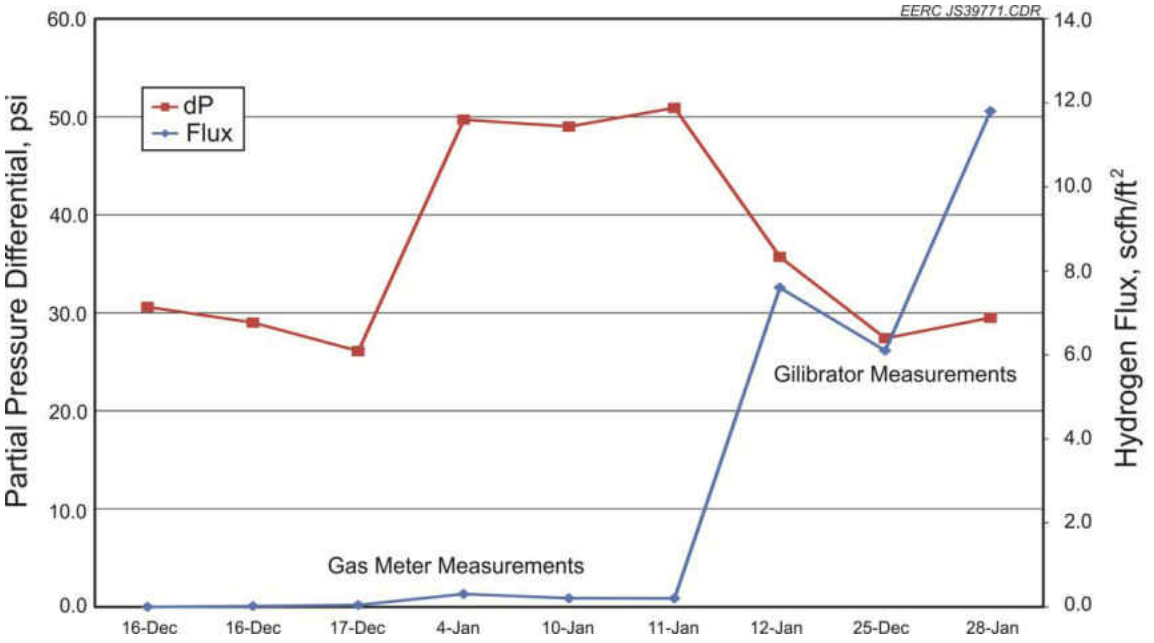

Figure 4.30. Hydrogen Flux across the SS2 Membrane during the Test Campaign.

flow for this membrane, but there does seem to be a flux increase with increasing partial pressure early in the week. Measurements made during the week of January 24 with the Gilibrator do seem to indicate increasing flux with increasing partial pressure differential.

There is no indication that contamination had an impact on flux rates, but more data points would be needed to verify this. The best performance for this membrane was observed at the end of the test campaign, but a significant leak was still observed.

4.7.3 Sievert's Law and Performance vs. DOE Targets

The highest hydrogen partial pressure differential achieved during the test program was 56 psi. This is well short of the DOE evaluation criteria of 100 psi. Therefore, Sievert's law was used to calculate the theoretical flux rate for the membranes at a partial pressure differential of 100 psi. Permeability for each membrane was calculated using the available data, and then that value was used in Sievert's law at 100 psi differential pressure. Table 4.51 shows the calculated values for each membrane. Only data derived from the Gilibrator measurements are presented for the slipstream membranes. The maximum flux achieved by the FS membrane was 21.4 scfh/ft^2, and this was during the time period that the membrane did not have a leak. Much lower hydrogen flux was observed when the membrane had a leak, indicating that the membrane material may have been poisoned to some degree during the test campaign.

SS1 membrane achieved much higher flux rates at 131 scfh/ft^2, but this was also when the membrane was thought to have a leak. A flux rate of 117 scfh was achieved when the membrane had no leak. SS2 membrane achieved 29.4 scfh/ft^2, but hydrogen purity was only about 60%.

Table 4.52 shows the DOE goals for membrane development in 2010 and 2015 and then evaluates the performance of the membranes in this test program versus those targets. It should be noted that this comparison represents the results found in this program only and does not represent other tests that have occurred on these membranes.

Table 4.51. Calculated Expected Membrane Flux at 100 psid using Sievert's Law

	Expected Flux @ 100 psid, scfh/ft^2		
Date	FS Membrane	SS1 Membrane	SS2 Membrane
16-Dec	3.5		
16-Dec	14.8		
17-Dec	20.1		
3-Jan	11.5		
10-Jan	21.3		
11-Jan	20.7		
12-Jan	20.3		
25-Jan	21.4		20.6
27-Jan	17.3	117.5	20.5
28-Jan	18.5	112.8	29.4
1-Feb	12.9	105.9	
2-Feb	11.1	93.6	
4-Feb	12.1	78.1	
17-Feb	13.4	115.0	
18-Feb	13.6	131.3	

All three membranes were below the 2010 target for flux rates, although SS1 membrane came the closest to achieving 200 scfh/ft^2. All three membranes were operated below the 2015 target temperature. Sulfur tolerance was not able to be specifically determined as part of this test campaign, because sulfur was kept well below 1 ppm for the duration of the testing. Undoubtedly, small levels of sulfur reached the membranes, and they were evaluated for sulfur poisoning in the post mortem analysis. Cost of the small separators is also not relevant to commercial-scale operations, and cost numbers were not provided by the membrane producers. The membranes did not appear to provide significant WGS activity, but this was difficult to determine in this test program because in order to achieve the highest possible partial pressure differential, the syngas was shifted as far as possible before hydrogen separation.

Table 4.52. Membrane Performance in this Test Campaign vs. DOE Targets

Performance Criteria	Units	2010 Target	2015 Target	FS Membrane	SS1 Membrane	SS2 Membrane
Flux (100 psi dP basis)	$ft^3/(hour*ft^2)$	200	300	21.3	117	29.4
Temperature	°F	572–1112	482–932	650	750	900
S Tolerance	ppmv	20	>100	ND	ND	ND
Cost	$/ft^2	100	<100	ND	ND	ND
WGS Activity	–	Yes	Yes	ND	ND	ND
ΔP Operating Capability	psi	Up to 400	Up to 800 to 1000	600	300	200
Carbon Monoxide Tolerance	–	Yes	Yes	Yes	Yes	Yes
Hydrogen Purity	%	99.5%	99.99%	99.99	99.2	59.7
Stability/Durability	Years	3	5	ND	ND	ND

Meets DOE 2015 goal.
Meets DOE 2010 goal.
Under DOE 2010 goal.

The FS membrane met the 2010 goal for differential pressure operation capability according to the specifications, even though it was not tested that high in this program. The others were rated far below the specification. The membranes all appeared to have CO tolerance, since none of them completely deactivated, with approximately 2% CO in the syngas during the test program. The FS membrane met the purity goal of 99.99% for the DOE 2015 target. The SS1 membrane came close to the DOE 2010 goal with 99.2% purity. SS2 membrane probably had a significant leak and did not meet the purity goals.

The stability and durability of the membranes are difficult to determine because of the relatively short test periods that were run. The FS membrane seemed to experience a reduction in flux toward the end of the program. Both the FS and SS1 membrane appeared to develop a significant leak during the course of the testing. The FS membrane was evaluated post mortem to understand if the leaks were developed in the membrane material, membrane joints, or the fittings. It is possible that the leaks developed in the fittings from the heat up and cool down experienced through the test program and not in the membrane material.

CHAPTER 5

ANALYSIS OF MEMBRANE MATERIAL AND FAILURE MODE

A significant leak was observed from the full stream membrane during the last two weeks of testing. The full stream membrane was returned to the supplier for an analysis of the module failure mode and estimate for module repair. The supplier was able to return a sample of the used membrane material, and the material was analyzed using several techniques. This chapter reviews the analysis of the membrane material and the likely cause of the failure.

5.1 Membrane Supplier Review

The supplier of the membrane disassembled the module and inspected each of the membrane disks for evidence of failure. The membrane was arranged in a stacked disk configuration, containing 50 discs. The supplier commented that one of the disks experienced a catastrophic failure, and that 27 of the disks did not pass the leak check. The disk that catastrophically failed physically tore away from the small diameter mounting flange. The supplier felt that the most likely cause of this failure and the other leaky disks was a reverse pressurization event. The disks are designed such that the pressure on the permeate side of the membrane cannot exceed the pressure on the feed side of the membrane. A reverse pressurization, or an event where pressure is greater on the permeate side, can cause significant damage to the disks. Based on the condition of the disks, the supplier felt that this type of an event likely occurred. The supplier also

commented that the internal components of the membrane were very clean, staining was minimal, and that it was apparent the failure did not occur as a result of a dirty gas feed stream.

The membrane supplier repaired the module by removing and replacing the torn disk. Upon request, the failed membrane disk was sent to the EERC for contaminant analysis. The disk was analyzed at EERC, and a portion of the disk was sent to two additional laboratories for contaminant analysis. Data mining was also undertaken to understand if a reverse pressurization event occurred during system operation.

5.2 Data Review for Reverse Pressurization

Based on the data available, the tear in the membrane occurred sometime between week four testing and week five testing. A gas bag sample taken approximately 10 hours before the shutdown of week four had indicated 100% hydrogen on the permeate side of the membrane. A gas bag taken two hours after startup of week five indicated approximately 90% hydrogen on the permeate side, with the balance having the composition of the syngas. The process logs for system operation and shutdown during week four and startup of week five were reviewed in detail for any evidence of a reverse pressurization event.

Figure 5.1 shows the permeate side pressure during the final operation and shutdown of the week four test. The data logging system records process values every five seconds. The system was shutdown at 07:40 on January 28th. A gas bag sample taken at 21:15 on January 27th contained 100% hydrogen and indicated that there was no leak in the membrane. Vacuum pressure was observed on the permeate side of the membrane after the shutdown. The vacuum is caused by the cooling of the stagnant

gases in the quench pots, and indicates there were no leaks in the membrane. The permeate side of the membrane was purged with nitrogen at 09:40, causing a momentary increase in pressure up to 37 in H_20. A log book entry indicated that when the membrane was shutdown, the feed side was isolated under pressure, and the log indicated that the membrane pressure was approximately 100 psi at 13:50. Therefore the membrane was under pressure when the permeate purge was on-line and no reverse pressurization occurred. The small spike in permeate purge pressure was insignificant compared to the pressure on the raffinate side. These data indicate that the failure of the membrane did not occur during the shutdown of the week four testing and must have occurred during the startup of the week five tests.

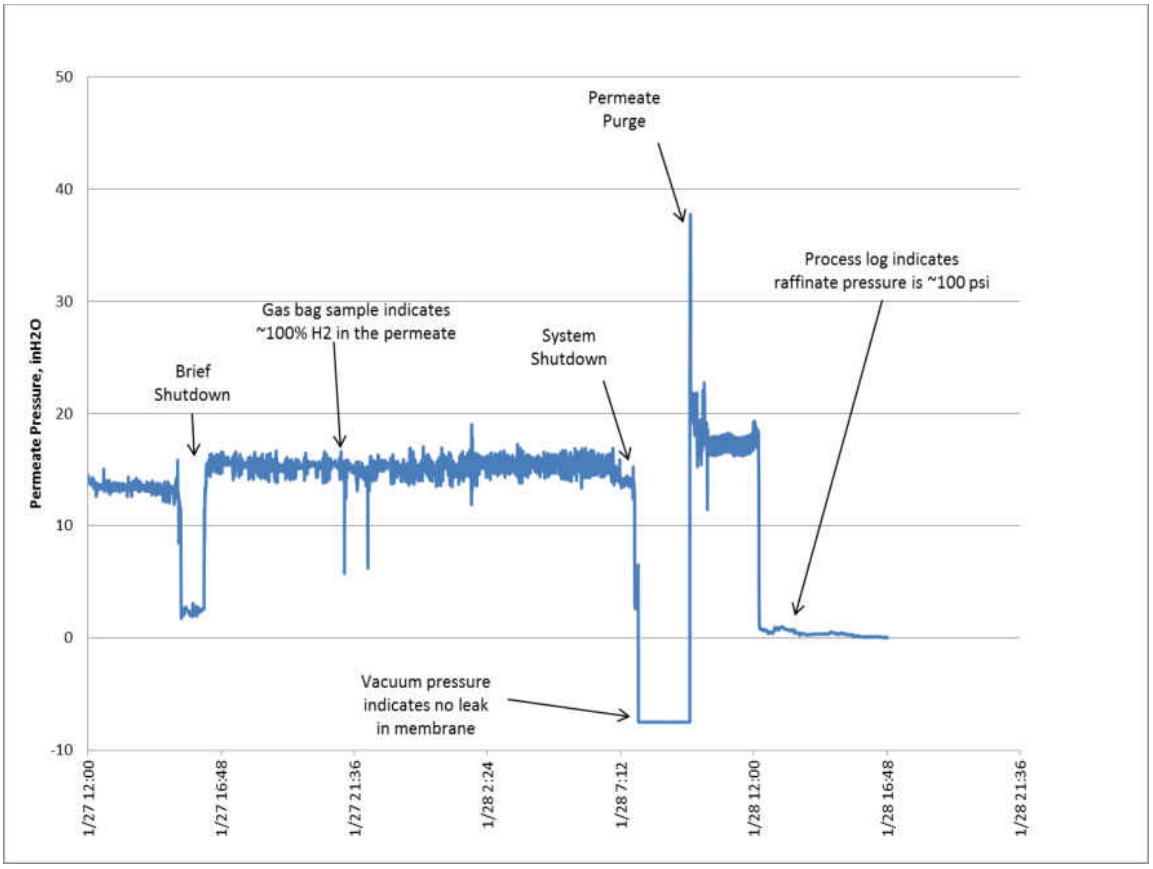

Figure 5.1. Permeate Pressure of the FS Membrane during Shutdown of Week 4 Testing.

The startup data was reviewed from week five testing to determine if an error during membrane startup resulted in the failure of the membrane material. Unfortunately, the operator did not turn on the data log for the membrane during startup and it was not turned on until after syngas was being sent to the membrane. Figure 5.2 shows the permeate pressure in the membrane once the data log was started. Based on the data available, it appears the leak was present when the membrane test was started. The operator noted in the log book that the dry gas meter for SS2 was not operating correctly, and therefore the operator was flowing nitrogen at 20 scfm through the permeate side of SS2 to try and calibrate the gas meter. It is possible that this testing caused a reverse pressurization event in the full stream membrane if a valve was not positioned correctly or the wrong purge mass flow controller was used. Unfortunately the data log is not indicative of whether a leak was present when the membrane was pressurized with nitrogen. The system was shut down later that day, and vacuum pressure was not created in the permeate line, confirming that a leak was present.

The syngas permeate flow rates were very similar at the end of week four and the start of week five. The incoming partial pressure of hydrogen was 75 psi at the end of week four and 83 psi at the start of week five. The permeate flow rates were 69.8 and 69.6 scfh during those periods. This consistency of flow despite the increase in partial pressure and a leak that had developed in the membrane also indicates an overall performance degradation of the membrane material. The performance degradation was minimal, but appeared to occur after four weeks of testing, which may be a concern for long-term operation. While interesting to note, the flow information does not indicate precisely when the tear in the membrane occurred.

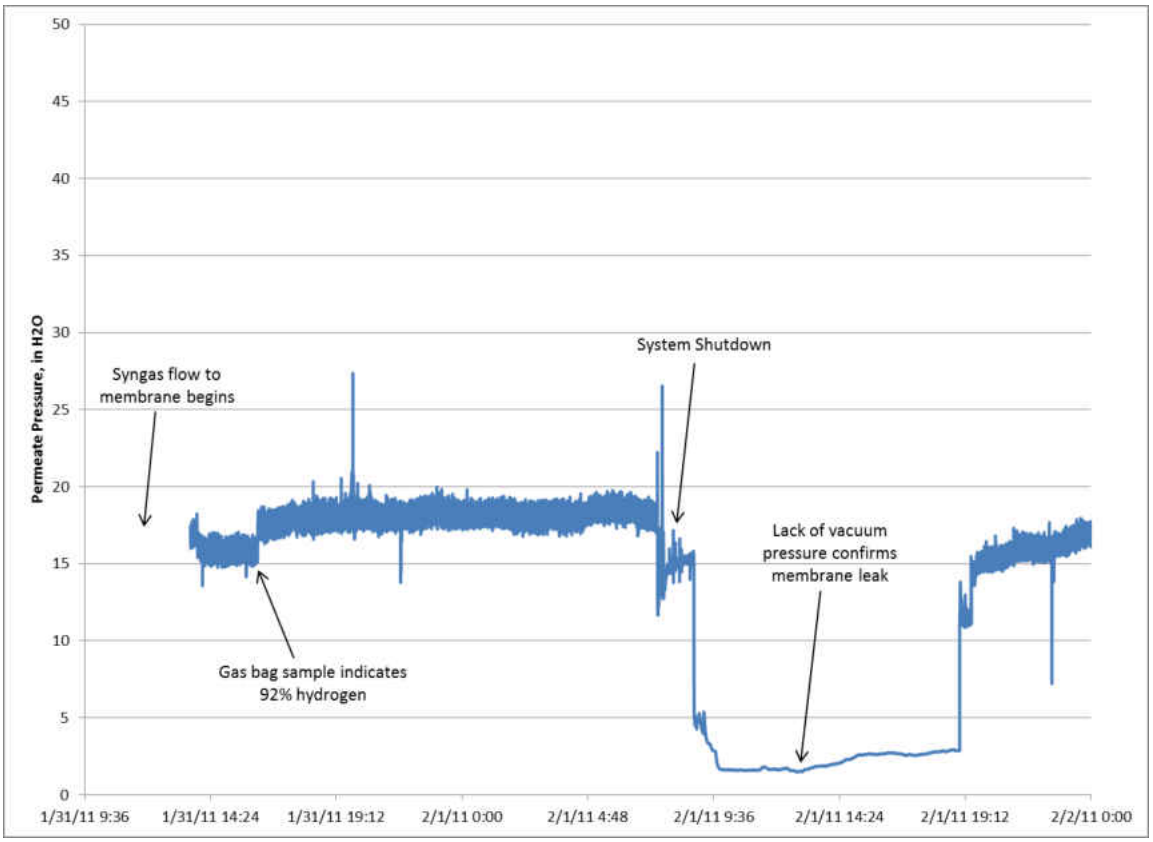

Figure 5.2. Permeate Pressure of the FS Membrane during Startup of Week 5 Testing.

5.3 Analysis of Membrane Materials and Analytical Techniques

The membrane disk was received from the supplier sealed in a plastic bag. The handling of the membrane material from removal to arrival is unknown, but it was packaged carefully for shipping. The packaging was labeled such that the face of the disk that is exposed to syngas and the inside (permeate side) of the membrane could be distinguished. A picture of the face of the membrane is shown in Figure 5.3, and the inside of the membrane is shown in Figure 5.4. The face of the material appeared relatively clean, and the inside appeared to have some discoloration or staining, which was consistent with comments from the supplier. The reason for the discoloration was not apparent upon visual inspection.

Figure 5.3. Face of the Membrane Material, Syngas Side.

Figure 5.4. Inside of the Membrane Material, Hydrogen Side.

The disk was carefully handled and cut into three separate pieces for analysis at three laboratories. Analysis was performed at the EERC, at the US Department of Energy's National Energy Technology Laboratory (NETL), and at United Technologies Research Center (UTRC). The goal of the analysis was to determine if there was any indication of impurities on the surface of the membrane, with an emphasis on sulfur contamination. Each of the laboratories employed similar techniques to determine the bulk makeup of the membrane and if any impurities were present.

Three main analytical techniques were used to evaluate the membrane material and look for signs of contamination. The laboratories used X-ray diffraction (XRD), scanning electron microscopy with energy dispersive X-ray spectroscopy (SEM/EDS), and X-ray photoelectron spectroscopy (XPS) depth profiling. XPS is often also referred to as electron spectroscopy for chemical analysis (ESCA).

5.3.1 X-ray Diffraction

XRD analysis is used to determine the crystal structure of a solid sample. In theory, the perfect crystal is a repetition of a very small unit cell such that the repetition makes up the entire volume of the crystal. Several different types of unit cells exist, and of the most basic are bcc and fcc which were reviewed in Chapter 2. The diffraction of X-rays by a periodic crystal structure in definite directions allows the determination of the nature of the crystal lattice. Figure 5.5 illustrates the diffraction process, which is often referred to as Bragg reflection (57). A sample is exposed to X-ray beams at varying angles of incidence, and the resulting intensity of the diffracted beams is measured. The Bragg equation, Equation 5.1, relates the wavelength of the reflected beam, λ, to the angle of incidence, θ.

$$n\lambda = 2D \sin \theta \qquad [5.1]$$

The symbol n is an integer, often called the order of the diffraction, and D is the distance between crystal planes. Peaks in X-ray diffraction intensity occur at specific intervals that are related to the crystalline structure of the sample. The peaks are compared to an existing database and past experience to identify the crystalline compounds present in the sample.

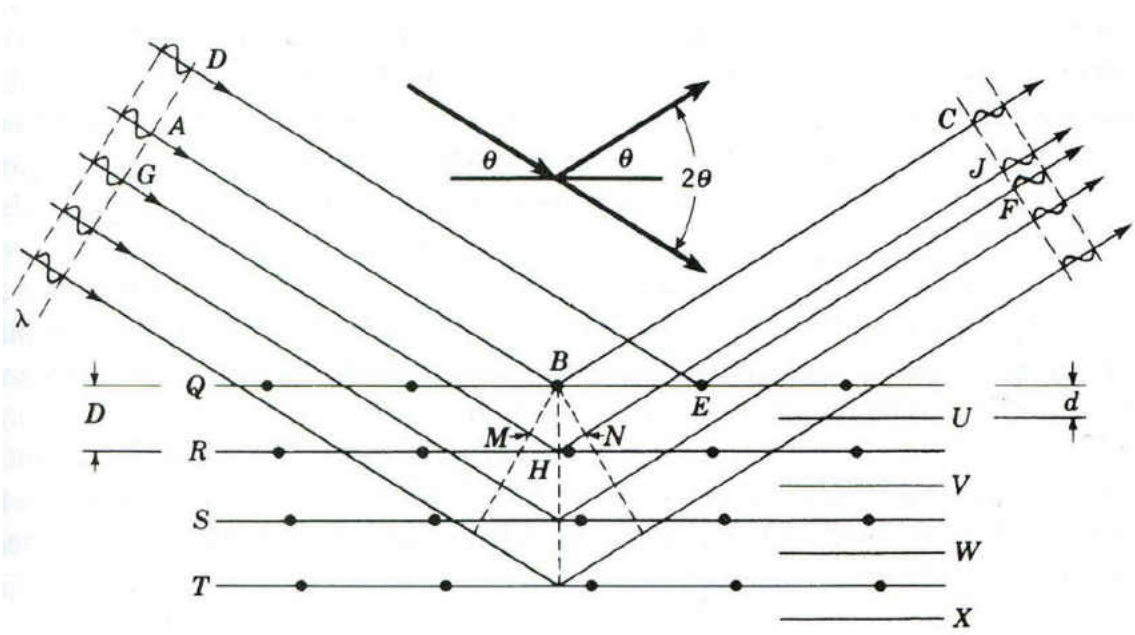

Figure 5.5. Illustration of the XRD Process (57).

5.3.2 Scanning Electron Microscopy with Energy Dispersive Spectroscopy

Detailed views of the membrane surface and chemical composition were accomplished using SEM/EDS. The SEM units use an electron gun to emit an electron beam that is swept in a raster pattern over the sample (58). The high energy beam produces backscatter electrons, secondary electrons, Auger electrons, and X-rays that can be collected in two separate detectors to provide detailed imaging and chemical

information about the sample. The SEM has capability to focus in on a certain area of interest on a sample and provide detailed chemical information about that focus area.

The incident electron beam interacts with the core-level electrons of an atom and ejects a secondary electron from the 1s orbital. This creates a hole in the core level which is filled by a higher electron. This filling is accompanied by an Auger electron emission or an x-ray emission, and the energy produced is characteristic of the atom from which it was emitted. Electron detectors collect the back-scattered and/or secondary electrons produced and compare the information gathered to the specific focus location of the electron beam to produce an image of the sample. Quantification of the x-rays produced in a given area produces chemical composition information about the sample (58).

5.3.3 X-ray Photoelectron Spectroscopy

XPS analysis (also known as ESCA) was used to characterize the chemical composition of the surface of the membranes. The technique enables the characterization of the very near surface of the material, as low as 1nm depth. It was also used in conjunction with an argon sputtering beam to provide a simultaneous depth profile and chemical analysis of the material, up to 40 nm depth. The operating principle for the XPS technique is that a sample is subjected to an x-ray beam which ejects photoelectrons (core-level electrons) from atoms in a sample. The kinetic energy of the photoelectrons produced is low enough that only surface level photoelectrons (1-10 nm) can escape the sample. This ensures that only the surface chemistry of the sample is evaluated. The kinetic energy of the emitted electron, E_k, is measured in an electron spectrometer. That information can be used to calculate the binding energy, E_b, of the electron according to the following equation, Equation 5.2:

$$E_b = hv - E_k - w \quad [5.2]$$

where hv is the energy of the X-ray beam, and w is the work function of the spectrometer, which is a correction factor for the electrostatic environment of the instrument (58). The binding energy of the photoelectron is characteristic of the atom from which it was produced, enabling determination of the chemical composition. Figure 5.6 illustrates this process (58).

When exposed to the X-ray beam, electrons from various orbital shells in each atom can be emitted, and the emission of these electrons is dependent on the oxidation state of the atom. The variations in bonds formed by the valence electrons impact the biding energies of the core electrons. A chemical shift in binding energy can be observed for various elements as a function of oxidation state. Therefore, the type of bonding that occurs in the sample can also be determined using XPS.

For XPS depth profiling, an argon ion beam is sputtered on the surface of the material. This beam etches away the material at an approximate rate of 8 nm/min. XPS measurements are taken continuously during the etching, allowing a profile of the very near surface contaminants as a function of depth into the sample. This technique is typically viable to 200nm depth into the sample, and the basic concept is illustrated in Figure 5.7 (58).

5.3.4 Analysis at EERC

The membrane sample was brought to EERC laboratories for analysis using SEM/EDS and SEM morphology. The morphology technique was used to determine the bulk composition of the membrane material and then to focus in on surface contaminants and determine the chemical composition. The analyzer used was a JEOL 5800 LV SEM,

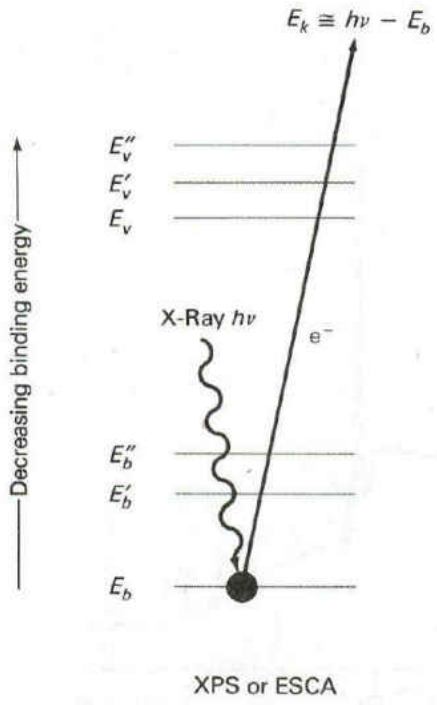

Figure 5.6. Schematic of the XPS Technique (58).

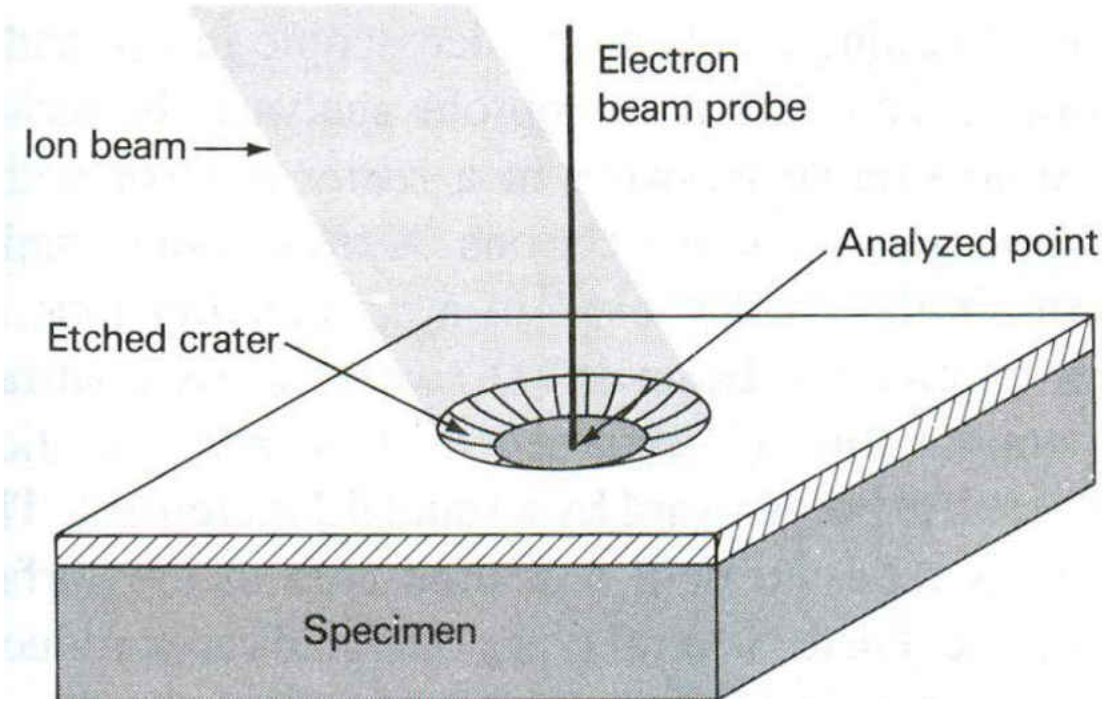

Figure 5.7. Illustration of the XPS Depth Profiling by Sputtering with an Argon Ion Beam (58).

capable of low vacuum (LV) imaging and analysis. The SEM is equipped with a Princeton Gamma Tech EDS Microanalysis system that used a nitrogen cooled lithium drifted silicon crystal (SiLi) detector. The system is capable of point analyses, line scans, and x-ray maps. Since the sample was already conductive, no sample preparation was performed prior to analysis and the sample was not coated with carbon.

The analysis at low magnification levels is shown in Figures 5.8 and 5.9 for the face and inside of the membrane material. The analysis confirms that the bulk membrane material is a palladium copper alloy. Traces of sulfur and chlorine were observed on the face of the membrane, but none of these components were detected on the inside of the material. The carbon levels observed were fairly consistent for all of the analyses, and the inside appeared to have higher levels of oxygen. Point number 1 on Figure 5.9 also shows the presence of an aluminum rich particle, possibly an aluminum oxide.

Particulates found on the surface of the membrane were analyzed in detail using higher magnification. The results of the analysis on the face of the membrane are shown in Figure 5.10. The nature of the particles examined has a wide variety of chemical compositions. The surrounding Pd and Cu is always picked up in the analysis, but high levels of C, O, S, Ni, and W are also observed. Elevated levels of carbon are often accompanied by high levels of tungsten. One possible source of this material would be from tungsten-carbide bits, which would indicate that some of the contaminants are an artifact of the membrane machining process. The arsine removal sorbent used upstream of the membranes contained Alumina oxide, copper oxide, and zinc oxide. Contamination from that sorbent would be indicated by elevated levels of aluminum, but no significant amounts were found. Any particles derived from the high temperature

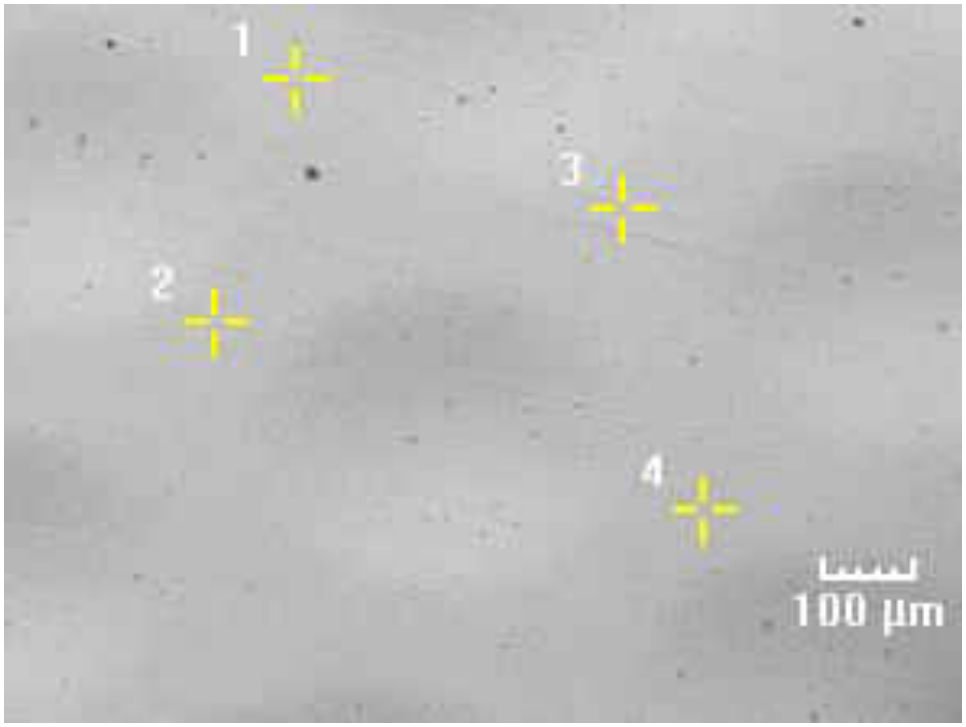

Tag	C	O	S	Cu	Pd	Ni	Cr	Si	Al	W	Cl
1	6.45%	0.00%	0.00%	25.01%	68.54%	0.00%	0.00%	0.00%	0.00%	0.00%	0.00%
2	5.57%	0.48%	0.00%	24.36%	68.79%	0.00%	0.00%	0.00%	0.00%	0.77%	0.02%
3	5.40%	1.14%	0.03%	24.67%	68.52%	0.00%	0.00%	0.00%	0.12%	0.00%	0.11%
4	6.04%	0.00%	0.00%	25.10%	68.18%	0.00%	0.08%	0.02%	0.00%	0.57%	0.00%

Figure 5.8. Low Magnification EDS Point Analysis of the Face of the Membrane Material, Values are in Wt%.

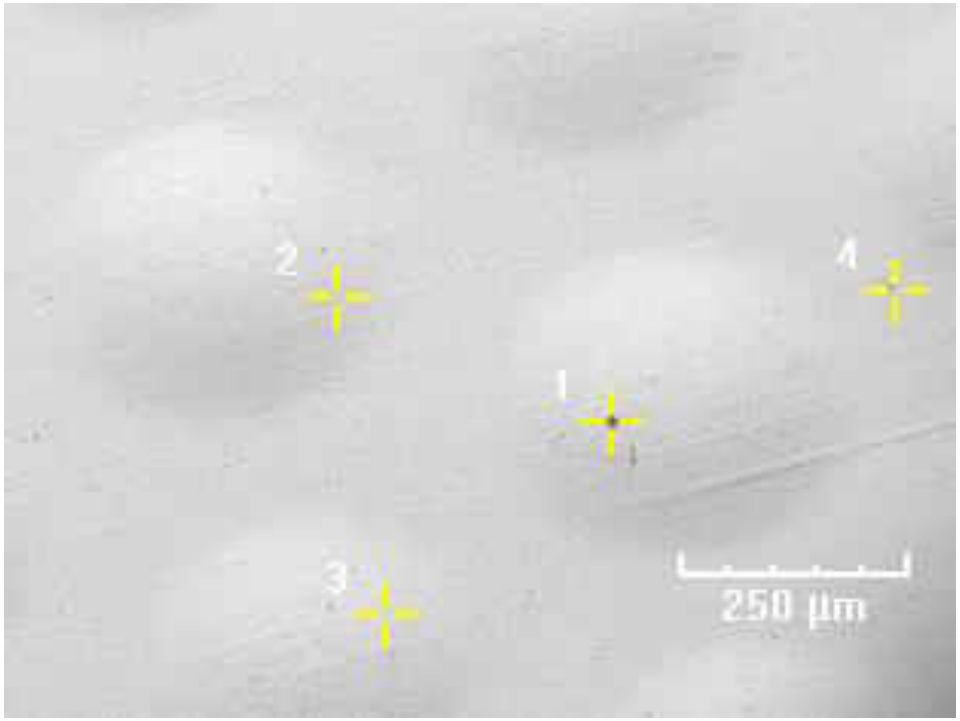

Tag	C	O	S	Cu	Pd	Ni	Cr	Si	Al	W	Cl
1	6.44%	15.39%	0.00%	8.17%	24.60%	0.14%	0.00%	0.06%	44.40%	0.61%	0.00%
2	4.71%	0.18%	0.00%	26.56%	68.52%	0.00%	0.03%	0.00%	0.00%	0.00%	0.00%
3	5.56%	0.58%	0.00%	25.66%	68.10%	0.00%	0.07%	0.02%	0.00%	0.00%	0.00%
4	4.97%	4.97%	0.00%	24.15%	60.14%	0.05%	0.00%	4.92%	0.14%	0.65%	0.00%

Figure 5.9. Low Magnification EDS Point Analysis of the Inside of the Membrane Material, Values are in Wt%.

stainless steel components would be expected to be high in Fe, Cr, and Ni. None of the particles were found to be enriched in all three of these elements. Some carbon particles found could be the result of coking. A few particles were found to be enriched in Si and Fe, which may indicate that they could be derived from the inorganic components in the feed coal, but there is not enough evidence to determine this with certainty. No chlorine was detected, indicating that the low levels of chlorine found in the coal was not depositing on the particles. The particulates observed may be random particles that were picked up from handling of the material.

The results of the particulate analysis on the inside surface of the membrane are shown in Figure 5.11. The results on the inside surface were similar to the results on the face of the membrane. A couple of particles rich in aluminum were found, but these are not likely from the arsine sorbent as they would also then be enriched in copper. The contamination observed from tungsten on the face was not detected in significant quantities on this side of the membrane. Trace amounts of chlorine were detected in the particles. Ni and Cr were both very low, indicating that the particles are not derived from stainless steel. Elevated silica levels were found on a couple of samples which could potentially be derived from coal ash.

In summary, the analysis at the EERC confirmed the base structure of the membrane material was Pd and Cu. Very low levels of sulfur and chlorine were detected on the surfaces of the membranes. Particulates found on the membrane surface contained a wide variety of elements, and were likely random contamination that was encountered due to material handling.

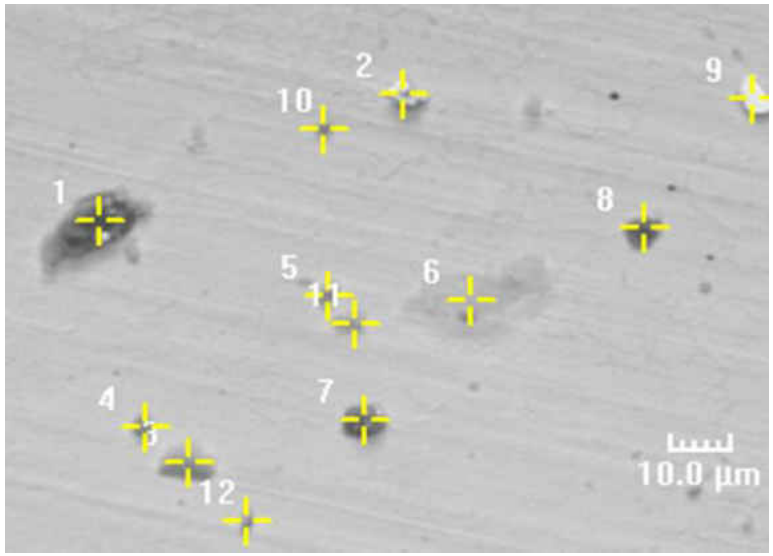

Tag	C	O	S	Cu	Pd	Ni	Cr	Si	Al	W	Cl	Ca	Fe
1	28.40%	0.52%	3.74%	13.13%	36.76%	0.01%	0.08%	6.28%	0.00%	8.14%	0.00%	1.91%	1.03%
2	9.04%	0.42%	6.46%	9.88%	37.74%	0.00%	0.00%	0.00%	0.30%	36.07%	0.00%	0.00%	0.09%
3	4.68%	11.67%	0.60%	17.66%	51.06%	0.19%	0.00%	5.45%	0.14%	0.00%	0.00%	0.00%	8.55%
4	5.17%	0.10%	0.00%	25.22%	67.81%	0.00%	0.02%	1.69%	0.00%	0.00%	0.00%	0.00%	0.00%
5	5.46%	4.47%	0.32%	22.95%	61.14%	0.00%	0.25%	1.33%	0.43%	0.13%	0.00%	0.00%	3.51%
6	7.34%	3.06%	0.19%	22.81%	64.02%	0.77%	0.55%	1.10%	0.00%	0.00%	0.00%	0.00%	0.17%
7	37.93%	0.00%	3.07%	11.57%	37.57%	2.60%	0.35%	1.28%	0.07%	4.32%	0.00%	0.00%	1.23%
8	25.02%	0.00%	0.42%	17.35%	52.31%	0.00%	0.00%	0.00%	0.04%	4.34%	0.00%	0.00%	0.53%
9	11.17%	0.00%	17.71%	6.56%	18.71%	0.00%	0.00%	2.30%	0.19%	43.37%	0.00%	0.00%	0.00%
10	6.85%	0.36%	1.00%	18.78%	44.16%	28.77%	0.09%	0.00%	0.00%	0.00%	0.00%	0.00%	0.00%
11	11.40%	7.57%	2.74%	20.19%	50.91%	1.39%	0.47%	0.90%	0.02%	0.00%	0.00%	0.00%	4.42%
12	8.88%	7.23%	1.23%	18.75%	53.45%	0.00%	7.03%	1.49%	0.00%	0.08%	0.00%	0.11%	1.75%

Figure 5.10. High Magnification EDS Point Analysis of the Particulates Found on the Face Membrane Surface, Values are in Wt%.

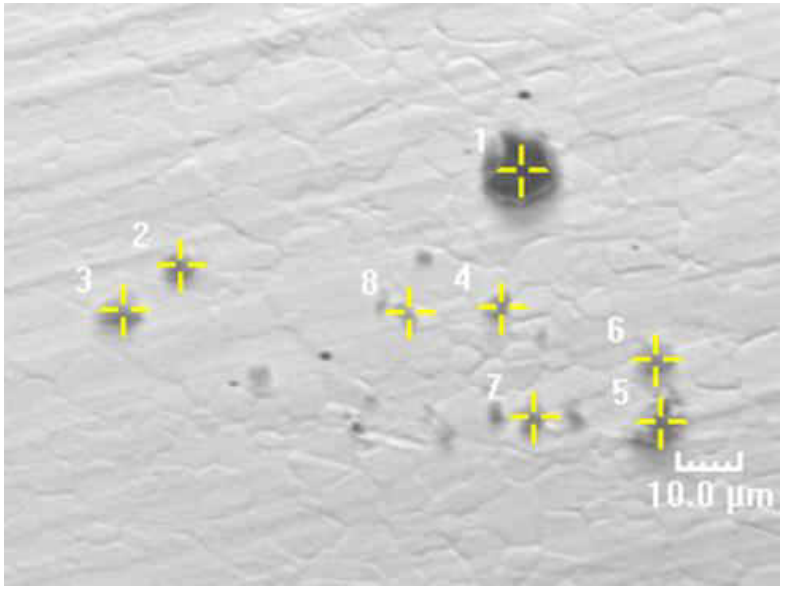

Tag	C	O	S	Cu	Pd	Ni	Cr	Si	Al	W	Cl	Ca	Fe
1	9.68%	15.53%	0.10%	5.67%	19.56%	0.14%	0.00%	0.32%	48.30%	0.14%	0.55%	0.00%	0.02%
2	19.18%	5.08%	0.27%	14.57%	45.29%	0.10%	0.02%	4.07%	0.69%	0.56%	0.58%	9.33%	0.26%
3	7.56%	1.81%	0.08%	21.06%	61.23%	0.06%	0.00%	2.20%	0.51%	0.46%	0.24%	4.62%	0.18%
4	5.91%	1.40%	0.00%	22.25%	61.13%	0.00%	0.00%	4.66%	0.68%	0.35%	0.24%	3.29%	0.09%
5	12.70%	15.71%	0.00%	17.83%	18.32%	0.00%	0.00%	0.85%	34.19%	0.23%	0.00%	0.00%	0.18%
6	13.17%	2.36%	0.38%	14.34%	50.53%	0.00%	0.00%	9.31%	1.15%	0.48%	0.86%	6.98%	0.45%
7	11.81%	19.56%	0.00%	9.48%	29.60%	0.00%	0.00%	19.58%	8.69%	0.56%	0.00%	0.43%	0.28%
8	7.49%	1.85%	0.02%	21.26%	63.06%	0.03%	0.00%	2.50%	0.33%	1.11%	0.00%	2.16%	0.20%

Figure 5.11. High Magnification EDS Point Analysis of the Particulates Found on the Inside Membrane Surface, Values are in Wt%.

5.3.5 Analysis at UTRC

The analysis at UTRC consisted of SEM/EDS imaging and analysis of the surface of the material and EDS analysis of a cross section of the material. Both the inside and the face of the material were analyzed. The SEM is a LEO 1455-VP. All images and analyses were performed at 15 kV accelerating voltage, and EDS was used for chemistry measurements and chemical analysis. The detector was an EDAX silicon drift detector with a 10 mm^2 window. The energy resolution of the detector is 135 eV. EDS semi-quantitative measured values were obtained using ZAF corrections (Z= atomic #, A= absorption, F= fluorescence).

Figure 5.12 shows the SEM/EDS analysis of the inside of the membrane. The area with the gold discoloration was referred to as the sulfur rich region, and the area without discoloration was referred to as the clean region. The analyses show that significant levels of oxygen and sulfur are present on the stained surface of the membrane material. The clean region shows much lower levels of both oxygen and sulfur. Carbon was also found to be present on the membrane surface.

Figure 5.13 shows the same analysis for the face of the membrane. Oxygen was detected in similar amounts as the inside of the membrane. Sulfur levels were slightly lower, and no sulfur was detected in the clean region of the membrane. A small amount of carbon was again detected in both the clean region and the sulfur rich region.

A cross section of the membrane material was taken and the inside of the membrane was analyzed using the SEM/EDS technique. This enabled an analysis to be performed on the material without interference of surface contaminants, and provided information on the possible penetration of materials into the membrane surface. The

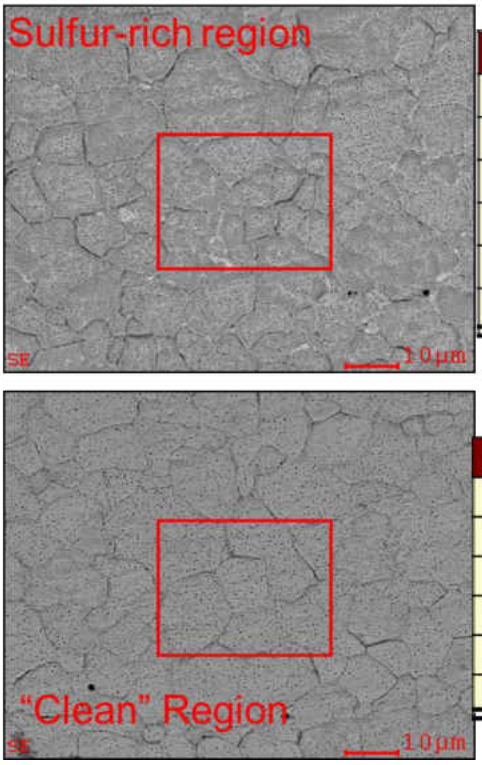

Element	Wt%	At%
CK	00.78	03.70
OK	09.67	34.51
SK	00.38	00.68
PdL	52.61	28.25
CuK	36.56	32.87
Matrix	Correction	ZAF

Element	Wt%	At%
CK	01.43	08.34
OK	02.33	10.25
SK	00.09	00.21
PdL	56.44	37.28
CuK	39.71	43.92
Matrix	Correction	ZAF

Figure 5.12. SEM/EDS Analysis of the Inside Surface of the Membrane.

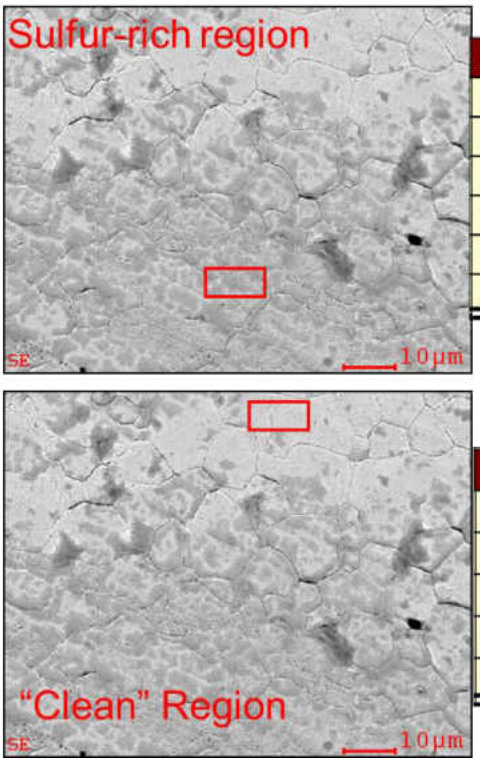

Element	Wt%	At%
CK	00.85	04.20
OK	08.43	31.10
SK	00.26	00.47
PdL	52.82	29.29
CuK	37.64	34.95
Matrix	Correction	ZAF

Element	Wt%	At%
CK	01.80	11.18
OK	00.67	03.12
PdL	61.13	42.91
CuK	36.40	42.79
Matrix	Correction	ZAF

Figure 5.13. SEM/EDS Analysis of the Face of the Membrane.

results of the analysis are shown in Figure 5.14. Only Pd and Cu were detected in the cross sectional analysis. No internal sulfide phases were found to be present. The ratio of Pd to Cu is consistent with a 60 wt.% Pd – 40 wt. % Cu alloy. The membrane thickness was measured to be about 25µm.

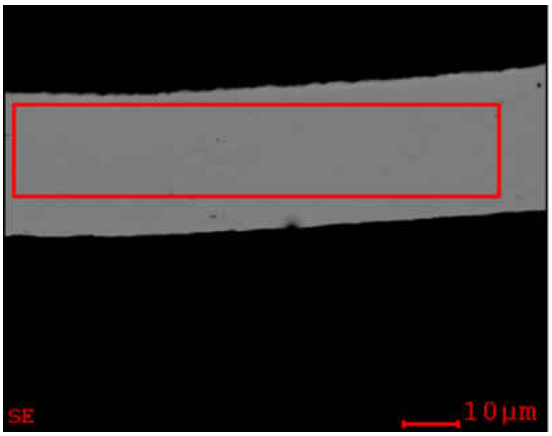

Element	Wt%	At%
PdL	60.97	48.26
CuK	39.03	51.74
Matrix	Correction	ZAF

Figure 5.14. SEM/EDS Analysis of the Membrane Cross Section.

In summary, the UTRC analysis indicated that there was some oxygen and sulfur present on the surface of the membrane, and that the corrosion products did not penetrate into the membrane material. The membrane in question was a 60 wt.% Pd – 40 wt. % Cu alloy that was 25µm thick.

5.3.6 Analysis at NETL

The analytical work at NETL was focused on determining the cause of the membrane failure. Three analytical techniques were used: SEM/EDS, XRD, and XPS (also known as ESCA) depth profiling.

The membrane sample was analyzed using an FEI Quanta 600 F scanning electron microscope equipped with an Oxford Inca X-act energy dispersive x-ray analyzer (SEM/EDS) to determine morphology and composition of membrane surface

features. Typically, 5 kV was used for imaging and 20 or 30 kV for EDS analysis at a working distance of 10 mm.

Backscatter SEM/EDS analysis of the inside of the membrane is shown in Figure 5.15. A more discolored portion is represented by point A, and a less discolored portion is represented by point B. The EDS analysis shows Pd, Cu, significant oxygen and trace amounts of sulfur, with variable S to O ratios. These areas appear to be surface deposits consisting of copper oxide, which accounts for the gold coloration observed on the disk. Point B on the figure shows mainly Pd and Cu, with minor amounts of oxygen. These areas are much less oxidized then the gold colored areas. Analysis of the face indicated Pd, Cu, and lower levels of oxygen than were observed on the inside.

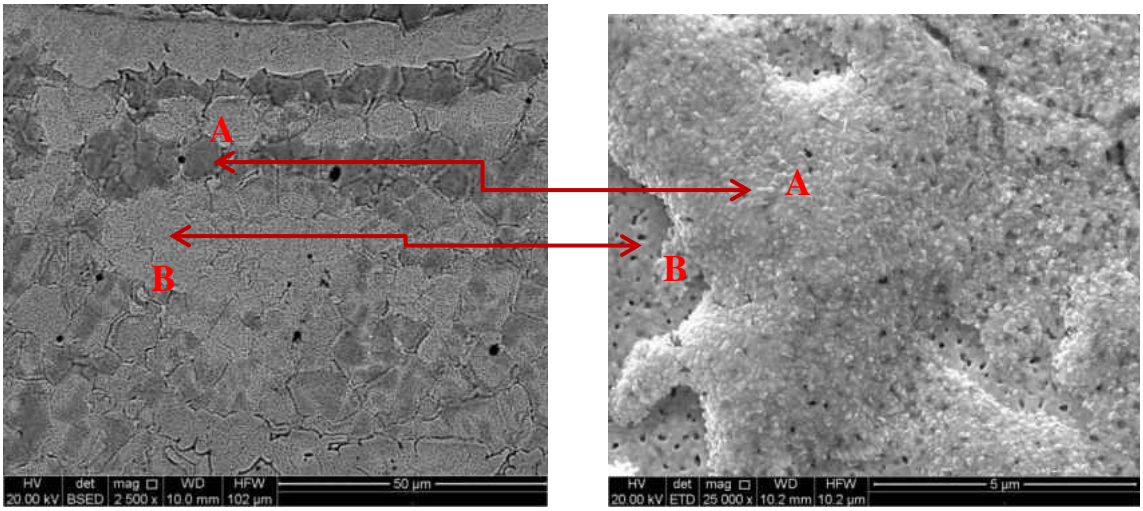

Figure 5.15. Backscatter SEM/EDS Analysis of the Inside Surface of the Membrane.

An SEM image analysis was also performed on the edges of the sample to potentially understand the failure mechanism. Figure 5.16 shows the inside edge and the outside edge of the membrane material. According to the supplier, the inside edge had torn away from the supporting flange. The SEM images show a rough edge on the inside, which is consistent with tearing. The outside edge is much smoother and appears to be

consistent with mechanical shearing. The analytical lab concluded that the inside edge likely tore away from its support, without having any prior knowledge of the suppliers comments.

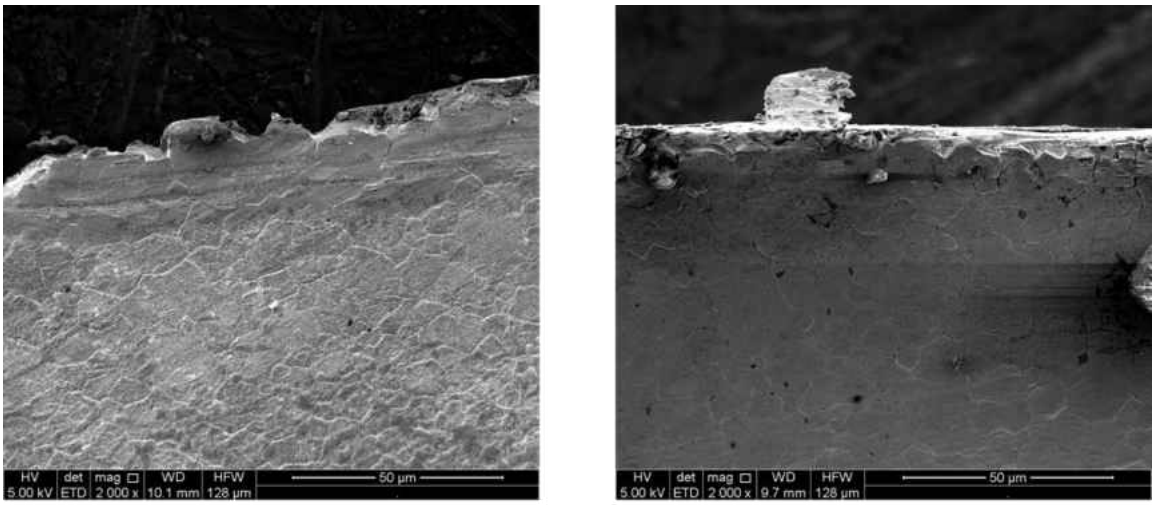

Figure 5.16. SEM Image Analysis of the Edges of the Membrane Material.

X-ray diffraction (XRD) characterization of the membrane sample to determine crystalline phase composition was conducted using a PANalytical X'pert Pro powder diffractometer with a Cu X-ray source at 45 kV and 40 mA and an X'Celerator detector equipped with a monochromator. The membrane foil was analyzed as received. The XRD patterns were recorded over a 2θ range of 10° to 90°. Phase identification was verified by comparison to the ICDD inorganic compound powder diffraction data base and NETL internal data.

The XRD analysis conducted at NETL is shown in Figure 5.17. The analysis indicates that the membrane is mainly made up of B2 (or bcc) PdCu with traces of fcc PdCu. A trace amount of copper oxide was detected on the inside of the membrane, which may explain the increase in fcc phase PdCu and Cu enrichment seen on the surface. This indicates that oxidation of the membrane surface can also lead to a phase

change in the palladium copper crystalline structure. The fcc phase is known to be less hydrogen permeable than the bcc phase (33) and therefore can result in lower overall permeation rates in the membrane. The face of the membrane contained lower levels of the fcc PdCu, and no oxides were detected. No crystalline sulfide phases were detected on either side of the membrane.

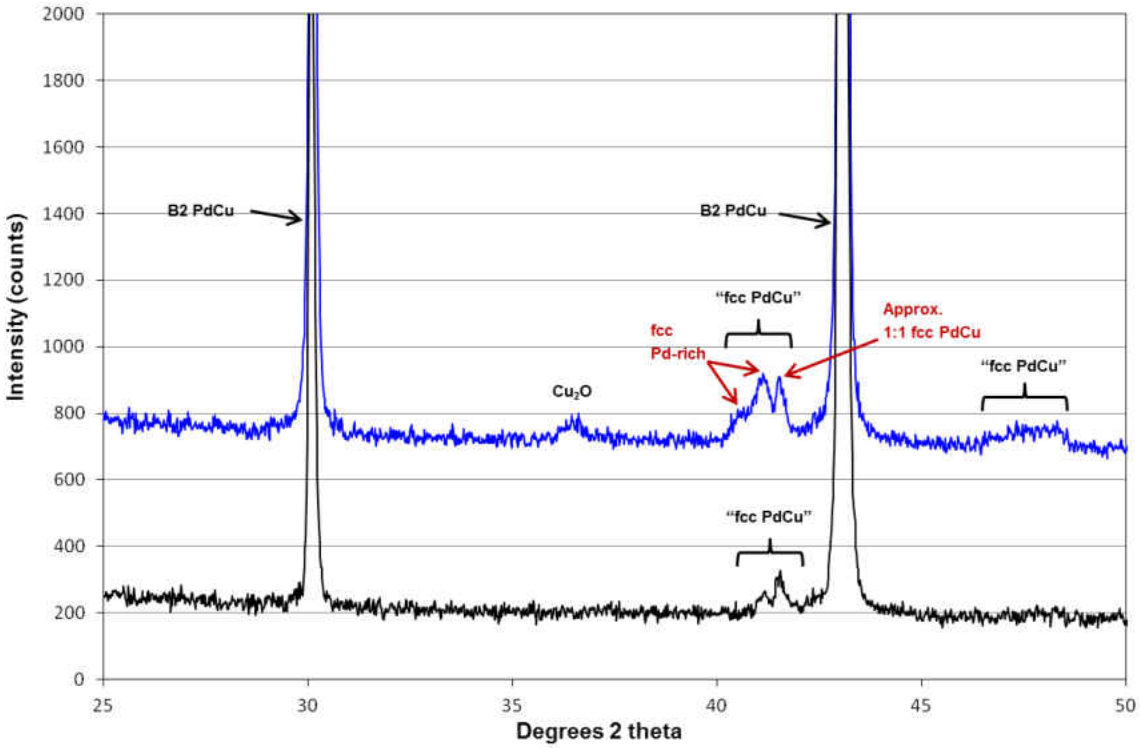

Figure 5.17. XRD Analysis of the Membrane Material at NETL. Blue Line is Inside, Black Line is Face of Membrane.

Surface analysis of the membrane was conducted using XPS depth profiling. The measurements were performed with a PHI 5600ci spectrometer using a monochromatic AlAl Kα X-ray source and analyzer pass energy of 58.7 eV. Elemental compositions were calculated from XPS peak areas by using sensitivity factors provided by the instrument manufacturer. The depth profile measurements were accomplished by sputtering the surface win an Ar+ ion beam. A differentially pumped ion gun was

operated at 1.5 x 10^{-2} Pa and 25 mA to deliver a sputtering rate of approximately 8.5 nm/min. At a maximum sputtering time of four minutes, a depth of approximately 34 nm into the membrane surface was achieved.

The results of the XPS analysis on the inside of the membrane is shown in Figure 5.18. The analysis confirms the copper enrichment observed during the SEM and XRD analyses. The enrichment extends "deep" into the surface (over 34 nm). The concentration of Pd is shown to be increasing toward the end of the analysis, corresponding to reduced concentrations of Cu. There are very thin but high levels of carbon observed on the surface of the membrane, which are contamination due to handling and possibly the result of storing in a polyethylene bag. Anything exposed to the environment or that has been handled is expected to have a carbonaceous surface residue. Very small amounts of sulfur were detected, and the sulfur was detected as sulfate. The sulfur was most likely originally present as sulfide, and had been converted to sulfate over time by exposure to the air. The enriched copper on the surface indicates the sulfate is most likely associated with copper, and is in the form of copper sulfate. Copper sulfate, copper oxide, and lower levels of palladium on the surface of the membrane could inhibit the rate of re-association of the hydrogen atoms.

The analysis of the face of the membrane is shown in Figure 5.19. The palladium copper ratio for the face of the membrane was close to the expected bulk composition of the membrane, and no enrichment is indicated. The sulfur levels were near zero on the face and were too low to determine the oxidation state. The same carbonaceous contamination that was observed on the inside of the membrane was also present in a very thin coating on the face of the membrane.

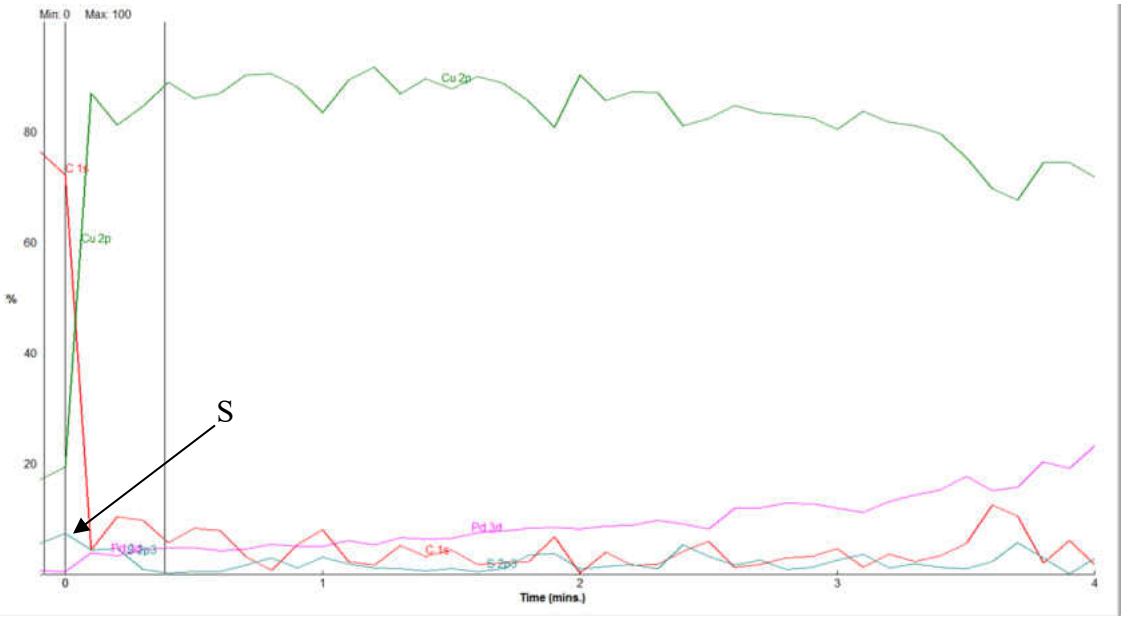

Figure 5.18. XPS Analysis of the Inside of the Membrane.

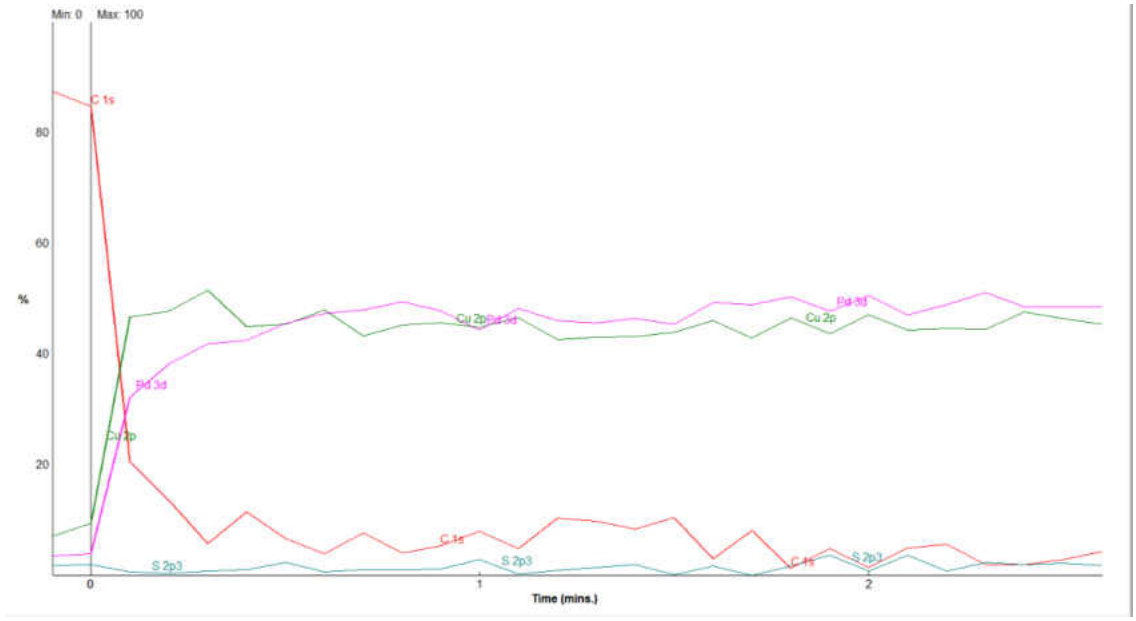

Figure 5.19. XPS Analysis of the Face of the Membrane.

In summary, the analysis at NETL indicated that there were more corrosion products on the inside surface of the membrane. The main corrosion product was copper oxide. The small amount of fcc Pd-Cu detected by the XRD appears to be copper depleted, and is expected due to the extraction of Cu as oxide. The XPS analysis shows

that Cu is highly enriched at the surface, and that the depth profile indicates this enrichment extends over 34 nm into the surface. Sulfur was detected on the inside of the membrane as sulfate. The face of the membrane did not have the same level of corrosion, did not have copper enrichment, and exhibited very low levels of sulfur.

5.4 Overall Analysis Summary and Failure Mechanism

The membrane material was analyzed at three different laboratories using three different techniques for surface analysis. The results of the analyses indicated that there was sulfur present on both surfaces of the membrane, but higher sulfur levels on the inside (hydrogen side) of the membrane as compared to the face (syngas side). The analysis also indicates that the staining observed on the inside of the membrane was indeed copper oxide. Sulfur in the form of sulfate was detected on the inside surface. Not enough sulfur was detected on the face to determine its chemical state. No significant sulfur penetration was observed. Some particulates were observed on the membrane surface, but their origin appeared to be random and an artifact of membrane handling. Copper enrichment as copper oxide was observed on the inside surface of the membrane, which caused localized higher levels of fcc phase copper. Increased levels of copper oxide on the inside of the membrane were likely responsible for reduced flux performance observed in weeks 5 and 6.

SEM analysis indicated that the inside small radius of the disk appeared to have torn away from its support. This finding was consistent with supplier findings of the membrane material. The supplier indicated that the failure of the material was likely due to a reverse pressurization event. Unfortunately, no process log data exists during the

startup period when the failure may have occurred, so this cannot be proven for certain. Given that no chemical failure was apparent, this was most likely the cause of the failure.

The results of the analysis bode well for the chemical durability of the membranes when exposed to coal derived syngas. The full stream membrane was exposed to coal derived syngas for 331 hours, and from a chemical standpoint, the material held up well. This is also an indication that existing warm gas cleanup technologies are adequate to clean syngas to levels required by hydrogen separation membranes that can tolerate very low levels of sulfur (< 1 ppm). Some performance degradation was observed over the 331 hours, but this could likely be overcome with commercial warm gas cleanup systems and next generation Pd-Cu based membrane materials.

CHAPTER 6

CONCLUSIONS

Three hydrogen separation membranes were exposed to coal-derived syngas for a total of 831 membrane-hours of exposure time. The syngas was produced from a PRB coal from the Antelope Mine in Wyoming. Particulate was removed with a hot-gas filter vessel, and solid sorbents were used to remove contaminants such as sulfur, chlorine, and mercury. Both high-temperature and low-temperature WGS catalysts were used to maximize the hydrogen content of the syngas and minimize CO concentration. A membrane skid was built that was capable of exposing one membrane to the FS syngas and two slipstream membranes to syngas simultaneously.

The warm gas cleanup train was able to remove sulfur to levels below 20 ppb, which is greater than 99.99% removal. Chlorine was typically observed at concentrations less than 1 ppm in the syngas. Mercury concentrations ranged from 1 to 7 ug/dNm3, representing removal efficiencies of 65 to 95%. Ammonia was not controlled and was measured to be less than 100 ppm during the EFG runs and ranged from 1000 to 2000 ppm during the HPFBG runs. Trace metal measurements were taken during weeks 4 and 5 and the measurements were consistent from week to week, with removals in the 90% range. The warm gas cleanup train performed well and very low levels of contaminants reached the membranes. This configuration is sustainable in a commercial operation if regenerable sorbents are used. Testing at Research Triangle Institute (RTI) with a

proprietary transport style solid sorbent has resulted in similar sulfur levels (59). Utilization of an eastern bituminous coal with higher concentrations of sulfur, chlorine, and mercury may lead to more difficulty in controlling contaminant levels.

The FS Pd-Cu membrane had very high hydrogen purity and good flux and recovery rates through the first few weeks of testing. Hydrogen purity was at least 99.99% through the first few weeks, and hydrogen recovery rates approached 50%. Hydrogen recovery would have been improved with increased partial pressure differential, but only 56 psi differential was achieved during the test run. Theoretical calculations with Sievert's law indicate that with a partial pressure differential of 100 psi, flux rates of 21.4 scfh/ft^2 may have been achieved. This falls well below the DOE 2010 goal of 200 scfh/ft^2. The highest flux was achieved during the earlier runs, despite the fact that partial pressure differential was higher for some of the membrane test runs later in the campaign. Also, a leak developed later in the test campaign that should have worked to increase flux for two reasons: 1) hydrogen bypasses the membrane and penetrates to the permeate side through the leak and 2) the other syngas components leaking through the membrane act as a sweep gas to increase partial pressure differential across the membrane. Even with the leak and the increased partial pressure, flux was decreased from where it was earlier in the test campaign. This indicates that there may have been some performance degradation because of syngas contaminants.

The Pd-Au SS1 membrane had good purity measurements, with readings up to 99.2% pure. Apparent flux rates were low initially until it was determined that the gas meter used to measure permeate flow was oversized. A low-range flowmeter was used starting in Week 4 testing, and it was determined that flux rates through the membrane

were significant, even though the hydrogen recovery rates were low. Based on the Sievert's law calculation, the membrane was capable of achieving flux rates of 117 scfh/ft^2. Higher rates were achieved during the last week of testing, but the membrane was also shown to have a small leak. It was difficult to determine if any performance degradation occurred for SS1 membrane because of the small leak that developed later in the tests and the lack of good flow measurements early in the test.

The Pd-Cu SS2 membrane seemed to have very low flux rates during the initial stages of the program because the gas meter was not capable of measuring the permeate flow rate and hydrogen purity was low. Once the low-flow flowmeter was brought online, flux measurements were shown to improve, but maximum hydrogen purity reached was about 60%. Theoretical flux rates calculated at 100 psi partial pressure differential were as high as 29.4 scfh, but this was also with 60% hydrogen purity. It was difficult to determine if any performance degradation occurred for SS2 membrane because of the lack of good flow measurements for most of the testing and a leak that appeared to be present for the duration of the test campaign.

DOE lists a 5-year membrane life as the durability target for 2015. It is difficult to derive the full life of the membranes over the duration tested. The leaks developed are certainly a concern but likely easily resolved with additional engineering. The FS membrane exhibited what appeared to be a slight degradation in performance over the 331 hours of exposure time, although the exact degradation in performance was difficult to quantify fully because of the leak. More exposure time would be necessary to determine the full potential impact of impurities. The testing did show that the membrane could still produce significant flux over several hundred hours of operation using

commercial or near-commercial technologies for warm-gas cleanup. This is a promising result as future membrane materials are developed. There was no conclusive reduction in flux for SS1 membrane, which is also a promising result. Overall, it is difficult to exactly determine the life of a membrane based on these data, but no significant showstoppers were discovered as a result of exposure to coal-derived syngas.

The membrane material from the FS membrane was analyzed at three different laboratories using three different techniques for surface analysis. The results of the analyses indicated that there was sulfur present on both surfaces of the membrane, with higher sulfur levels on the inside (hydrogen side) of the membrane as compared to the face (syngas side). The analysis also indicates that the staining observed on the inside of the membrane was indeed copper oxide. Sulfur in the form of sulfate was detected on the inside surface. Not enough sulfur was detected on the face to determine its chemical state. No significant sulfur penetration was observed. Some particulates were observed on the membrane surface, but their origin appeared to be random and an artifact of membrane handling. Copper enrichment as copper oxide was observed on the inside surface of the membrane, which caused localized higher levels of fcc phase copper. Increased levels of copper oxide on the inside of the membrane were likely responsible for reduced flux performance observed in weeks 5 and 6.

SEM analysis indicated that the inside small radius of the disk appeared to have torn away from its support. This finding was consistent with supplier findings of the membrane material. The supplier indicated that the failure of the material was likely due to a reverse pressurization event. Unfortunately, no process log data exists during the startup period when the failure may have occurred, so this cannot be proven for certain.

Given that no chemical failure was apparent, a reverse pressurization event was most likely the cause of the failure.

The results of the analysis bode well for the chemical durability of the membranes when exposed to coal derived syngas. The full stream membrane was exposed to coal derived syngas for 331 hours, and from a chemical standpoint, the material held up well. Some level of sulfur was noted on the membrane surface, which did appear to degrade membrane performance. This work has shown that existing warm gas cleanup technologies are adequate to clean syngas to levels required by hydrogen separation membranes if the membranes can withstand low levels (< 1 ppm) of sulfur. Membranes with zero tolerance for sulfur species will likely not maintain high flux rates for long durations with the gas cleanup train employed.

This work has demonstrated that existing warm gas cleanup techniques are adequate to remove contaminants from syngas to levels required for consistent, long-term membrane operation if very low levels of sulfur can be tolerated. The next steps in researching the impact of coal-derived impurities will be to expose promising membrane materials to higher levels of contaminants. This could be accomplished by removing the sulfur polishing, chlorine guard, and mercury removal beds. A sour shift water-gas shift catalyst upstream of the sulfur removal beds could be used in place of the high and low temperature shift beds to overcome the impact of chlorine on the low temperature shift bed. Additional fuel types also need to be tested, including eastern bituminous coals high in sulfur, chlorine, and mercury. Understanding the impact of a wide variety of fuels on warm gas cleanup and membrane performance will increase the prospects for commercializing this promising technology.

REFERENCES

1. Kluiters, S.C.A; Status Review on Membrane Systems for Hydrogen Separation; December 2004.

2. *Effects of a Transition to a Hydrogen Economy on Employment in the United States, Report To Congress;* US. Department of Energy, July 2008.

3. Ellis, S.; *Honda Fuel Cell Vehicle Progress*; Presented at the Advancing the Hydrogen Economy Action Summit II; Grand Forks, ND; September 4, 2008.

4. Holmes, M..; *Coal-to-Hydrogen*; Presented at the Advancing the Hydrogen Economy Action Summit II; Grand Forks, ND; September 4, 2008.

5. Black, J.; *Cost and Performance Baseline for Fossil Energy Plants Volume 1: Bituminous Coal and Natural Gas to Electricity*; Revision 2; DOE/NETL-2010/1397; 2010.

6. Gerdes, K.; *Current and Future Technologies for Gasification Based Power Generation, Volume 2: Carbon Capture, Revision 1*; DOE/NETL-2009/1389; 2010.

7. Klara, J.M.; *IGCC: Coals Pathway to the Future; Presented at the Gasification Technologies Conference*; October 4, 2006.

8. Sondreal, E.A.; Swanson, M.L.; Benson, S.A.; Holmes, M.J.; Jensen, M.D. A *Review of Gasification Technology for Coproduction of Power, Synfuels, and Hydrogen from Low-Rank Coals*. In Proceedings of the 20th Symposium on Western Fuels; Marriott Denver Tech Center, Denver, CO; Oct 24–26, 2006.

9. Gerdes, Kristen; *The Potential of Advanced Gasification Pathways to Reduce CO2 Capture Costs*; Presented at the Gasification Technologies Conference, Colorado Springs CO; October 2009

10. Hoffman, Jeff; *Cost and Performance for Low-Rank Coal Power Plants*, Presented at the Gasification Technologies Conference, Colorado Springs CO, October 2009.

11. Plunkett, John; *Performance & Cost Comparisons of Alternate IGCC based Carbon Capture Technologies*, Presented at the Gasification Technologies Conference, Colorado Springs CO, October 2009.

12. Stanislowski, Joshua; Laumb, J; *Gasification of Lignites to Produce Liquid Fuels, Hydrogen, and Power*; Presented at the Pittsburgh Coal Conference, September 2009.

13. Stocker, J., Whysall, M., Miller, G.; *30 Years of PSA Technology for Hydrogen Purification*; UOP LLC; 1998.

14. Adhikari, S., Fernando, S.; *Hydrogen Membrane Separation Techniques*; ACS Publications Industrial & Engineering Chemistry Research; 2006.

15. DOE Hydrogen Program; *FY 2008 Annual Progress Report*; http://www.hydrogen.energy.gov/index.html; December 2008.

16. Ockwig, N.; Nenoff, T.; *Membranes for Hydrogen Separation*; ACS Publications Chemical Review 2007.

17. Rothenberger, K.; Howard, B.; Killmeyer, R.; Ciocco, M.; Morreale, B.; Enick, R.; *Palladium-Copper Alloy Membrane Performance Under Continuous H_2S Exposure.*; www.netl.doe.gov.

18. Morreale, B.; Ciocco, M.; Howard, B.; Killmeyer, R.; Cugini, A.; Enick, R.; *Effect of hydrogen-sulfide on the hydrogen permanence of palladium-copper alloys at elevated temperatures*; Journal of Membrane Science; 241 (2004) 219-224.

19. Subramanian, P.; Laughlin, D.; *Binary Alloy Phase Diagrams – Second Edition*, ed. Massalski, T.; ASM International; 1990; p.1454-1456.

20. Volkov, A.; Kazantsev, V.; Kourov, N.; Kruglikov, N.; *Formation of the Structure and Properties of Cu-Pd Alloys during the A1-B2 Phase Transitions*; The Physics of Metals and Metallography; 2008.

21. Kamakoti, P.; Sholl, D.; *Ab initio lattice-gas modeling of interstitial hydrogen diffusion in CuPd alloys*; Physical Review B 71, 014301 (2005).

22. Sholl, D.; *Using density functional theory to study hydrogen diffusion in metals: A brief overview*; Journal of Alloys and Compounds 446-447 (2007) 462-468.

23. Kamakoti, P.; Sholl, D.; *A comparison of hydrogen diffusivities in Pd and CuPd alloys using density functional theory*; Journal of Membrane Science 225 (2003) 145-154.

24. Kamakoti, P.; Sholl, D.; *Towards first principles-based identification of ternary alloys for hydrogen purification membranes*; Journal of Membrane Science; 279 (2006) 94-99.

25. Hao, S.; Sholl, D.; *Selection of dopants to enhance hydrogen diffusion rates in MgH2 and NaMgH3*; Applied Physics Letters 94, 171909 (2009).

26. Hao, S.; Sholl, D.; *Comparison of first principles calculations and experiments for hydrogen permeation through amorphous ZrNi and ZrNiNb films*; Journal of Membrane Science; 350 (2010) 402.

27. Hao, S.; Sholl, D.; *The role of interstitial H_2 in hydrogen diffusion in light metal borohydrides*; Phys. Chem. Chem. Phys., 11 (2009) 11106.

28. O'Brien, C.; *Sulfur Poisoning of Pd and PdCu Alloy Hydrogen Separation Membranes*; Doctoral Thesis; Carnegie Mellon University; 2011.

29. Gabitto, J.; Tsouris, C.; *Sulfur Poisoning of Metal Membranes for Hydrogen Separation; International Review of Chemical Engineering*; 2009.

30. Ma, Y.; Pomerantz, N.; Chen, C.; *Sulfur-Tolerant Pd/Cu and Pd/Au Alloy Membranes for Hydrogen Separation with High Pressure CO_2 Sequestration*; Periodic Progress Report, 2007.

31. Yang, J.; Nishimura, C.; Komaki, M.; *Hydrogen permeation of $Pd_{60}Cu_{40}$ alloy covered V-15Ni composite membrane in mixed gases containing H_2S*; Journal of Membrane Science; 309 (2008) 246-250.

32. U.S. Department of Energy; *Hydrogen from Coal Program RD&D Plan for the Period 2009 through 2016*; External Draft; September 2009.

33. Cicero, D.; *The U.S. DOE's Hydrogen from Coal Program*; Presented at the 235th ACS National Meeting; April 2008.

34. O'Brien, C.; Miller, J.; Gellman, A.; Howard, B.; Morreale, B.; *Hydrogen Transport through Palladium-Based Separation Membranes in the Presence of Hydrogen Sulfide*; Presented at the Pittsburgh Coal Conference, Pittsburgh, PA; September 2009.

35. Howard, B.; Morreale, B.; *Poisoning and Corrosion of Pd-Alloy Hydrogen Separation Membranes by H_2S*; Presented at the Pittsburgh Coal Conference, Pittsburgh, PA; September 2009.

36. Eltron Research and Development Tech Brief; *Maximum, Economical CO_2 capture for IGCC Power Plants*; www.eltronresearch.com; 2009.

37. Jack, D.; CO_2 *Capture and Hydrogen Production in IGCC Power Plants*; Presented at the Gasification Technologies Conference, Washington D.C.; October 2008.

38. Schwartz, J.; Damle, A.; *Integrated Ceramic Membrane System for Hydrogen Production*; DOE Annual Merit Review Meeting; May 2007.

39. Emerson, S.; *Experimental Demonstration of Advanced Palladium Membrane Separators for Central High-Purity Hydrogen Production*; FY 2008 Annual Progress Report.

40. Balachandran, U.; Lee, T.; Chen, L.; Song, S.; Picciolo, J.; Dorris, S.; *Hydrogen Separation by Dense Cermet Membranes*; Fuel 85 (2006) 150-155.

41. Balachandran, U.; Lee, T.; Park, C.; Lu, S.; Dorris, S.; *Development of Cermet Membranes for Hydrogen Separation from Coal Gasification Stream*; Presented at the Pittsburgh Coal Conference, Pittsburgh, PA; September 2009.

42. Oyvind, H.; Gade, S.; Keeling, M.; Thoen, P.; Davidson, A.; Way, D.; *Membranes for Hydrogen Separation and Production: History, Fabrication Strategies, and Current Performance*; Separation and Purification Technology; 2008.

43. Way, J.; Thoen, P.; *Palladium/Copper Alloy Composite Membranes for High Temperature Hydrogen Separation*; Annual Progress Report; 2005.

44. Ma, Y.; *Composite Pd and Pd Alloy Porous Stainless Steel membranes for Hydrogen Production and Process Intensification*; U.S. Department of Energy Project Facts; April 2009.

45. Ayturk, M.; Ma, Y.; *Electroless Pd and Ag deposition kinetics of the composite Pd and Pd/Ag Membranes synthesized from agitated plating baths*; Journal of Membrane Science; 330 (2009) 233-245.

46. Ma, Y.; *Composite Pd and Pd Alloy Porous Stainless Steel membranes for Hydrogen Production and Process Intensification*; Department of Energy Hydrogen Program 2009 Annual Merit Review Proceedings; May 2009.

47. Guazzone, F.; Catalano, J.; Mardilovich, I.; Kniep, J.; Pande, S.; Wu, T.; Lambrecht, R.; Datta, S.; Kazantzis, N.; Ma, Y.; *Gas permeation field tests of composite Pd and Pd-Au membranes in actual coal derived syngas atmosphere; Journal of Hydrogen Energy*; 37 (2012) 14557-14568.

48. Barton, T.; Argyle, M.; *Integration of a Structural Water Gas Shift Catalyst with a Vanadium Alloy Hydrogen Transport Device*; Department of Energy Hydrogen Program 2009 Annual Merit Review Proceedings; May 2009.

49. Abdollahi, M.; Yu, J.; Liu, P.; Ciora, R.; Sahimi, M.; Tsotsis, T.; *Ultra-pure hydrogen production from reformate mixtures using a palladium membrane reactor system*; Journal of Membrane Science; 390-391 (2012) 32-42.

50. Liu, P.; Muhammad, S.; Tsotsis, T.; *Process intensification in hydrogen production from coal and biomass via the use of membrane-based reactive separations*; Current Opinion in Chemical Engineering; 2012, 1:342-351.

51. Abdollahi, M.; Yu, J.; Liu, P.; Ciora, R.; Sahimi, M.; Tsotsis, T.; *Hydrogen production from coal-derived syngas using a catalytic membrane reactor based process*; Journal of Membrane Science; 363 (2010) 160-169.

52. Li, H.; Dijkstra, J.; Pieterse, J.; Boon, J.; van den Brink, R.; Jansen; D.; *Towards full-scale demonstration of hydrogen-selective membranes for CO_2 capture: Inhibition effect of WGS-components on the H_2 permeation through three Pd membranes of 44 cm long*; Journal of Membrane Science; 363 (2010) 204-211.

53. Li, H.; Dijkstra, J.; Pieterse, J.; Boon, J.; van den Brink, R.; Jansen; D.; *WGS-mixture Separation of WGS Reaction Test in a Bench-scale Multi-tubular Membrane Reactor*; Energy Procedia; 4 (2011) 666-673.

54. Air Liquide; *MEDAL™ Membrane Technology*; http://www.airliquide.com/en/oil-gas/equipment-11/medal-membrane-technology-2.html.

55. Air Products; *Hydrogen Recovery and Purification*; http://www.airproducts.com/Products/Equipment/PRISMMembranes/page08.htm

56. Driscoll, D.; *NETL Test Protocol – Testing of Hydrogen Separation Membranes*; DOE/NETL-2008/1335; Oct 2008.

57. Shoemaker, D.; Garland, C.; Nibler, J; *Experiments in Physical Chemistry*, Sixth Edition; McGraw-Hill; 1996.

58. Skoog, D.; Leary, J.; *Principles of Instrumental Analysis*, Fourth Edition; Saunders College Publishing; 1992.

59. Denton, D.; *Pre-Commercial Demonstration of High-Efficiency Low-Cost Syngas Cleanup Technology for Chemical, Fuel, and Power Applications*; Presented at the 2012 Gasification Technologies Conference; Washington, DC; October 2012.